THE HYDROCHEMICAL EVOLUTION AND WATER BALANCE OF THE EMAKAT LAKE IN THE NORTHERN CRATER HIGHLAND OF TANZANIA

Godwin Lucas

A Dissertation Submitted in Partial Fulfilment of the Requirements for the Degree of Master's in Hydrology and Water Resources Engineering of the Nelson Mandela African Institution of Science and Technology

Arusha, Tanzania

July, 2023

ABSTRACT

This study aimed to ascertain the hydrochemical evolution and water balance of Emakat Lake, of the Empakaai Crater. Water and rock samples were collected from the lake and springs on the inner and outer crater rims, and at the foot of the Empakaai Crater. The results showed that the lake is a highly alkaline (pH > 10) and saline (electrical conductivity (EC) = 28,860 - 29,460 µs/cm) with the concentration of total dissolved solids (TDS) ranging from14,432 to 14723 mg/L. Springs exhibited lower pH (6.85 - 8.69), EC (562 - 1584 µs/cm) and TDS (276 - 1016 mg/L). The dominant ions in Emakat Lake were Na^+ and CO_3^{2-}+HCO_3^- which occupy about 80% and 85% of the cation and anion phases with ion distribution of $Na^+ > K^+ > Ca^{2+} > Mg^{2+}$ and $(CO_3^{2-} + HCO_3^-) > Cl^- > SO_4^{2-} > F^- > NO^{3-} > PO_4^{3-}$. Piper, chloro-alkaline indices, Chadha, and Gibbs plots revealed that Na-K-HCO_3 water type dominated Emakat Lake, and a majority of springs exhibited mixing characteristic water type. Base ion-exchange dominated the hydrochemical evolution of both lake and springs, influenced by evaporation and water-rock interaction for the lake and springs respectively. The water balance of Emakat Lake was highly influenced by groundwater flow which accounted for 49% of the inflow and 56% of the outflow. This suggest that Emakat Lake plays a major role in the hydrological system in the area alongside the springs which are the sources of the major rivers of Engaruka and Engaresero.

DECLARATION

I, Godwin Lucas do hereby declare to the Senate of the Nelson Mandela African Institution of Science and Technology that this dissertation is my original work and that it has neither been submitted nor being concurrently submitted for degree award in any other institution.

Godwin Lucas

The above declaration is confirmed by:

Prof. Hans Charles Komakech

Dr. Ceven Shemsanga

COPYRIGHT

CERTIFICATION

The undersigned certifies that they have read and hereby recommend for acceptance by The Nelson Mandela African Institution of Science and Technology a dissertation entitled: "*The Hydrochemical Evolution and Water Balance of the Emakat Lake in the Northern Crater Highland of Tanzania",* in partial fulfillment of the requirement for the degree of Master's in Hydrology and Water Resources Engineering of the Nelson Mandela African Institution of Science and Technology.

Prof. Hans Charles Komakech

Dr. Ceven Shemsanga

ACKNOWLEDGEMENTS

First, I would like to express my sincere gratitude to the Almighty God for His endless love and mercies that had made me pursue my research while healthy. It is His grace that made me accomplish my targets, and without Him, there is nothing that can be accomplished.

Secondly, my sincere gratitude goes to my supervisors Prof. Hans Komakech and Dr. Ceven Shemsanga for their quick acceptance of being my supervisors just after the death of my late supervisor Prof. Alfred Muzuka. Their tireless efforts of instructing, advising, improving, and ensuring that this work met the required research standards have greatly made me work hard and complete my dissertation.

Thirdly, I would like to acknowledge the Water Infrastructure and Sustainable Energy Futures (WISE-Futures) for funding and providing an opportunity to pursue my studies and research. Through this funding, the WISE futures has put a mark that can never be forgotten since, without this, I would have never pursued my studies and research.

My special appreciation goes to the Nelson Mandela African Institution of Science and Technology (NM-AIST) and its community, specifically to the School of Materials, Energy, Water, and Environmental Sciences (MEWES) for assistance and directives which have contributed much to the research. Special thanks to Prof. Revocatus Machunda, Dr. Judge Eliaman Laltaika, Prof. Kelvin Mtei, Prof. Jande Chande, Mr. Justine Lwekoramu, Ms. Theresia Urio, Dr. Grite Nelson and Dr. Anna Msigwa. My sincere gratitude goes to my research team which assisted me in data collection at Emakat Lake and its surroundings, namely: Mr. Deogratias Kabengo, Mr. Steven Solomon, Mr. Boniphace Machele, and the Eliaman Laltaika Family for hosting us at their home when we were conducting our sampling. Also, the Ngorongoro Conservation Area Authority (NCAA) for granting permission to conduct research and granting security.

Lastly, my sincere gratitude goes to my family; my wife Ms. Editruda Fausitine, our daughters; Secilia and Mercy and our son; Harris for their love and benevolence, and my fellow students Ms. Rosette Nyiranziza, Mr. Mohamed Mwabumba, Ms. Rosemary Kavishe, Mr. Paulo Sanka, and Ms. Mercy Kundu for their help during my studies.

May God bless you all.

Thank you

DEDICATION

I dedicate this work to my lovely family; my lovely wife Ms. Editruda Fausitine, my two daughters; Cesilia and Mercy; our son; Harris and to my parents Lucas and Justina for their encouragement and trust in me.

TABLE OF CONTENTS

ABSTRACT i

DECLARATION ii

COPYRIGHT iii

CERTIFICATION iv

ACKNOWLEDGEMENTS v

DEDICATION vi

TABLE OF CONTENTS vii

LIST OF TABLES x

LIST OF FIGURES xii

LIST OF ABBREVIATIONS AND SYMBOLS xiv

CHAPTER ONE 1

INTRODUCTION 1

1.1 Background of the Problem 1

1.2 Statement of the Problem 2

1.3 Rationale of the Study 3

1.4 Research Objectives 3

1.4.1 General Objective 3

1.4.2 Specific Objectives 4

1.5 Research Questions 4

1.6 Significance of the Study 4

1.7 Delineation of the Study 4

CHAPTER TWO 5

LITERATURE REVIEW 5

2.1 Overview of the Empakaai Crater 5

2.2 Hydrochemical Evolution of Crater Lakes 6

2.3 Lake Water Balance 7
2.3.1 Water Balance for Closed and Ungauged Lake 8
2.3.2 Lake Water Balance in Tanzania 9
2.4 Models and Theories 10
2.4.1 Runoff Estimations by Curve Number Model 10
2.4.2 The DeBruin–Keijman Model of Evaporation 14
2.4.3 The Craig and Gordon Evaporation Model 17
2.4.4 Lake-Groundwater Flow 21
CHAPTER THREE 23
MATERIALS AND METHODS 23
3.1 Study Area 23
3.1.1 Geographical Location 23
3.1.2 Climatic Condition 24
3.1.3 Land use 24
3.1.4 Geomorphology and Drainage 24
3.1.5 Geology and Geochemistry 25
3.2 Sampling and Analysis 27
3.2.1 Water Sampling and Analysis for Hydrochemical Parameters 27
3.2.2 Rocks Sampling and Analysis 28
3.2.3 Geospatial and Statistical Analysis of the Results 29
3.3 The Water Balance Estimation of Emakat Lake 29
3.3.1 Lake Volume and Volume Change 29
3.3.2 Rainfall 30
3.3.3 Runoff 31
3.3.4 Evaporation over Emakat Lake 32
CHAPTER FOUR 33

RESULTS AND DISCUSSION 33
4.1 Hydrochemistry of Empakaai Crater 33
4.1.1 Hydro-Chemical Characteristics 33
4.1.2 Hydrochemical Evolution of Emakat Lake 36
4.1.3 Geological Contribution to the Hydrochemical Evolution 39
4.1.4 Solute Sources in Emakat Lake 41
4.2 Water balance of Emakat Lake 49
4.2.1 Water Balance Parameters Estimations 49
4.2.2 Isotopic characteristics 60
4.2.3 Water Balance Parameters from other Lakes in the Vicinity 64
4.2.4 Water Balance Estimtions 66
CHAPTER FIVE 67
CONCLUSION AND RECOMMENDATIONS 67
5.1 Conclusions 67
5.2 Recommendations 68
REFERENCES 70
RESEARCH OUTPUTS 84

LIST OF TABLES

Table 1: Landcover classification and the respective hydrological condition 11

Table 2: The soil classifications with their respective runoff potential and infiltration rate characteristics 12

Table 3: The slope classification based on their respective percentage and runoff potentials 12

Table 4: The Hydrologic Soil Groups (HSG) with their respective infiltration rate and runoff potential 12

Table 5: The Antecedent Runoff condition for America and the modified for East Africa 13

Table 6: The slope classification criteria for the Empakaai Crater Catchment 32

Table 7: Location of sampling points and physical parameters of water samples from Emakat Lake and the associated springs 34

Table 8: Chemical parameters for Emakat Lake and the associated springs 35

Table 9: The dominant geochemical phases of the hosting geological formation as per XRD results 40

Table 10: The ionic ratio of Na/Cl can aid in identifying the source of Na and Cl 42

Table 11: The correlation coefficients of chemical constituents for Emakat Lake and the associated springs 43

Table 12: Saturation indices of Emakat Lake and associated springs by which positive values indicate super-saturation, whereas negative values reflect sub-saturation 47

Table 13: The data performance for validation of the CHIRPS data with three stations: Monduli, Nainokanoka, and Ngorongoro HQ stations 51

Table 14: Analysis results for the soil sample collected at Empakaai Crater 53

Table 15: The summary of the hydrological soil-cover complex table corresponding to the hydrological characteristics of Empakaai catchment 56

Table 16: The weighted curve number calculation from the hydrological soil-cover complex 57

Table 17: The monthly rainfall of Empakaai Crater obtained as an average of six CHIRPS point grids for the time series of 2006 to 2018 with their respective monthly runoff obtained through the curve number method 58

Table 18: Parameters for evaporation computation by D-K Model..... 59

Table 19: The isotopic composition of Emakat Lake and the associated springs..... 61

Table 20: The rainfall and evaporation amount from Manyara, Duluti and Babati Lakes as compared to Lake Emakat..... 65

Table 21. The summary of the isotopic mass balance for estimation of the groundwater flow 66

LIST OF FIGURES

Figure 1: The schematic presentation of the Craig-Gordon Model (Horita *et al.,* 2008) ..19

Figure 2: (i) The Tanzania map showing the location of the study area (ii) The Northern Crater Highlands map showing the Empakaai Crater (iii) The Empakaai Crater map showing the sampling locations.....23

Figure 3: The Cross Section showing the vertical representation of the major lithological units and structures along the line AB of the geological map in Fig. 2 (Guest *et al.,* 1961).....25

Figure 4: The Cross Section showing the vertical representation of the major lithological units and structures along the line CD of the geological map (Guest *et al.,* 1961) 26

Figure 5: Schoeller plot showing the solute concentration comparison for Emakat Lake and the associated springs 37

Figure 6: (A) Piper diagram showing the main hydrochemical characteristics of the Emakat Lake and associated springs (B) Chadha plot (Chadha, 1999) (C) Chloro-Alkaline indices (CAI-1 and CAI-2)plot (Liu *et al.,* 2020), and Gibbs plots (D) TDS versus $Cl/(Cl+HCO_3)$ and (E) TDS versus Na/(Na+Ca) (Gibbs, 1970) 38

Figure 7: The graphical representation of the chemical characteristics for the springs associated with Emakat Lake.....44

Figure 8: Major solute concentration of Emakat Lake plotted against Cl, a conservative ion over the evaporative.....46

Figure 9: (A) Lakes classification based on the nature of their neutralization source (B) Assessment of cation source based on the comparison of pH and total cation of the Emakat Lake 49

Figure 10: The bar charts for the trend analysis test of rainfall for ground collected and the CHIRPS data; (a) Ngorongoro HQ for 2013 to 2018 (b)Nainokanoka for 2006, 2007, 2013, 2014, 2017, and 2018 (c) Monduli for 2012 to 2016 50

Figure 11: The graphs of the coefficient of determination (R2) test of the ground collected data against the CHIRPS data: (a) Monthly test at Ngorongoro HQ for 2013-2018; (b) Monthly test at Nainokanoka for 2006, 2007, 2013, 2014, 2016 and 2018; (c)

Monthly test at Monduli for 2012-2016; (d) Average monthly test at Ngorongoro HQ for 2013-2018; (e) Average monthly test at Nainokanoka for 2006, 2007, 2013, 2014, 2016; and 2018 (f) Average monthly test at Monduli for 2012-2016 52

Figure 12: The LU/LC Map based on vegetation distribution 53

Figure 13: The slope classification map obtained from DEM for the Empakaai Crater 54

Figure 14: The map showing the hydrologic soil groups (HSG) classification 55

Figure 15: The map of the Empakaai Crater Catchment showing the three hydrological soil cover complex 55

Figure 16: The graph showing the isotopic variation of δ^2H Vs $\delta^{18}O$ along the Global (GMWL) and Tanzania (TML) Meteoric lines 60

Figure 17: Variation of δ^2H and $\delta^{18}O$ with major ions for Emakat Lake and associated springs: (a) $\delta^{18}O$ Vs EC for Emakat Lake; (b) $\delta^{18}O$ Vs EC for Emakat Lake; (c) $\delta^{18}O$ Vs EC for Emakat Lake and springs; (d) $\delta^{18}O$ Vs d-excess; (e) $\delta^{18}O$ Vs NO_3^- (f); Cl^- Vs δ^2H (g) δ^2H Vs d-excess for Emakat Lake (h)) δ^2H Vs d-excess for springs 63

Figure 18: The graph showing Rainfall and Evaporation change with altitude 65

LIST OF ABBREVIATIONS AND SYMBOLS

A	Atmosphere
AMC	Antecedent Moisture Condition
AMCSD	American Mineralogist Crystal Structure Database
ANN	Artificial Neural Network
ARC	Antecedent Runoff Condition
B	Turbulent Flow
C-G	Craig-Gordon Model
CHIRPS	Climate Hazards Group Infrared Precipitation with Station data
CN	Curve number
DEM	Digital elevation model
D-K	De Bruin–Keijman Model
DOY	Day of the year
dr	Inverse earth−sun relative distance
E	Evaporation
EC	Electrical conductivity
ESDAC	European Soil Data Centre
GIS	Geographical information system
GIUH	Geomorphological Instantaneous Unit Hydrograph
GMWL	Global meteoric water line
GPS	Global positioning system
G_{sc}	Solar constant
H	Relative humidity
HDPE	High-density polyethylene
HSG	Hydrological soil group
i	Heavy isotopes
I	Initial rainfall infiltration
ITCZ	Intertropical Convergence Zone
J	Julian day
K	Potential Maximum Retention after runoff
L	Lamina liquid phase
LU/LC	Land use/land cover
M	Laminar vapour phase

MAMSL	Meters above mean sea level
MNRT	Ministry of Natural Resources Tanzania
NCAA	Ngorongoro Conservation Area Authority
NSE	Nash Sutcliffe model efficiency coefficient
ORP	Oxidation reduction potential
P	Rainfall/Precipitation
pH	Power of hydrogen
PHREEQC	pH, redox, equilibrium, program written in C
Q_t	Heat storage changes
R	Runoff
Ra	Extra-terrestrial radiation
RMSE	Root mean square error
Rn	Net radiation
Rs	Solar radiation
S	Liquid/Interface boundary
SCS	Soil Conservation Services
T	Temperature (T)
TDS	Total dissolved solids
TMA	Tanzania meteorological agency
TMWL	Tanzania meteoric water line
To	Surface Temperature
UBCWM	University of British Columbia Watershed Model
UNESCO	United Nations Educational, Scientific and Cultural Organization
URT	United Republic of Tanzania
USDA	United States Department of Agriculture
USGS	United States Geological Survey
V	Vapour/Interface boundary
XRD	X-ray diffraction
Ze	Elevation of the station
α	Fractionation factor
γ	Psychometric constant
δ	Isotopic composition
ρ	Transport resistance
ρw	Density of water

φ	Latitude
ω_s	Sunset hour angle in radians
λ	Latent heat of vaporization
$\frac{\mathrm{d}}{\mathrm{dt}}(\mathrm{s})$	Storage change over time
ε_k	Kinetic isotope fractionation factor
ε	Effective enrichment factor
$\propto$	Albedo
I_g	Subsurface inflows
O_g	Subsurface outflows
I_s	Surface inflow
O_s	Surface outflows
Δ	Slope of saturation

CHAPTER ONE

INTRODUCTION

1.1 Background of the Problem

Lakes contribute about 90% of the world's fresh surface water (Karmakar & Musthafa, 2020). Their existence results from the interaction of hydrological components such as precipitation, evaporation, surface, and groundwater flows, which ensure adequate water supply (Chen *et al.,* 2020). However, the factors mentioned above result in rapid population growth around the lakes, which, coupled with natural factors such as climate change, have resulted in increased siltation, acidification, toxic contamination, and eutrophication of lakes, thus affecting their water quality and quantity (Karmakar & Musthafa, 2020). Lakes influence the regional hydrological characteristics while providing a variety of economic services and hence promoting economic growth and well-being in their vicinity and downstream (Avery & Tebbs, 2018; Karmakar & Musthafa, 2020). Understanding the lake's hydrological system is crucial to ensure the sustainable utilization and effective management of lakes and other resources available in their catchments (Karmakar & Musthafa, 2020).

The hydrological water balance is a widely used technique in the world to understand the interaction of components of the hydrological cycle, including lakes and their catchments (Duan *et al.,* 2018; Kansoh *et al.,* 2020; Karmakar & Musthafa, 2020). It utilizes the mass conservation principle that gives the input-output relationship of the hydrologic components in an area at a given time, balanced by the change of storage (Kansoh *et al.,* 2020). In lakes, water balance provides the quantitative assessment of theoretical and practical hydrological problems such as change predictions in hydrological systems, rational use, distribution of water in time and space, and determination of unknown hydrological components through the analysis of known components (Avery & Tebbs, 2018; Zhang *et al.,* 2021).

Hutchinson (1957) classified lakes into 11 main types, one being the crater lakes formed when water permanently occupies a volcanic feature such as a crater or a caldera and may remain active or inactive in influencing the water chemistry (Rouwet *et al.,* 2015; Kalacheva *et al.,* 2022). However, the crater lake chemistry is influenced mainly by the geology of the lake catchment, the climatic conditions of the area, and the extent of heat and gas inputs from volcanic activities (Kalacheva *et al.,* 2022). The water balance of the crater lakes depends mainly on the nature of their hydrological system. For instance, the open lake hydrological system is characterized by surface inflow and outflow. In contrast, the closed lake hydrological

system is characterized by a lack of surface inflow and outflow, with evaporation and seepage playing a significant role in this system (Avery & Tebbs, 2018; Kansoh *et al.,* 2020; Zhang *et al.,* 2021).

Emakat Lake is a closed crater lake occupying part of the Empakaai Crater, an extinct and intact crater of the Elanairobi Volcano of the Northern Crater Highlands (Ryner *et al.,* 2008). According to Muzuka *et al.* (2004) and Deacampo and Renaut (2016), the lake is alkaline, characterized by high pH and dominated by Na^+ and K^+ ions originating from the weathering of bedrock, hydrothermal reactions, and rainfall. Ecological studies (Frame *et al.,* 1975; Childress *et al.,* 2007) and paleoclimate studies (Muzuka *et al.,* 2004; Ryner *et al.,* 2006; Ryner, 2007; Ryner *et al.,* 2007; Ryner *et al.,* 2008) undertaken on the Empakaai Crater, reveal the lake's sources are the few streams flowing from the inner crater rims, direct precipitation, and groundwater. Nevertheless, Emakat Lake is important in paleoclimate studies because it is a closed lake in the ecologically-sensitive area of the Ngorongoro Conservation Area Authority (NCAA) (Ryner, 2007). Despite the importance of Emakat Lake, its hydrological component still needs to be discovered. Important rivers such as Engaruka and Egaresero support the population on the foot of the crater and downstream originate from the springs on the crater's outer walls. Their interrelationship with Emakat Lake, however, also needs to be revised. Therefore, the current study aimed to unveil the hydrological aspect of Emakat Lake with a major concentration on its hydrochemical evolution, water balance, and its interrelationship with the water sources on the outer crater rims. Since the lake is ungauged, the study utilized the environmental isotopes ($\delta^{18}O$ and $\delta^{2}H$) through the isotope mass balance approach to compute the water balance (Gibson *et al.,* 2018).

1.2 Statement of the Problem

The hydrological components of lakes provide insights for proper conservation and protection plans to ensure their sustainability and that of their watersheds (Mohajerani *et al.,* 2021). Due to limited data, the hydrology of most inland lakes, including Tanzanian lakes, is poorly understood. Since most lakes are poorly gauged or ungauged and lack piezometric monitoring data (Deus *et al.,* 2013), their hydrological computations involve extensive estimations of most parameters (Mbanguka *et al.,* 2016). This is the case of Emakat Lake since it is ungauged and lacks hydrometeorological data despite being located on the highlands, which are considered to be potential recharge areas and water resources for agriculture in the outer slopes of the crater (Boone *et al.,* 2006; Westerberg *et al.,* 2010). In the past 20 years, the population in the NCAA, including the Empakaai Crater, has increased five times the population of the 1950s,

which goes parallel with the increase in livestock population, particularly cattle, sheep, and goats (Lyimo *et al.,* 2020). The population increase may result in reduced water recharge from rainfall, increased runoff due to changes in land use/cover, overexploitation, and changes in the precipitation regime, affecting the downstream users (Ávila-Carrasco *et al.,* 2023).

According to the United Republic of Tanzania (URT) (2022), about 47 130 people depend on the Engaruka and Engaresero Rivers, which originate from the springs emerging from the outer rims of the Empakaai Crater, but their hydrological interrelationship remains unstudied. Therefore, this study aimed to assess the hydrology of Emakat Lake, with a major focus on the lake's hydrochemical evolution and quantification of groundwater contribution to the lake, together with their interrelationship to the water sources on the outer crater rims.

1.3 Rationale of the Study

The fertility of the slopes of the Empakaai crater attracted people to reside in the area and depend on groundwater for domestic uses and cattle watering (Boone *et al.,* 2006). Due to its beautiful scenery and uniqueness, the Empakaai Crater is promoted as a tourist attraction site and contributes to the economy of the residents and the income of the NCAA (Sitchler & Jung, 2017).

The Crater highlands and Empakaai Crater Lake are considered to be potential recharge areas that sustain rich and diverse ecosystems (Ryner *et al.,* 2008) as well as the water resources for agriculture in the outer slopes of the crater (Boone *et al.,* 2006; Westerberg *et al.,* 2010). However, the increasing population in the conservation area, including the Empakaai Crater, which has increased the number of cattle, continue to threaten the sustainability of Emakat Lake (Ávila-Carrasco *et al.,* 2023). This challenge calls for an urgent study on the hydrodynamics of the lake and its catchment to know its sustainability in the wake of its challenges.

1.4 Research Objectives

1.4.1 General Objective

To assess the hydrochemical evolution and water balance of the Emakat Lake of the Crater Highland in Northern Tanzania.

1.4.2 Specific Objectives

(i) To assess the influencing factors for the hydrochemical evolution of the Empakaai Crater.

(ii) To investigate the water balance and relative contribution of subsurface flow to the Emakat lake.

1.5 Research Questions

(i) What are the sources and mechanisms of dissolved ions in the Empakaai Crater, and how do they evolve over time?

(ii) What are the key components of water balance of the Empakaai Crater hydrological system?

1.6 Significance of the Study

This work provides a framework for informed decision-making, ecological conservation, wildlife management, sustainable tourism practices, and water resource planning within the Empakaai Crater by the NCAA. Since the crater is a source of the main rivers of Engaruka and Engaresero, which sustain the ecosystem and population downstream, the study will provide crucial information for effective decision-making, resource planning, and conservation efforts to meet the water-related challenges and promote the well-being of the communities relying on the water resources originating from the Empakaai Crater.

1.7 Delineation of the Study

The hydrochemical evolution and water balance of Empakai Crater are crucial for water resource management, biodiversity conservation, understanding ecosystem functioning, assessing climate change impacts and supporting local communities, which contributes to thesustainable management and preservation of the Crate's unique ecplogical and cultural heritage. Thia study unveils the hydrological aspect of Emakata Lake with a Major concetration on its hydrochemical evolution, water balance, and its interrelation with the water sourses on the outer Crater' rims. It inegrates the stable isotopes approach and the remote sensing data to estimate the water balance as the Emakat Lake located in the Crater is ungauged.

CHAPTER TWO

LITERATURE REVIEW

2.1 Overview of the Empakaai Crater

The Empakaai Crater is a volcanic caldera in northern Tanzania's Ngorongoro Conservation Area. It is part of the more extensive East African Rift System, known for its geologic activity and rich biodiversity (Ryner *et al.,* 2008). According to Muzuka (2004) and Deacampo and Renaut (2016), the lake is alkaline, characterized by high pH and dominated by Na^+ and K^+ ions originating from bedrock weathering, hydrothermal reactions, and rainfall. The crater is located at the highest point of the Northern Volcanic Crater Highlands receiving rainfall ranging from 600 to 1000 mm with spatial variation from the western to eastern slopes, respectively. However, the topographical enhancement can result in as higher as 1500 mm of annual rainfall (Ryner *et al.,* 2006, 2008). The crater area is about 35 km^2, surrounded by steep walls and contains a central lake, Lake Empakaai, which covers an area of about 8.15 km^2.

Several studies have been undertaken on the Empakaai Crater in geology, paleoenvironment, biodiversity and conservation, volcanic hazards, and anthropological and archaeological studies. The geological studies conducted in Empakaai Crater are based on understanding the formation and structure of the Empakaai Crater. These studies analyzed the volcanic history, tectonic processes, and the relationship between the crater and the surrounding landscape. According to Mollel *et al.* (2008), the formation of the Empakaai Crater is associated with the rifting processes of the Eastern African Rift Valley. The first rifting process, ca. 20 Ma, resulted in fissures and faults, which were then transformed into volcanic centres. The eruption centres formed volcanic summits (Empakaai, Olmot, Loolmasin, Ngorongoro, Lemagrut, Sadiman, and Oldean), which were growing while merging and then formed the Crater Highlands at ca. 2 Ma (Scoon, 2018).

The second rifting process took place ca. 1.26 Ma and formed the current north-south fault in the eastern boundary of the Crater Highland. It created some other fissures crossing the Empakaai, emptying the magma chamber beneath as a result of the summit's collapse and hence the Empakaai Crater formed (Żaba & Gaidzik, 2011). The crater was then occupied with water to form Emakat Lake. The other volcanic mountains, such as Kerimasi and Oldoinyo Lengai, formed later after Ca. 1 Ma to the present.

The paleoenvironment studies were conducted in the Empakaai Crater to reconstruct the past climate and ecosystem dynamics through analysis of sediment cores obtained from the Emakat Lake and the surrounding areas, pollen analysis, diatom, geochemical proxies and radiocarbon dating (Muzuka, 2004; Ryner *et al.,* 2008; Ryner, 2007). Studies concluded that the area has been experiencing prolonged dry and wet seasons where the recurring lake level fluctuation has been experienced in the last 1200 years, accompanied by increased human activities, of which all these events are preserved in the Empakaai Crater.

Ecological studies in the Empakaai Crater focus on investigating the interactions between organisms and their environment, as well as the overall functioning and dynamics of the ecosystem. The studies covered ecosystem services within the crater, habitat preferences and resource utilization patterns of various plant and animal species, and key species' population dynamics (Childress *et al.,* 2007).

The conducted studies in the Empakaai Crater did not cover the hydrological investigation aspect. Instead, they relied on field experience where it was concluded that water sources for the Emakat Lake are the few streams flowing from the inner crater rims, direct precipitation, and groundwater (Ryner *et al.,* 2008). Understanding the hydrological component of the hydrochemical evolution and water balance of the Empakaai Crater is crucial as it is the recharge zone at the highest point receiving high rainfall. Springs from the outer crater rims drain the surrounding plains and form major rivers such as Engarasero and Engaruka Rivers, sustaining the rich and diverse ecosystem as well as the water resources for agriculture in the outer slope of the crater and downstream (Boone & BurnSilver, 2002; Westerberg *et al.,* 2010).

2.2 Hydrochemical Evolution of Crater Lakes

Crater lakes are volcanic lakes associated with polygenetic volcanic systems involving explosive eruptive processes that create a deep and large depression that may hold water due to climatic, local hydrogeology, and permanent degassing (Kalacheva *et al.,* 2022). The hydrochemistry of the crater lakes is influenced mainly by local geology, the climatic condition of the area, and the extent of the heat and gas inputs from the volcanic activities of the crater (Chikita *et al.,* 2022). Lakes on active craters are characterized by low pH, sulfur-rich chemistry, elevated concentration of dissolved rock-forming elements, high temperature, and conductivity, while those on inactive craters are dominated by bicarbonate together with high pH and low conductivity (Rouwet *et al.,* 2015; Chikita *et al.,* 2022).

The hydrochemical evolution of crater lakes starts from the inflow of the lakes through the acquisition of solutes from reactions with the hosting geology (local or regional) and inputs from the atmosphere (Kalacheva *et al.,* 2022). Usually, the solute composition reflects the dominant rock type of the catchment area regarding its distribution, the nature of the reaction with natural water, and the resulting solute types, which are then released into lakes' inflows and distributed in them (Deocampo, 2018). The hydrothermal input also plays a significant role in the closed lake evolution, hydrological process and setting influence post-lake hydrochemical evolution processes such as water mixing, reaction, and resident time (Deocampo, 2018).

The crater lakes in East Africa are associated with the Rift Valley activity, and their hydrochemistry is closely related to hydrology, climate, and geology (Deacampo & Renaut, 2016). Most of these lakes are alkaline, with solutes originating from direct precipitation, weathering of the hosting rocks, and hydrothermal fluids (Deacampo & Renaut, 2016). The solute concentration of crater lakes in East Africa reflects the normal weathering impact of the alkaline feldspathoids of volcanic formations of the East African Rift System (Deocampo, 2004). The Rift Rivers and Springs solute composition has higher Na^+ and K^+ than Ca^{2+} and Mg^{2+}. This condition reflects the dissolution reaction of nepheline, which involves the uptake of H+ ions and the subsequent release of Na^+ and K^+ into the solution while forming zeolite as a secondary mineral (Greenwood, 2014).

Concerning the relative solubility, Mg^{2+} and Ca^{2+} act as non-conservative ions since they are removed from the solution through precipitation as clay and carbonate minerals (Deocampo, 2018). Atmospheric input also contributes to the hydrochemical evolution of the East African crater lakes since it is the primary source of CO_2 which dissolves in rainwater to form carbonic acid, which generally dissociates into HCO3- and H- (Schagerl, 2016). Besides, rainfall is also considered the source of all Cl^- in East Africa (Schagerl, 2016). The higher CO_3^- in the East African crater lakes is also closely linked to the weathering of carbonatite from the Oldoinyo Lengai that forms soluble calcite as the secondary product (Schagerl, 2016).

2.3 Lake Water Balance

The water balance in lakes is computed using the water balance equation, which was developed based on the principle of mass conservation, which states that for any arbitrary volume and during any period, the difference between total input and output will be balanced by the change of water storage within the volume (Duan *et al.,* 2018; Kansoh *et al.,* 2020; Karmakar &

Musthafa, 2020). According to Sokolov and Chapman (1974), the water balance equation can be expressed in terms of the difference in the total inflows and the outflow balanced by the change of storage (Equation 1). The inflows include precipitation such as rainfall (P), Runoff (R), and surface and subsurface inflows (I_s and I_g), while the outflows include evaporation (E) and surface and subsurface outflows (O_s and O_g) (Mohajerani *et al.,* 2021).

$$\frac{d}{dt}(S) = P + R + I_s + I_g - E - O_s - O_g \quad (1)$$

Whereby:

P =rainfall , R = Runoff, and inflows I_s surface inflows, I_g = subsurface inflows

E = evaporation, O_s = surface outflow and O_g = subsurface outflows

2.3.1 Water Balance for Closed and Ungauged Lake

The simple hydrology of the closed crater lake provides an easy way of computing water balance since a significant portion of its catchment is located in the crater's inner walls (Mohajerani *et al.,* 2021). The water balance in such lakes largely depends on the precipitation, subsurface groundwater contribution and springs and runoff from the inner crater walls as inflows and evaporation, evapotranspiration, and seepage as outflows (Rouwet *et al.,* 2015). With this assumption, Equation 1 can be modified by neglecting the surface inflow and outflow as in Equation 2.

$$\frac{d}{dt}(S) = P + R + I_g - E - O_g \quad (2)$$

Among all lake water balance components, determining groundwater inflow/outflow components is the most complicated during water balance computation (Dinka, 2020). However, conventional methods can be used by installing some piezometers, which despite being very expensive, only give the absolute results of the interaction (Mohajerani *et al.,* 2021). The stable isotopes of water (^2H and ^{18}O) are naturally occurring tracers of water that are used to compute the inflow-outflow of water to lakes through the isotopic mass-balance approach system (Gibson *et al.,* 2018). The isotopic mass-balance method requires the determination of the isotopic composition of all components of the hydrological balance such as the lake water

(δ_L), precipitation (δ_P), evaporation (δ_E), groundwater (δ_g) and surface-water inflows and outflows (Özaydin *et al.,* 2001). Therefore, the isotopic mass-balance equation for the closed lake can be written as Equation 3 from Equation 2 by adding the isotopic content on the respective component of the lake water balance.

$$\frac{d}{dt}(\delta_L S) = \delta_p P + \delta_p R + \delta_g I_g - \delta_E E - \delta_L O_g \quad (3)$$

The isotopic composition of the isotopic mass-balance components such as a lake, groundwater, precipitation, and runoff can be obtained through laboratory analysis of collected field samples. Evaporation, being one of the complex parameters to estimate among water-balance parameters, can be estimated using the Craig-Gordon (C-G) Evaporation Model (Craig & Gordon, 1965) that utilizes the mentioned data to estimate the isotopic composition of evaporation on an open water body by evaluating changes in the stable isotopes of water (^{2}H and ^{18}O) in its different phases, namely liquid, vapour and the transition phase of the two phases (Gibson *et al.,* 2016).

2.3.2 Lake Water Balance in Tanzania

Most of the water balances for lakes in Tanzania are based on the utilization of the traditional water balance computation method (Branchu & Bergonzini, 2004; Tate *et al.,* 2004; Kumambala & Ervine, 2010; Mbanguka *et al.,* 2016). These methods rely on field measurements and calculations based on hydrological principles. They are simple to use as they use straightforward measurement techniques and calculations that are easy to understand and implement and involve direct field measurements hence allowing site-specific considerations (Mohajerani *et al.,* 2021). However, they have some spatial and temporal coverage limitations due to often relying on point measurements, the potential for measurement errors from calibration issues, human error, or equipment limitations and the inability to account for future scenarios (Mbanguka *et al.,* 2016). Similarly, estimating groundwater contribution using the traditional method requires an extensive and expensive piezometer network (Krabbenhoft *et al.,* 1990; Özaydin *et al.,* 2001). Since most Tanzanian lakes are poorly gauged or ungauged and lack piezometric monitoring data (Deus *et al.,* 2013), their water balance computations involve extensive estimations of most parameters (Mbanguka *et al.,* 2016).

Stable isotopes of water are widely used in hydrological studies, including water balance, due to their conservative nature providing unique information about water sources, movement, processes, and interactions within a hydrological system (Mohajerani *et al.,* 2021). Its application has grown recently due to its simplicity, cost-efficiency and ease of use, as one-time sampling can provide accurate water balance of a hydrological system (Gibson *et al.,* 2018). Recent studies utilizing stable isotopes in water balance include Masse-Dufresne et al. (2021), who utilized the stable isotopes to quantify the floodwater impact on lake water balance. Gibson *et al.* (2018) employed the stable isotope to survey and quantify the water balance of 560 lakes with one-time data collection, which proved effective. Akiyama *et al.* (2018) used the stable isotope water balance to monitor the groundwater recharge in the Hyper-Arid Gogi Desert.

In Tanzania, stable isotopes are also used in hydrological studies, including water balance. Atomic *et al.* (1970) coupled the stable isotopes ($\delta^{18}O$ and $\delta^{2}H$) and the radioactive isotope ($\delta^{3}H$) to evaluate the water balance of Lake Chala as a decision-making tool regarding the lake's feasibility of supplying irrigation water. Other earlier stable-isotope applications include the one conducted at Makutupola and Hombolo basins which used the $\delta^{18}O$ and $\delta^{2}H$ to assess the source of aquifer recharge and nitrates in Dodoma (Nkotagu, 1996a, 1996b).

The most recent applications of stable isotopes are those conducted on the Arusha aquifer that involved groundwater dating and establishment of the recharge mechanism, coupled with the $\delta^{3}H$ and the stable isotopes of water ($\delta^{18}O$ and $\delta^{2}H$). Chacha *et al.* (2018) and Mduma *et al.* (2016) utilized the stable isotopes to assess the water balance and the dominant components sustaining Lake Duluti. Since the Emakat Lake is a closed lake and ungauged lacking ground collected data for the interval of time, therefore a one-time data collection approach coupled with the stable isotope mass balance approach is a proper water balance method for the lake.

2.4 Models and Theories

2.4.1 Runoff Estimations by Curve Number Model

Estimating runoff amount and rate for ungauged catchment is problematic since most conventional methods require field-collected hydrological and meteorological data (Askar, 2013). Several methods of estimation of runoff for ungauged catchment exist, such as the University of British Columbia Watershed Model (UBCWM), Artificial Neural Network (ANN), Soil Conservation Services Curve Number SCS-CN model, and Geomorphological Instantaneous Unit Hydrograph (GIUH). However, the SCS-CN model is widely used because

it combines the catchment characteristics and climatic factors in one component known as the curve number (CN) (Askar, 2013; Satheeshkumar *et al.,* 2017). Although the method is designed for a single storm event, it can be scaled to find average annual runoff values.

The method is efficient in small catchment areas, and its efficiency increases when coupled with the geographical information system (GIS) to prepare input data. Although the initial idea for developing this method was for runoff estimation for a single storm event, it is now utilized for annual runoff estimations (Askar, 2013). The method requires rainfall data and CN as input data. The CN for ungauged catchments is determined based on the hydrologic soil group, land use, and hydrologic condition of the respective catchment (Askar, 2013; Guswa *et al.,* 2018). Since the performance of the SCS-CN model differs depending on land use, customization should be done to reflect the environment under study (Parasuraman *et al.,* 2007).

(i) Land Use-Land Cover Map

The Land Use-Land Cover (LU/LC) Map is used to evaluate the effect of the land cover on runoff giving poor, fair, and good hydrological conditions (Table 1) (Askar, 2013). The determination of the land cover can be through satellite images, aerial photographs, land use maps, and direct mapping from the field (USDA, 1975).

Table 1: Landcover classification and the respective hydrological condition

No	Vegetation Cover	Hydrological Condition
1	< 30%	Poor
2	30 - 70%	Fair
3	> 70%	Good

Askar (2013)

(ii) Hydrologic Soil Groups

The Hydrological Soil Groups (HSG) refer to soil classification based on the runoff potential determined by the soil infiltration and saturation rate when the soil is not covered (Askar, 2013; Ross *et al.,* 2018; USDA, 1975). The classification considers soil texture class, bedrock depth, and groundwater table (Ross *et al.,* 2018). Soils with a high percentage of fine clay have a high runoff potential compared to those with a high percentage of coarse sand. The reason behind this is that the course material has many pore spaces, hence, high permeability and easy infiltration of water, whereas fine clay tends to expand when wet and block pore spaces, thus reducing permeability and causing low infiltration (Table 2) (Rezaei *et al.,* 2015).

Table 2: The soil classifications with their respective runoff potential and infiltration rate characteristics

No	Soil Texture	Infiltration Rate	Runoff Potential
1	Sand > 90% and Clay < 10%	High	Low
2	50% < Sand < 90% and 10% < Clay < 20%	Moderately-high	Moderately-low
3	Sand < 50% and 20% < Clay < 40%	Moderately-low	Moderately-high
4	Sand < 50% and Clay > 40%	Low	High

Ross *et al.* (2018)

Bedrock depth and groundwater table both determine the thickness of the unsaturated zone of the soil profile whereby, the shallower the depth of the unsaturated soil zone, the faster the rate of saturation, hence high runoff potential and vice-versa (Vereecken *et al.,* 2019). However, slope also plays a significant role in the classification of soil since it controls soil moisture, soil type, groundwater flow, and soil movement, hence, an increase in slope decreases soil thickness, and subsequently increases runoff potential (Table 3) (Fazlollahi *et al.,* 2016; Rezaei *et al.,* 2015).

Table 3: The slope classification based on their respective percentage and runoff potentials

No	Slope Class	Percentage	Runoff Potential
1	Flat	0 - 3%	Very low
2	Undulating	3 - 8%	Low
3	Moderately-sloping	8 - 15%	Moderately-low
4	Hilly	15 - 30%	Moderate
5	Moderately-steep	30 - 45%	Moderate-high
6	Steep	45 - 65%	High
7	Very steep	> 65%	Very high

Pamela *et al.* (2018)

Therefore, soil falls under four HSG (A, B, C, and D) based on the infiltration rate and runoff potential (Table 4) (Askar, 2013; Satheeshkumar *et al.,* 2017; USDA, 1975).

Table 4: The Hydrologic Soil Groups (HSG) with their respective infiltration rate and runoff potential

Hydrologic Soil Group (HSG)	Infiltration Rate	Runoff Potential
HSG A	High	Low
HSG B	Moderately-high	Moderately-low
HSG C	Moderately-low	Moderately-high
HSG D	Low	High

USDA (1975), Askar (2013) and Satheeshkumar *et al.* (2017)

(iii) Curve Number Determination

The determination of CN for a specific hydrological unit involves the combination of the identified hydrological conditions due to the landcover of the area and the respective hydrological soil groups. The matrix of the hydrological condition and hydrological soil groups

also known as a hydrological soil-cover complex, established by the United States Department of Agriculture-Soil Conservation Services (USDA-SCS) gives the runoff CN of a specific hydrological unit (USDA, 1975).

(iv) Antecedent Runoff Condition

The Antecedent Runoff Condition (ARC), also known as Antecedent Moisture Condition (AMC) is the measure of the amount of moisture available in the soil before rainfall (Askar, 2013). The ARC is classified into three classes as AMC I, AMC II, and AMC III to represent dry, average, and wet soil conditions. The CN estimated under the hydrological soil-cover complex is under the average condition (AMC II) while AMC I and AMC III can be obtained through the modification of AMC II using Equations 4 for AMC I and Equation 5 for AMC III (Askar, 2013; Ritzema, 1994; Satheeshkumar *et al.,* 2017). The AMC values for the different classes for 5-day moisture content remaining after the previous rainfall was developed for America only, however Ritzema (1994) modified and established those which match the East African condition (Table 5).

Table 5: The Antecedent Runoff condition for America and the modified for East Africa

AMC Class	5 days Antecedent Rainfall in America		5 days Antecedent Rainfall in East Africa
	Dormant Season (mm)	Growing Season (mm)	
(i)	< 13	< 36	< 23
(ii)	13 - 28	36 - 53	23 - 40
(iii)	>28	>53	>40

Ritzema (1994)

$$AMCI = \frac{CNII}{(2.281 - 0.01281CNII)} \quad (4)$$

$$AMCIII = \frac{CNII}{(0.427 + 0.00573CNII)} \quad (5)$$

(v) Runoff Estimation

The runoff estimation by CN methods involves the combination of factors such as land cover, soil type, and ARC during CN determination (Ritzema, 1994). With precipitation data, the runoff is obtained by Equations 6, 7, and 8 while for a large catchment with more than one hydrological unit, the CN is obtained as a sum of CN for all hydrological units in the catchment as Equation 9.

$$R = \frac{(P - I)^2}{(P - I) + K} \quad (6)$$

Whereby, R = Runoff, P =Rainfall and I = Initial Rainfall infiltration, K = Potential Maximum Retention after runoff

But $I = 0.2K$

Then

$$R = \frac{(P - 0.2K)^2}{(P + 0.8K)} \quad (7)$$

However, according to Satheeshkumar *et al.* (2017), the Potential Maximum Retention after a runoff (S) can be obtained from Equation 8.

$$K = (\frac{24500}{CN}) - 254 \quad (8)$$

Whereby, CN = Curve Number and K = Potential Maximum Retention after runoff

Since the catchment covers an area with different hydrologic units, the weighted CN representing the whole catchment is obtained as the sum of the CN from every individual hydrologic unit of the catchment (Askar, 2013; Satheeshkumar *et al.,* 2017):

$$CN = \frac{\sum_1^n CN_n A_n}{A} \quad (9)$$

Whereby, CN = Weighted Curve Number of the catchment, CN_n = Curve Number of the n^{th} hydrologic unit, A_n = The area of the n^{th} hydrologic unit, A is the total area of the catchment.

2.4.2 The DeBruin–Keijman Model of Evaporation

The evaporation from open lakes can be estimated through various methods such as pan evaporation, mass balance, energy budget, mass transfer, equilibrium temperature, empirical

factors, and combination methods (Finch & Calver, 2008). Among these methods, the combination method, which amalgamates the energy budget and mass transfer methods, performs better in open-water evaporation estimates (Elsawwaf *et al.,* 2010; Rosenberry *et al.,* 2007). Various evaluations performed on the combination methods concluded that the DeBruin–Keijman (D-K), Penman, and Priestley–Taylor methods provide better estimates; however, in most cases, the D-K outperformed other methods (Duan & Bastiaanssen, 2017; Elsawwaf *et al.,* 2010; Rosenberry *et al.,* 2007; Winter *et al.,* 1995; YAO, 2009).

Also, the D-K method is relevant to ungauged lakes like Emakat Lake since it requires a few input data, which are mostly freely available online from satellite providers (Duan *et al.,* 2018). The estimation of the open lake by the D-K method requires the surface temperatures (To) and net radiation (Rn) among others as input data as shown in Equation 10.

$$E = \frac{\Delta(R_n - Q_t)}{0.85\Delta + 0.63\gamma} \times \frac{86.4}{\lambda \rho_w} \tag{10}$$

Whereby, E is the lake evaporation rate (mm/day), Δ is the slope of saturation (Equation 11) of vapour pressure-temperature curve at air temperature (k Pa/°C), its calculation requires average air temperature (T), λ is the latent heat of vaporization which is 2.45 MJ/ kg, and ρw the density of water (1000 kg/m).

$$\Delta = \frac{498 \times \left[0.6108 \times \exp\left(\frac{17.27 \times T}{T + 237.3} \right) \right]}{(T + 237.3)^2} \tag{11}$$

Whereby, γ is the Psychometric constant (k Pa/°C) computed from the elevation of the station (Ze) which is measured from the mean sea level gives the atmospheric pressure (P) and is given with Equations 12 and 13. Rn is the net radiation (W/m^2) and Q_t the water heat flux density at the water–atmosphere interface (W/m^2) also known as heat storage changes(Q_t).

$$\gamma = 0.665 \times 10^{-3} \times P \tag{12}$$

$$P = 101.3 \times \left(\frac{(293 - 0.0065 \times z_e}{293} \right)^{5.26} \quad (13)$$

The Rn can be computed from the slob's equation as in Equation 14 whereby albedo ($\propto$) and Rs can be obtained from online satellite services however a default value of 0.05 for α can be used (Duan & Bastiaanssen, 2015). The extra-terrestrial radiation (Ra) (W/m^2) is the theoretical parameter that is computed from latitude and day of the year (DOY) (Equation 15). The G_{sc} is the solar constant which is 0.082 MJ/m^2min, φ is the latitude in radians, dr is the inverse earth−sun relative distance given by Equation 16, δ is the solar declination in radians given by Equation 17, J is the DOY also known as Julian day where for monthly values is given as in Equation 18 and ω_s is the sunset hour angle in radians given as Equation 19.

$$R_n = (1 - \propto)R_s - 110\frac{R_s}{R_a} \quad (14)$$

$$R_a = 11.6 \times \frac{24 \times 60}{\pi} G_{sc} d_r (\omega_s \sin(\varphi)\sin(\delta) + \cos(\varphi)\cos(\delta)\sin(\omega_s)) \quad (15)$$

$$dr = 1 + 0.033\cos(\frac{2\pi J}{365}) \quad (16)$$

$$\delta = 0.4093\sin(2\pi\frac{J + 282}{365}) \quad (17)$$

$$J = 30.42 \times \text{Month} - 15.23 \quad (18)$$

$$\omega_s = \arccos(-\tan\delta) \quad (19)$$

The Q_t for the lake is an important component that is, however, neglected in some studies due to its complexity in its computations and lack of appropriate data but it can result in large errors especially in the computation of monthly evaporation values (Duan & Bastiaanssen, 2015). The hysteresis Equation 20 developed for the computation of the lake heat storage change as a function of net radiation can aid in the computations. The constants a, b, and c can be computed with the procedures explained by Duan and Bastiaanssen (2015).

$$Q_t = aR_n + b + c\frac{dR_n}{dt} \tag{20}$$

The function requires the monthly lake To and Rn computed from Rs. The range ($T_{O\text{-}Range}$), standard deviation ($T_{O\text{-}SDV}$), and mean ($T_{O\text{-}Mean}$), and the lake To change with time (ΔTo). Since the heat storage change (Q) is minimum and maximum when the lake To change (ΔTo) is minimum and maximum respectively, then the $Q_{t\text{-}min}$ is computed using Equation 21 while $Q_{t\text{-}max}$ is the opposite of the $Q_{t\text{-}min}$.

$$Q_{t-min} = -7.55T_{0-STD} - 71.47 \tag{21}$$

The Rn values of the respective months with minimum and maximum ΔTo are considered as the x values and hence two coordinates are obtained which are (Rn at ΔTo_{min}, $Q_{t\text{-}min}$) and (Rn at ΔTo_{max}, $Q_{t\text{-}max}$). The coordinates are plotted in the XY axis to obtain a linear model in Equation 22 which gives the estimates of the a and b constant values of Equation 20. The constant value c is computed by Equation 23 to obtain all the constant values for the hysteresis function and the obtained expression is specifically for the respective lake and can be used to compute the heat storage change of the respective lake.

$$Q_t = aR_n + b \tag{22}$$

$$c = -15.95T_{0-Range} + 48.76T_{0-STD} - 6.46 \tag{23}$$

2.4.3 The Craig and Gordon Evaporation Model

Most of the evaporation estimates for lakes rely on the field data measurements such as water flows, lake level changes, and comprehensive weather data, which become impractical and

expensive in areas that need more appropriate infrastructure (Gibson *et al.,* 2015). However, the straightforward approach is through the determination of the stable isotopes of lake water and precipitation and integration with the primary weather data such as rainfall, wind, temperature, humidity, and solar radiation(Craig & Gordon, 1965; Gibson *et al.,* 2015; Horita *et al.,* 2008). The C-G Evaporation Model (Craig & Gordon, 1965) utilizes the mentioned data to estimate the evaporation on an open water body by evaluating the changes in the stable isotopes of water (^{2}H and ^{18}O) in its different phases, namely liquid, vapour, and the transition phase between the two phases (Gibson *et al.,* 2015).

The model is based on the assumptions that the liquid-vapour interface layer is bounded by laminar and turbulent layers in both the liquid and vapour phases (Fig. 1), dominated by molecular diffusion and eddy diffusion transport of molecules, respectively (Craig-Gordon, 1965). The evaporation flux is modelled according to the Rideal–Langmuir linear-resistance model, where fluxes in each layer are proportional to the differences in isotopic concentration between the upper and the lower boundary of the layer (Craig & Gordon, 1965; Horita *et al.,* 2008; Özaydin *et al.,* 2001). The model assumes that under a steady state, water's evaporation flux (E) is constant throughout the cross-section (Craig & Gordon, 1965). The evaporation flux for the light and heavy isotopes of water from the liquid surface to the free atmosphere can be expressed as in Equations 24 and 25 (Craig & Gordon, 1965; Gat *et al.,* 2001).

$$E = \frac{1-h}{\rho} \tag{24}$$

Whereby, $\rho = \rho_M + \rho_B$ and h stands for relative humidity normalized to the free atmosphere as $h = \frac{h}{aH_2O}$ by which aH_2O stands for the lake water activity coefficient which is close to one however in hypersaline water it may reduce to up 0.67 (Horita *et al.,* 2008).

$$E_i = \frac{\alpha_{V/L} R_L - hR_A}{\rho_i} \tag{25}$$

Whereby, $\rho_i = \rho_i M + \rho_i B$ and $\alpha_{V/L} = \frac{1}{\alpha_{L/V}}$, the letters E stands for evaporation flux, *i* for heavy isotope, A for free atmosphere, M for laminar layer, B for turbulent layer, L for liquid

phase, V for vapour phase, and R for heavy to light isotopic ratio. The symbols ρ and α stands for the transport resistance and the isotopic fractionation factors respectively and hence ρ_M and ρ_B stands for transport resistances for light isotopes in laminar and turbulent phases respectively while $\rho_{i,M}$ and $\rho_{i,B}$ stands for transport resistances of heavy isotopes in laminar and turbulent phases respectively. $\alpha_{L/V}$ stands for equilibrium fractionation factor from liquid to vapuor phase.

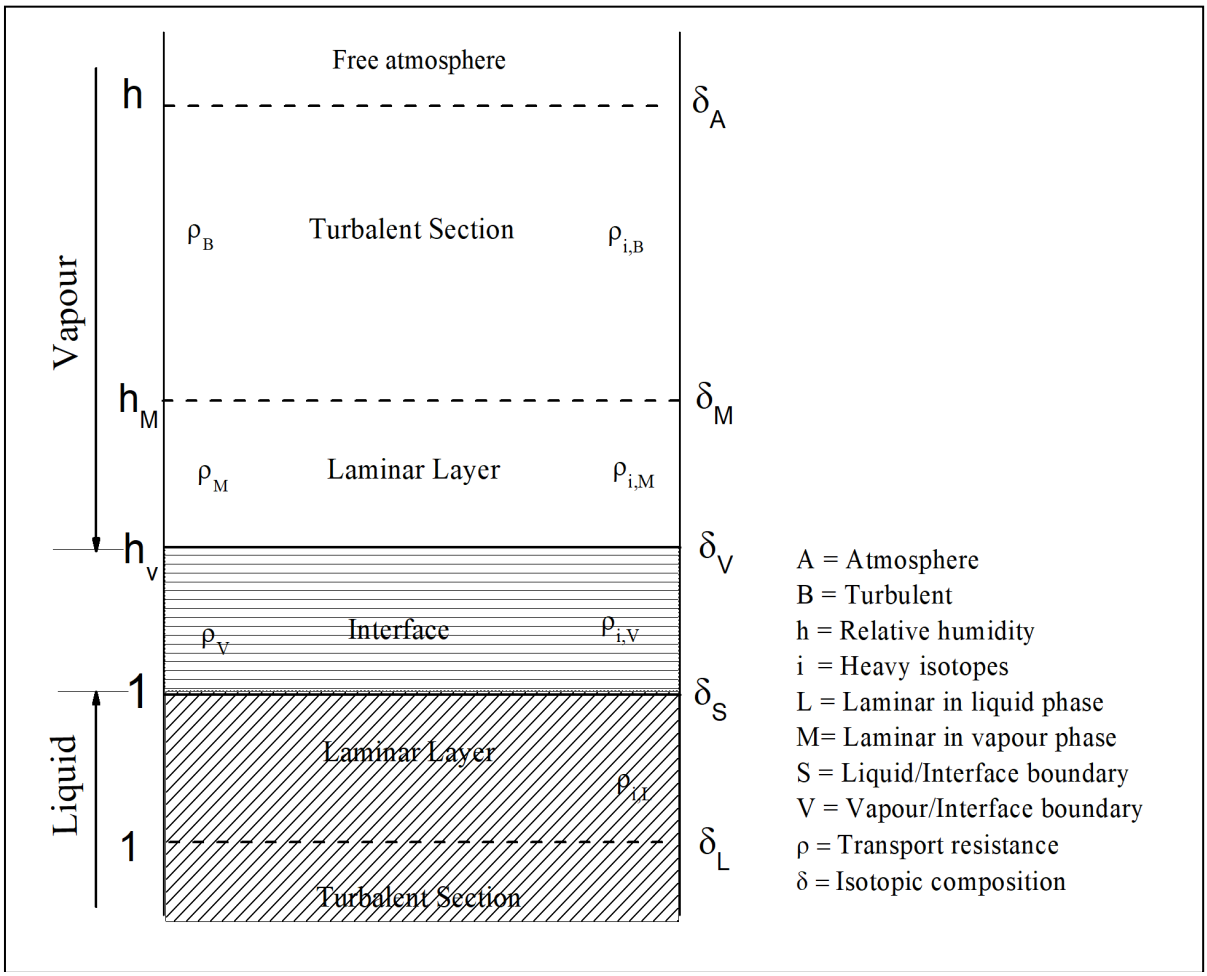

Figure 1: The schematic presentation of the Craig-Gordon Model (Horita *et al.*, 2008)

Then the isotopic composition of E can be given by the ratio of E for the heavy isotopes to that of the light isotopes (Craig & Gordon, 1965; Gat *et al.,* 2001) as in Equation 26:

$$R_E = \frac{E_i}{E} = \frac{(\alpha_{V/L} R_L - hR_A)\rho}{\rho_i(1-h)} \tag{26}$$

Expressing Equation 26 in δ terms substituting the R with the respective 1+ δ yield the expression for calculating the isotopic composition of vapour evaporating from the lake surface (Equation 27) (Craig & Gordon, 1965; Gat *et al.,* 2001; Horita *et al.,* 2008).

$$\delta_E = \frac{\alpha_{V/L} \times \delta_L - h\delta_A - \varepsilon}{(1-h) + \varepsilon_k} \tag{27}$$

Whereby, ε is the effective enrichment factor expressed as $\varepsilon = \varepsilon^* + \varepsilon_k$ by which $\varepsilon^* = (1 - \alpha_{V/L})$ and ε_k is the kinetic isotope fractionation factor resulted due to vapour transport through the three layers namely interface, laminar and turbulent. The δ_E, δ_L and δ_A stands for the isotopic composition of vapour, lake, and the atmosphere, respectively and $\alpha_{V/L}$ stands for the isotopic fractionation factor at the vapour-liquid interface.

Most of the parameters in Equation 27 can be obtained from field data collection whereby δ_L can be obtained from sampling and analysis of the isotopic composition of the lake under study. The isotopic composition of the free atmosphere (δ_A) can be obtained from sampling and analysis of the isotopic composition of precipitation (δ_P) assuming that local precipitation and atmospheric moisture are obviously in isotopic equilibrium(Horita *et al.,* 2008). However, it is standardized through the simple expression as in Equation 28 (Gibson *et al.,* 2015; Özaydin *et al.,* 2001):

$$\delta_A = \alpha_{V/L} \times \delta_P - (1 - \alpha_{V/L}) \tag{28}$$

The isotopic equilibrium fractionation factor at the liquid-vapour interface $\alpha_{L/V}$ can be obtained by the expression developed by Majoube (1971) during the laboratory experiment for the temperature between 0ºC and 100ºC for ^{18}O and ^{2}H and T is in Kelvin and obtained expressions as in Equations 29 and 30 (Horita *et al.,* 2008; Majoube, 1971; Özaydin *et al.,* 2001).

$$\ln \alpha_{L/V}\ (^{18}O) = [-2.667 - 415.6(T^{-1}) + 1137000(T^{-2})] \times (10^{-3}) \tag{29}$$

$$\ln \alpha_{L/V} \ (^{2}H) = [52.612 - 76278(T^{-1}) + 24844000(T^{-2})] \times (10^{-3}) \quad (30)$$

However, the experiment conducted by Horita and Wesolowski (1994) for the temperature range from 0ºC to 374ºC for ^{18}O and ^{2}H yielded Equations 31 and 32, respectively while utilizing T in Kelvin (Horita *et al.,* 2008; Horita & Wesolowski, 1994).

$$\ln \alpha_{L/V} \ (^{18}O) = [-7.685 + 6712.3(T^{-1}) - 1666400(T^{-2}) + 350410000(T^{-3})] \times (10^{-3}) \quad (31)$$

$$\ln \alpha_{L/V} \ (^{2}H) = [(1.1588 \times 10^{-6}) T^{3} - (1.6201 \times 10^{-3}) T^{2} + 0.79484 T - 161.04 + 2.9992 \times 10^{9} (T^{-3})] \times (10^{-3}) \quad (32)$$

The diffusion-controlled isotope fractionation during water-vapour state change in the C-G model is represented as the kinetic fractionation factor (ε_k) by which its calculation is as Equations 33 and 34 for ^{18}O and ^{2}H, respectively (Horita *et al.,* 2008).

$$\varepsilon_k (^{18}O) = 14.2(1 - h) \quad (33)$$

$$\varepsilon_k (^{2}H) = 12.5(1 - h) \quad (34)$$

2.4.4 Lake-Groundwater Flow

The groundwater inflow-outflow of the lake is another component that is difficult to determine due to the complicated flow pattern especially when using the conventional methods through the installation of a network of piezometers (Özaydin *et al.,* 2001). However, the combination of water balance and isotopic mass balance equations (Equations 2 and 3) provides an easy way to quantify the lake groundwater interactions which are groundwater outflow (O_g) and groundwater inflow (I_g) as in equations 35 and 36.

$$O_g = \frac{N - \delta_g M}{\delta_g - \delta_L} \tag{35}$$

And

$$I_g = \frac{N - \delta_L M}{\delta_g - \delta_L} \tag{36}$$

Where;

$$M = I_g - O_g \text{ and } N = \delta_g I_g - \delta_L O_g$$

CHAPTER THREE

MATERIALS AND METHODS

3.1 Study Area

3.1.1 Geographical Location

The Empakaai Crater is located within NCAA and forms part of the Northern Volcanic Crater Highlands associated with the Eastern arm (Fig. 2) of the East African Rift Valley (Gregory). It is about 110 kilometres North West of Arusha City and approximately bounded by latitudes ($2^0 52' 48'' S$ and$2^0 55' 48'' S$), Longitudes ($35^0 47' 24'' E$ and $35^0 51' 36'' E$) and an elevation of about 2300 metres above mean sea level (MAMSL) (Fig. 2). The crater occupies about 35 km^2 of the conservation area while a closed, depth of about 80 meters, saline-alkaline lake, known as Emakat Lake occupies part of its floor (about 3.2 km diameter) (Muzuka, 2004; Ryner *et al.,* 2006).

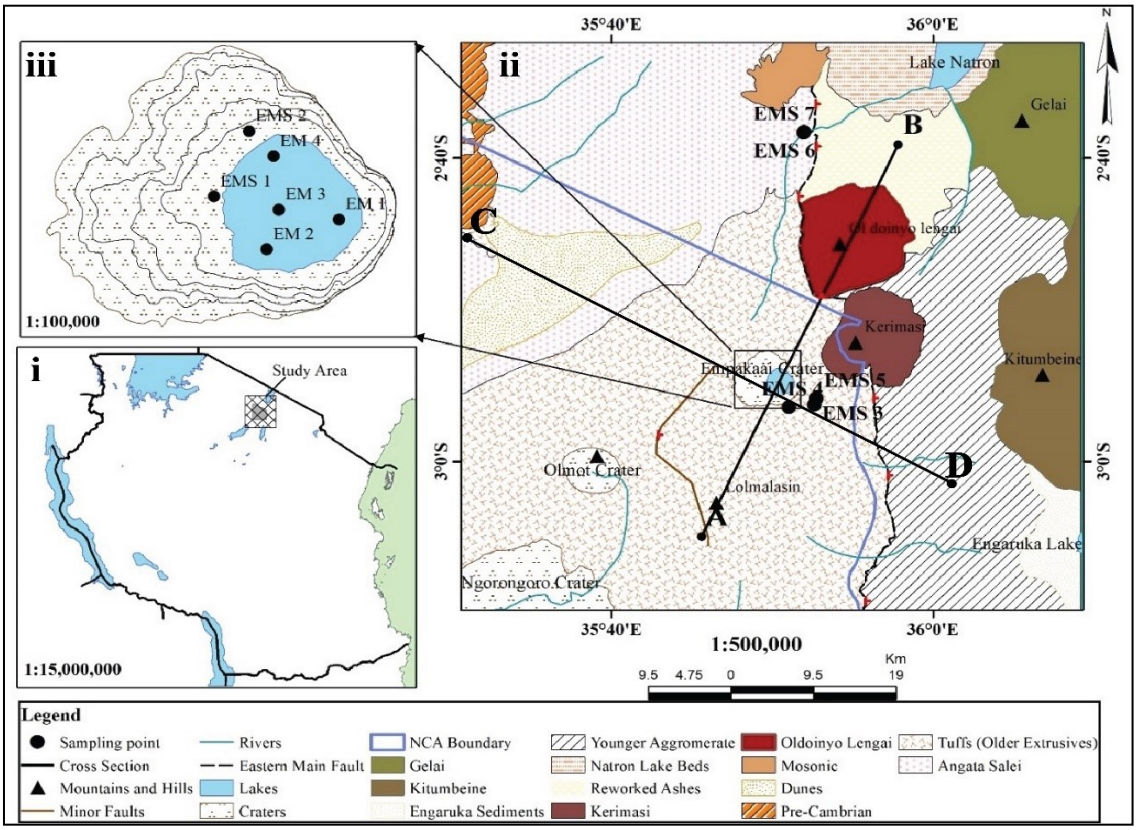

Figure 2: (i) The Tanzania map showing the location of the study area; (ii) The Northern Crater Highlands map showing the Empakaai Crater; (iii) The Empakaai Crater map showing the sampling locations

3.1.2 Climatic Condition

The rainfall in the Northern Crater Highlands is seasonal and occurs between November and May with its peak in April and May. The annual rainfall range between 600 to 1000 mm with spatial variation from the western to eastern slopes respectively, however, the topographical enhancement can result in as higher as 1500 mm annual rainfall (Ryner *et al.,* 2006; Ryner *et al.,* 2008).

3.1.3 Land use

The Empakaai Crater is located in NCAA, which is a protected area. However, the Maasai people reside on its outer rims, where they practice agriculture and animal keeping. Their population has been increasing from time to time, leading to an increased number of cattle and demand for food, with the only solution being to allow crop cultivation to support the population. The persistent aridity, population increase, food scarcity, and overgrazing have led to encroachment into the outer crater walls (Boone & Silver, 2002). These have implications on the land-use change impacting the vegetation protecting water catchments and the amount and chemistry of the lake water (Boone & BurnSilver, 2002; NCAA & MNRT, 1996). Due to the steep slopes and the saltiness of the lake water, cattle cannot access the lake. Hence, only wild animals reside in the place.

3.1.4 Geomorphology and Drainage

Emakat Lake is on the most elevated volcanic shield, the Empakaai Crater of the Elanairobi Shield in the Northern Crater Highland. The crater walls are not uniformly elevated as the western wall raise to about 3200 m while the eastern wall raises to about 2800 MAMSL (Fig. 3). The Elanairobi Volcano marks the Northern-Eastern end of the old Crater highlands. At the same time, the Oldoinyo Lengai protrudes along the major fault with a north-south trend connecting the highlands with the plain at the foot of the fault in the eastern part of the major faults. Therefore, the Elanairobi Volcano is flanked by Oldoinyo Lengai in its North East while Olmot Crater is in its southwest, though separated by a plain. The north to the western side of the crater is surrounded by the Angata Salei plain, while in the north to the east are the Natron and Engaruka plains, where all plains extend from the foot of the Empakaai Crater.

Since the crater is at the highest point and receives the highest rainfall, then it is the recharge zone downstream for sustaining the rich and diverse ecosystem (Frame *et al.,* 1975) as well as the water resources for agriculture in the outer slope of the crater and downstream (Boone *et*

al., 2006; Westerberg *et al.,* 2010). The springs from the outer crater rims drain the surrounding plains and form major rivers such as Engarasero and Engaruka Rivers (Fig. 2), which sustain the population downstream before entering Lake Natron and Engaruka, respectively (Widgren & Sutton, 2004).

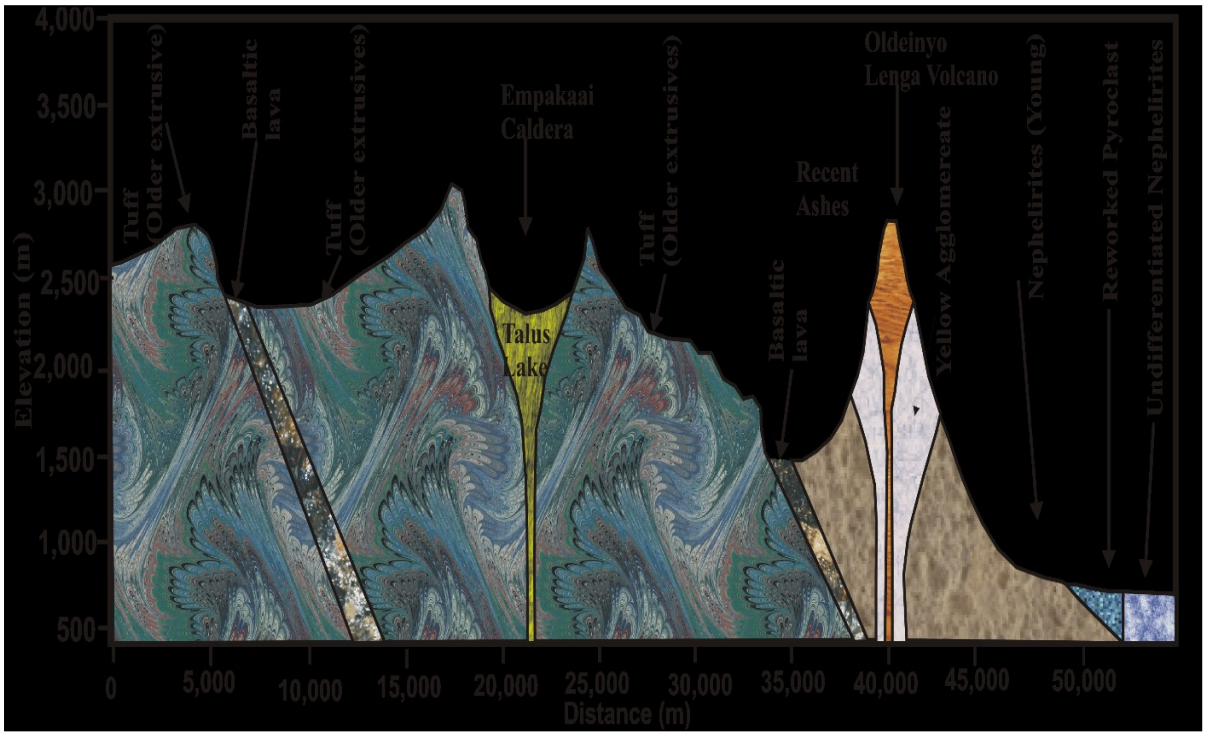

Figure 3: The Cross Section showing the vertical representation of the major lithological units and structures along the line AB of the geological map (Guest *et al.,* 1961)

3.1.5 Geology and Geochemistry

The formation of the Empakaai Crater is associated with the rifting processes of the Eastern African Rift Valley (Mollel *et al.,* 2008). The first rifting process, ca. 20 Ma, resulted in fissures and faults, which were then transformed into volcanic centres. The eruption centres formed volcanic summits (Empakaai, Olmot, Loolmasin, Ngorongoro, Lemagrut, Sadiman, and Oldean), which were growing while merging and then formed the Crater Highlands at ca. 2 Ma (Gaidzik, 2011).

The second rifting process took place ca. 1.26 Ma and formed the current north-south fault in the eastern boundary of the Crater Highland. It created some other fissures crossing the Empakaai, emptying the magma chamber beneath as a result of the summit's collapse and hence the Empakaai Crater formed. The crater was then occupied with water to form Emakat Lake.

The other volcanic mountains, such as Kerimasi and Oldoinyo Lengai, formed later after Ca. 1 Ma to the present.

The local geology of the area, as indicated by the map (Fig. 2), the cross-sections AB (Fig. 3), and CD (Fig. 4) show that the older formation is the metamorphosed Precambrian formation of the Oldoinyo Ogol group in the northwest of the Empakaai Crater while the remaining formations formed in the Miocene or later. The faults on the northeast and southeast of the Elanairobi Volcano, as presented as right and left faults, respectively, on the Cross-section AB, indicate that the landmass of Elanairobi Volcano was uplifted along the faults while allowing the Oldoinyo Lengai Mountain to form on top of the fault in the northwest. In the west of Elanairobi, the depositional basin formed due to the longitudinal dunes lying on top of the tuffs of Angata Salei (Fig. 4). The lower part of the Empakaai Crater is composed of nephelinites and mica-augite tuffs, the intermediate part is composed of agglomerates made of red scoria and tuffs, and the top part of the crater rim is composed of phonolite (Greenwood, 2014; Guest *et al.,* 1961).

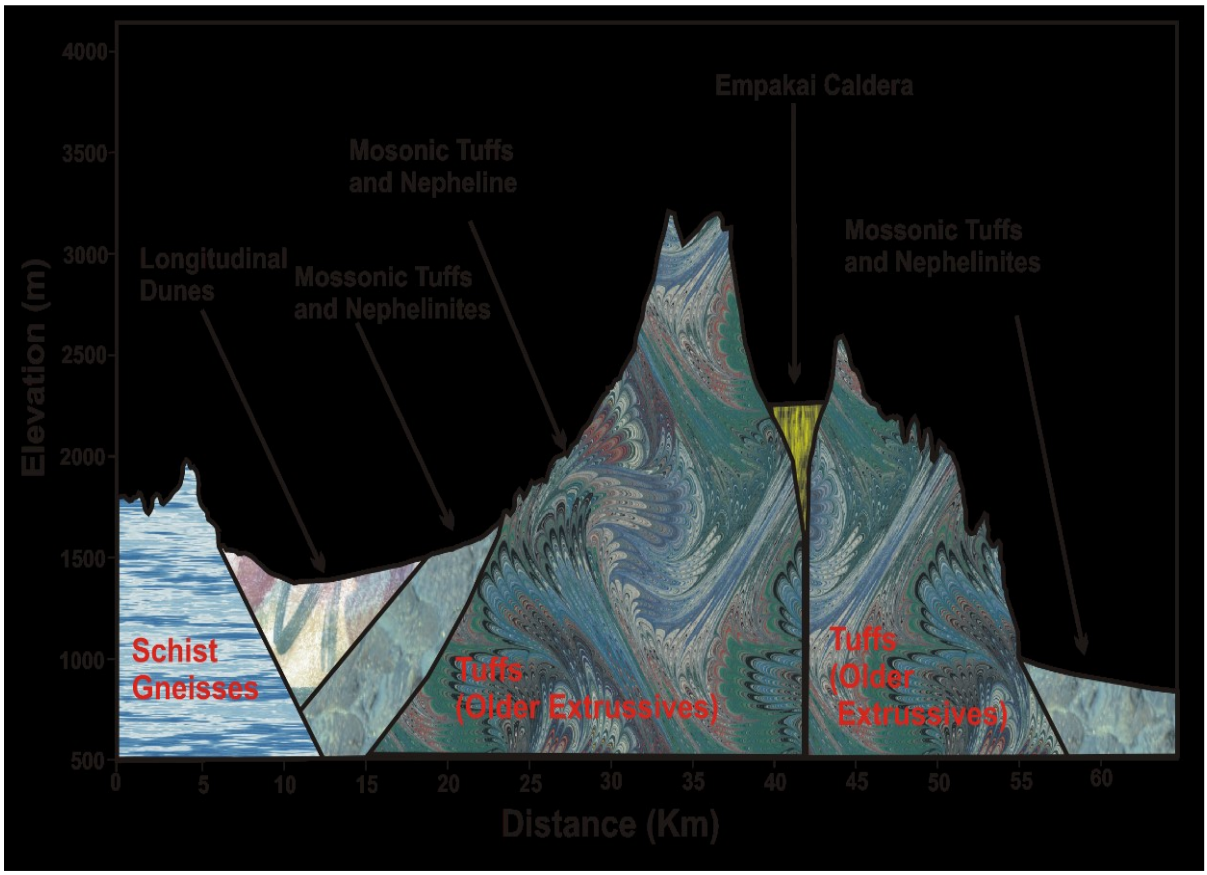

Figure 4: The Cross Section showing the vertical representation of the major lithological units and structures along the line CD of the geological map (Guest *et al.,* 1961)

The Empakaai Crater is composed mainly of feldspathoids, with the mineral assemblage consisting of nepheline, augite, andradite, melilite, apatite, and titanomagnetite. In contrast, the phenocryst consists of nepheline, augite, garnet and occasion melilite, and apatite (Mollel, 2007). Secondary minerals like calcite and zeolites (analcime, phillipsite, and chabazite) also occur in the area due to alterations of primary minerals (Greenwood, 2014). The rock formation forming the crater wall is largely altered since it is associated with secondary minerals of calcites and zeolites enriched in Ca, Mn, and P while depleted in Na and K (Greenwood, 2014). However, the presence of high calcite content can also be associated to be the result of the alteration of carbonatite erupted from Oldoinyo Lengai and Kerimasi (Greenwood, 2014).

3.2 Sampling and Analysis

3.2.1 Water Sampling and Analysis for Hydrochemical Parameters

The sampling campaign was done between 30th May and 25th November 2019 from 15 sampling points. In order to address the issue of spatial variation such as lake stratification, varied sedimentation and inflow type of the lake which may result to varied hydro physical and chemical properties of water (USGS, 2018), sampling was done at seven different location on surface and sub-surface of the Emakat Lake to an average depth of 25 m. Nevertheless, two springs from the inner crater rims (Ngurumani and Oleigero springs), three springs from the outer crater rims (Ngopironi spring, Marite spring 1, and Marite spring 2) and two springs from the foot of the Empakaai Crater (Emparakachi spring 1 and Emparakachi spring 2). Sampling for precipitation was done at one sampling point located at Karatu about 45 km south-west of the Empakaai Crater.

Standard procedures for water sampling as described by APHA, AWWA (2005) was utilized. Sampling was done in acid prewashed bottles which were then rinsed five times with the respective sample on-site during sampling time. Water samples for major cations such as Na^+, K^+, Ca^{2+}, and Mg^{2+} were sampled in the 500 mL bottles acidified with HNO_3 while samples for major anions such as F^-, Cl^-, HCO_3^-, SO_4^{2-} except NO_3^- were sampled in the non-acidified bottles of 250 mL. Water samples for NO_3^- analysis were sampled in 50 mL falcon tubes acidified with sulphuric acid while water samples for analysis of PO_4^{3-} were done in 50 mL amber glass bottles. Water samples for stable isotope (^2H and ^{18}O) from the lake and springs were collected with high-density linear polyethylene (HDPE) bottles of 100 mL which were immersed in sampled water ensuring bubble-free then tighten to avoid evaporation. Event based rainwater samples collection was done according to IAEA/GNIP Precipitation Sampling Guide (IAEA/GNIP, 2014) where a five litres gallon installed with a funnel and added with a

paraffin film. Then samples were daily transferred to the HDPE bottles of 100 mL by immersing in collected water ensuring bubble-free then tighten to avoid evaporation.

The samples were labelled with special codes which included code name, date of sampling and the respective parameter to be analysed for the respective sample in the respective bottle. Detailed information of the respective sample such as the location number, sample code, sampling location, coordinates of the sampling location were obtained by a hand-held GPS which provided the eastings, northings, and the altitude was recorded. For the samples collected in the lake, the depth below the lake surface was also recorded. All water samples collected were stored at 4ºC in cooler boxes with ice blocks during the field works and in the refrigerator before analysis and they were analysed immediately after the field works

The water sample analysis involved the onsite measurements by which temperature, pH, electrical conductivity (EC), total dissolved solids (TDS), salinity, and oxidation-reduction potential (ORP). The analysis was done with the HANNA Instruments HI 9829 multi-parameter. The standard method for analysis of major cations (Ca^{2+}, Mg^{2+}, $Na^{+,}$ and K^{+}) and major anions (SO_4^{2-}, NO_3^{-}, PO_4^{3-}, F^{-}, CO_3^{2-} and HCO_3^{-}) were utilized according to APHA, AWWA (2005) whereby the analysis for Ca^{2+}, Mg^{2+}, Cl^{-}, CO_3^{2-} and HCO_3^{-} was performed by the titration method, the analysis of SO_4^{2-}, NO_3^{-}, PO_4^{3} using the Hatch Spectrophotometer (Dr 2900), and the analysis of Na^{+} and K^{+} using the Flame Photometer (FP6440). The analysis of stable isotopes of water (δ^2H and $\delta^{18}O$) was done by the Dual Inlet-Isotope Ratio Mass Spectrometer.

3.2.2 Rocks Sampling and Analysis

In addition to water samples, three-rock samples were collected from the inner, outer crater walls and at the foot of the Empakaai Crater for geochemical analysis. The rock samples were collected from the outcrops which represented the formation of the respective lithological units. The rock samples were kept in the special sample bags which were labelled with a special code that included the sampling location number, code, and date of sampling. Analysis of the rock samples was done by using the inXitu's Terra portable powder XRD instrument whereby the rock samples were ground and sieved with 150 ɥm sieves to obtain powdered samples, of which about 50 g of each were loaded on the XRD for analysis. The final results were extracted from the instrument and processed by using the XPowder (Ver. 2010.01.35 PRO) software utilizing the American Mineralogist Crystal Structure Database (AMCSD).

3.2.3 Geospatial and Statistical Analysis of the Results

Data processing was done using different tools and software like Excel for assembling, calculating, and presenting data in tables in an organized manner. The ArcGIS software was used for the spatial presentation of data, data extraction incorporating with the python tool together with performing some calculations such as area and lake volume. The graphical presentation of data and results was performed using Origin Pro 8.5.

The hydrochemical evolution of Emakat lake and the associated springs was analysed using the Schoeller plot (Schoeller, 1965), piper plot (Piper, 1944), Chloro-Alkaline indices plot (Liu *et al.,* 2020), Chadha plot (Chadha, 1999), and Gibbs plot (Gibbs, 1970) while the quantification of groundwater flow in Emakat Lake was determined using a combination of the water balance and isotopic mass balance equations (Equations 2 and 3).

3.3 The Water Balance Estimation of Emakat Lake

A combination of the traditional water balance equation (Equation 2) and the isotopic mass balance equation (Equation 3) aided in the computation of the groundwater flow (Özaydin *et al.,* 2001). The estimation of hydrometeorological parameters of the water balance such as lake volume change, rainfall, runoff, and evaporation was estimated through different approaches as discussed in the following subsections.

3.3.1 Lake Volume and Volume Change

The lake volume and volume change can be calculated from a combination of the digital elevation model (DEM), the topographical map, and the bathymetry data for the respective lake (Mbanguka *et al.,* 2016). Other methods such as the combination of satellite altimetry are also available but are limited to relatively large reservoirs such as oceans, large lakes, and large rivers (Troitskaya *et al.,* 2012). For small lakes like Emakat, the aforementioned methods are the relevant techniques for the determination of the lake volume and the annual lake volume change. The DEM which is freely available from https://earthexplorer.usgs.gov/ is utilized in delineating the catchment and the lake topography whereas the lake bathymetry gives the lakes subsurface topography.

The lake volume and volume change of Emakat Lake were determined by a combination of DEM, lake bathymetry, and the surface water level determined by the GPS during water sampling. The DEM enabled the delineation of the Empakaai Crater catchment and the determination of lake topography. The lake subsurface topography was determined using the

bathymetry map by Ryner *et al.* (2007) whereby the map was extracted then georeferenced to generate the georeferenced bathymetry contours. The two generated topography were merged in ArcGIS 10.5 to generate the full lake map. The avearge lake surface elevation of 2216.57 m recorded by the hand held GPS during water sampling was considered as the maximum water level as the data collection was done in May which marked the end of the high-rain season for the study area (Ryner *et al.,* 2007).

According to Ryner *et al.* (2008), the inter-annual lake variation for Emakat Lake is 0.4 m and from this point of view, the minimum water level was estimated to calculate the minimum volume the lake can attain during the dry season. The lake volumes during the wet and dry seasons were calculated with the aid of the 3D analyst tool in ArcGIS 10.5. The difference between the two volumes was considered as the annual volume change for Emakat Lake.

3.3.2 Rainfall

The Empakaai Crater lacks a weather station on the lake and the land surface for weather data recording making the accurate estimation of the rainfall impossible. Satellite data are available for such cases; however, these also require validation from ground-collected data (Duan *et al.,* 2018). Different satellite resources are available and several attempts to validate them over East Africa have been done by Dinku *et al.* (2007), Maidment *et al.* (2017), and Dinku *et al.* (2018). However, the recently released Climate Hazards Group Infrared Precipitation with Station data (CHIRPS), provides the higher resolution rainfall data 0.05^{o} data for > 30 years (Katsanos *et al.,* 2016). The validation and performance evaluation of the CHIRPS data by Dinku *et al.* (2018) concluded that the resource has a higher performance over East Africa including Tanzania, despite some challenges in the coastal and mountainous regions.

In the current study, a point-to-grid comparison was used to validate the CHIRPS data from three ground measurements which are the Monduli, Ngorongoro, and Nainokanoka, the first being the weather station and the last two automatic min-weather stations. The gridded raster CHIRPS images (in .tif format) which are freely-available online were downloaded from https://climateserv.servirglobal.net/ for the respective stations.

The available ground-collected rainfall data had remarkable gaps that limiting the extent of the time series for validation attempt. To address this challenge, CHIRPS data were extracted for the respective time depending on the availability of data for the respective station. The validation for Monduli station was done for the data with time series from 2012 to 2016, Ngorongoro HQ station, between 2013 to 2018, and Nainokanoka station, 2013, 2014, 2017,

and 2018. The validation was done based on the standard statistical methods which are trend analysis through average monthly rainfall distribution graph, root mean square error (RMSE), Nash Sutcliffe model efficiency coefficient (NSE), bias, and Coefficient of determination (R^2) (Dinku *et al.,* 2007).

To estimate the rainfall of the Empakaai Crater, six points from the six grids of CHIRPS that cover the catchment were identified and considered as the point stations for the CHIRPS data in the catchments, then their coordinates were extracted by ArcGIS 10.5. The daily rainfall for the respective CHIRPS point stations of the Empakaai Catchment were extracted then exported as time series rainfall data by using python 3.7 (64 bits) utilizing the Spyder (Anaconda 3) algorithm. The monthly rainfall for each grid was computed from the extracted CHIRPS daily rainfall values for the time series of 2005 to 2019. The monthly rainfall for each year was computed and their respective average monthly gave the average predicted rainfall for the Empakaai Catchment.

3.3.3 Runoff

The runoff from the Empakaai Crater inner walls was estimated by the CN Model (Askar, 2013; Satheeshkumar *et al.,* 2017). The LU/LC map was obtained from the vegetation cover map of the Empakaai Crater by Ryner *et al.* (2006). The map was digitized to identify the boundaries of the vegetation covers of the inner crater rims of the Empakaai Crater.

The land cover was classified in accordance to the vegetation type to determine the hydrological condition whereby areas with thicket vegetation and the montane forest were considered to exhibit good hydrological conditions and the wooded grassland, fair hydrological condition. The soil map of Tanzania published by the Geological Department, Dodoma Tanzania was retrieved from the European Soil Data Centre (ESDAC) website (Samki & Baker, 1977) then georeferenced and overlain with the Empakaai Catchment boundary.

Since the Empakaai Crater is confined with very steep walls, then the slope was considered in the classification as a possible major controlling factor for the soil class and type of the Empakaai Crater catchment (Ritzema, 1994). The DEM image downloaded from the United States Geological Survey (USGS) (https://earthexplorer.usgs.gov) aided in the delineation of the Empakaai Catchment and slope classification. The slope classification was founded on the five classes (Table 6) based on the modification of the slope classification by Pamela *et al.* (2018).

Table 6: The slope classification criteria for the Empakaai Crater Catchment

No	Slope Class	Percentage
1	Lake	0 - 0.5%
2	Gentle	0.5 - 8%
3	Moderately Gentle	8 - 25%
4	Moderately Steep	25 - 45
5	Steep	>45

The soil map was then generated with the consideration of slope as the major factor controlling the texture, type, and thickness of the soil then it was compared with a soil sample collected from the crater for physical characteristics. To generate the hydrological soil-cover complex, the two maps; the land cover and the soil classification maps were superimposed to identify the soil cover complex.

3.3.4 Evaporation over Emakat Lake

The evaporation over Emakat Lake was estimated by the D-K Model. Despite its high performance, the D-K method is relevant to the lake which is ungauged like Emakat Lake since it requires few input data which mostly are freely available from online satellite providers (Duan *et al.,* 2018). The monthly average temperatures (T) were computed from the daily temperature data acquired from the Ngorongoro HQ station for the year 2018. The net short wave R_s and To were obtained freely from https://lpdaac.usgs.gov/ in .hdf format then the point data were extracted with the aid of the ArcGIS and the python algorithm.

The R_n was computed by the slob equation with the utilization of the obtained satellite R_s as the average of the daily recorded data for 2018 and 2019, standard $\propto$ for the lake of 0.05 and the slob's constant of 110 W/m^2 (Duan *et al.,* 2018). The R_a was computed by utilizing the G_{sc} of 0.082 MJ/m^3 min latitude, and DOY as described by Duan and Bastiaanssen (2015).

The monthly average lake surface temperature computed from satellite daily recorded data from 2014 to 2019 and the computed monthly R_n were used to develop the expression for computing the Q_t for Emakat Lake (Equation 37) where the constants in the equation were estimated as explained by Duan and Bastiaanssen (2015).

$$Q_t = 0.5972R_n - 252.61 - 13.6342^{dR_n}/_{dt} \quad (37)$$

CHAPTER FOUR

RESULTS AND DISCUSSION

4.1 Hydrochemistry of Empakaai Crater

4.1.1 Hydro-Chemical Characteristics

The results from the in-situ measurements and laboratory analysis are presented in Table 7 and Table 8, respectively. The pH range of the lake is between 10.04 and 10.20, which is higher compared to the pH of the springs that ranged from 6.85 to 8.18 for the springs located on the inner and outer rims of the crater. The EC and TDS of Emakat Lake ranged from 28 860 to 29 460 µs/cm and 14 432 to 14 723 mg/L, respectively (Table 7) while those for springs ranged from 562 to1584 µs/cm and 276 to 1016 mg/L, respectively. The ORP of the lake ranged between 72.3 and 168.5 mV.

The ionic balance done on the hydrochemical results ranged between -9 and 4% which might be a result of temperature storage challenges which might have raised due to the transport distance form site to Laboratory. However, it was in the allowable range of -10 to 10% (Rice *et al.,* 2012). The concentration of Na^+, K^+, $Ca^{2+}$and Mg^{2+} for Emakat Lake ranged from 7182.49 to 8518.45 mg/L, 1214.67 to1479.18 mg/L, 53.80 to 111.39 mg/L and 13.73 to 26.15 mg/L, respectively while for the springs, the ranges were from 13.89 to 352.74 mg/L, 6.55 to 42.67 mg/L, 6.73 to 64.50 mg/L and 2.28 to 28.01 mg/L, respectively (Table 8). The concentration of Cl^-, SO_4^{2-}, F^-, PO_4^{3-} and NO_3^- in Emakat Lake ranged from 1014.48 to 1145 mg/L, 586.34 to 629.52 mg/L, 226.65 to 261.35 mg/L, 0.10 to 2.50 mg/L and 92.95 to 224.28 mg/L, respectively, whereas for the springs, the ranges were from 2.63 to 154.58 mg/L, 1.00 to 256.00 mg/L, 0.31 to 11.64 mg/L, 0.10 to 0.80 mg/L and 0.00 to 27.39 mg/L, respectively (Table 8).

These results show that Emakat Lake is dominated by higher Na^+, K^+, and higher HCO_3^- and CO_3^{2-} and hence highly alkalinity (Schagerl, 2016). The major cations and anions for Emakat lake show the decreasing order of distribution of $Na^+ > K^+ > Ca^{2+} > Mg^{2+}$ which is the normal characteristics for the eastern Africa soda lakes (Getenet *et al.,* 2022), while the anions distribution exhibit a pattern of $(CO_3^{2-} + HCO_3^-) > Cl^- > SO_4^{2-} > F^- > NO^{3-} > PO_4^{3-}$ (Table 8).

Table 7: Location of sampling points and physical parameters of water samples from Emakat Lake and the associated springs

Code	Source	Location			Ph	Temp	EC	TDS	Salinity	ORP
		Eastings	Northings	Altitude (MAMSL)		ºC	µS/cm	mg/L	PSU	mV
EM 1.1	Lake	816749	9676571	2215	10.08	21.25	29330	14662	18.17	168.3
EM 1.2	Lake	816749	9676571	2209	10.09	20.64	29400	14700	18.25	123.4
EM 2.1	Lake	814774	9676619	2219	10.2	23.15	29100	14545	18.01	118.9
EM 2.2	Lake	814774	9676619	2204	10.05	22.04	29090	14542	17.99	123.8
EM 2.3	Lake	814774	9676619	2199	10.04	21.11	30530	15261	17.62	107.5
EM 3.1	Lake	815392	9677462	2217	10.04	21.03	29390	14691	18.24	136.2
EM 3.2	Lake	815392	9677462	2202	10.06	19.96	29460	14723	18.25	122.7
EM 4.1	Lake	815481	9678925	2214	10.09	20.61	28860	14432	17.87	106.8
Mean				**2209.88**	**10.08**	**21.22**	**29395.00**	**14694.50**	**18.05**	**125.95**
Standard Deviation				**7.01**	**0.05**	**0.92**	**469.44**	**233.81**	**0.21**	**18.29**
EMS 1	Spring on inner crater rim	814250	9677555	2219	8.18	15.24	562	276	0.26	109.2
EMS 2	Spring on inner crater rim	815066	9679151	2219	8.03	15.42	567	284	0.28	138.9
EMS 3	Spring on outer crater rim	820187	9675362	2162	8.69	15.75	670	335	0.33	191.2
EMS 4	Spring on outer crater rim	819956	9674571	2209	8.16	15.3	687	344	0.34	187.7
EMS 5	Spring on outer crater rim	817010	9674290	2577	8.09	17.72	673	336	0.33	189.5
EMS 6	Spring at Crater foot	818784	9707692	831	6.92	25.5	1504	978	0.74	275.3
EMS 7	Spring at Crater foot	818830	9707797	826	6.85	24	1584	1016	0.76	272.2
Mean				**1863.29**	**7.85**	**18.42**	**892.43**	**509.86**	**0.43**	**194.86**
Standard Deviation				**666.85**	**0.64**	**4.10**	**415.28**	**309.23**	**0.20**	**57.34**

Table 8: Chemical parameters for Emakat Lake and the associated springs

Code	Source	F	Cl	SO4	NO3	PO2	HCO3	CO3	Na	K	Mg	Ca	SiO	Balance
		mg/L	mg/L	mg/L	mg/L	mg/L	mg/L	mg/L	mg/L	mg/L	mg/L	mg/L	Mg/L	
EM 1.1	Lake	196.41	827.6	330.62	55.21	0.1	3110.94	4247.06	4169.41	797.74	9.76	44.74	658.34	-7
EM 1.2	Lake	184.47	856.5	316.86	52.17	1.45	3292.33	4537.2	4283.73	813.71	8.75	43.4	543.54	-8
EM 2.1	Lake	191.7	870.69	316	89.52	0.2	3858.8	4261.15	4252.4	819.87	11.18	49.52	593.06	-8
EM 2.2	Lake	185.67	861.28	319.76	52.6	0.4	3315.82	4569.57	4319.51	820.55	8.89	39.35	561.04	-8
EM 2.3	Lake	139.61	588.03	348.69	80.94	0.33	3880.24	4803.15	4479.47	825.38	10.12	40.72	517.39	-8
EM 3.1	Lake	191.33	897.15	326.33	90.99	0.3	3655.41	3767.59	4068.25	783.5	7.53	42.33	655.12	-7
EM 3.2	Lake	191.91	902.84	338.12	48.71	0.2	3271.61	4508.65	4179.41	804.24	9.7	46.74	633.13	-9
EM 3.3	Lake	145.96	614.77	364.55	84.62	0.18	4056.71	5021.6	4683.2	862.92	10.58	42.57	497.91	-8
EM 4.1	Lake	184.67	992.72	326.17	55.83	0.8	3783.35	4375.27	4583.23	875.87	14.2	43.04	679.65	-6
Mean		**179.08**	**823.51**	**331.90**	**67.84**	**0.44**	**3580.58**	**4454.58**	**4335.40**	**822.64**	**10.08**	**43.60**	**593.24**	
Standard Deviation		**19.81**	**126.55**	**15.20**	**17.02**	**0.41**	**317.95**	**337.43**	**193.28**	**27.98**	**1.78**	**2.90**	**62.78**	
EMS 1	Spring on inner crater rim	0.8	5.04	51.67	0.92	0.5	210.92	3	50.4	19.5	4.13	41.25	19.34	3
EMS 2	Spring on inner crater rim	0.7	8.61	15.07	7.29	0.5	206.92	2.08	42.87	17.74	3.88	26.15	18.32	4
EMS 3	Spring on outer crater rim	3.7	12.63	10	14	0.1	305.13	14.05	47.7	18.8	5.29	64.5	2.75	-2
EMS 4	Spring on outer crater rim	2.46	10.52	29	0.9	0.3	250.12	3.4	48.3	23.9	17.13	13.75	5.65	-5
EMS 5	Spring on outer crater rim	2	46.31	1	1	0.8	218.74	2.53	48.3	27.4	7.9	25.5	6.78	-4
EMS 6	Spring at Crater foot	3.59	74.98	188	14.4	0.1	507.1	0.4	238	40.2	11.42	30	1.23	-3
EMS 7	Spring at Crater foot	3.86	86.97	210	5.8	0.11	527.15	0.35	239	41.6	16.4	29.25	5.11	-5
Mean		**2.44**	**35.01**	**72.11**	**6.33**	**0.34**	**318.01**	**3.69**	**102.08**	**27.02**	**9.45**	**32.91**	**8.45**	
Standard Deviation		**1.24**	**31.89**	**81.84**	**5.51**	**0.25**	**129.80**	**4.37**	**86.30**	**9.31**	**5.21**	**14.91**	**6.79**	

In the cation dominance, Na^+ exhibit the highest proportion which accounted about 80% followed by K^+ which accounted for about 16% of total cation while anions were dominated by (CO_3^{2-}+HCO_3^-) that accounted for about 85% followed by Cl^- which accounted for about 9% of total anions. This implies that the lake is dominated by the Na^+-HCO_3^- water type. The low concentration of Ca^{2+} and Mg^{2+} in Emakat Lake can be associated with their non-conservative nature by which they are removed from the system by mineral precipitation or adsorption (Deocampo, 2004). The overall total cation of springs in the study area were dominated by Na^+ (60%) followed by K^+ (19%) with cationic distribution of $Na^+ > K^+ > Ca^{2+} > Mg^{2+}$ and anionic characteristics of (CO_3^{2-}+HCO_3^-) > SO_4^{2-} > Cl^- > NO^{3-} > F^- > PO_4^{3-} with CO_3^{2-}+HCO_3^- (74%) and SO_4^{2-} (16%). This also indicate that, springs are dominated by Na^+-HCO_3^- water type where higher Na^+ and K^+ are attributed by the ion exchange process in groundwater where Na^+ and K^+ are replaced by Ca^{2+} and Mg^{2+} in the solid phase (Ma *et al.,* 2021).

4.1.2 Hydrochemical Evolution of Emakat Lake

The acidity and alkalinity of water can be assessed based on its level of pH (Liu *et al.,* 2020). Based on the present results, Emakat Lake exhibited higher pH of > 10 which implies that it is a highly alkaline lake. The lake is classified as higly saline lake due to its higher EC and TDS ranging between 28 860 and 29 460 µs/cm and 14 432 and 14723 mg/L, respectively (Rusydi, 2018). These values might be subjected to seasonal variation as it was reported for Lake Natron by Philip and Mosha (2012). However, the variation in Emakat Lake might be not as great as of Lake Natron due to limited inflow. The springs on the study area were characterized by neutral to slightly higher pH ranging between 6.85 and 8.69. The EC and TDS ranged between 562 to 1584 µs/cm and 276 to 1016 mg/L, respectively. The existence of ORP ranging from 72.3 to 168.5 mV and 109.2 to 275.3 mV for lake and springs, respectively indicates the presence of some oxidation condition in the lake and the groundwater (Campodonico *et al.,* 2019).

For comparison on the abundance of the solutes concentration in Emakat Lake and the associated springs, the Schoeller plot was employed (Schoeller, 1965). The overall solute concentration of the lake was higher than the springs (Fig. 5). Emakat Lake has a relatively high HCO_3^- and CO_3^{2-} but the concentration of CO_3^{2-} is lower compared to HCO_3^- for the springs. The Ca^{2+} and Mg^{2+} exhibited intermediate concentration while $PO4^{3-}$ exhibited the least concentration both in the lake and the springs. While all springs had high HCO_3^- in

common, those with high Na^+ had a relatively high concentration of either SO_4^{2-} or Cl^- which implies that multiple hydrochemical processes are influencing the geochemistry of the springs as a result of the mixed water characteristics (Fig. 5).

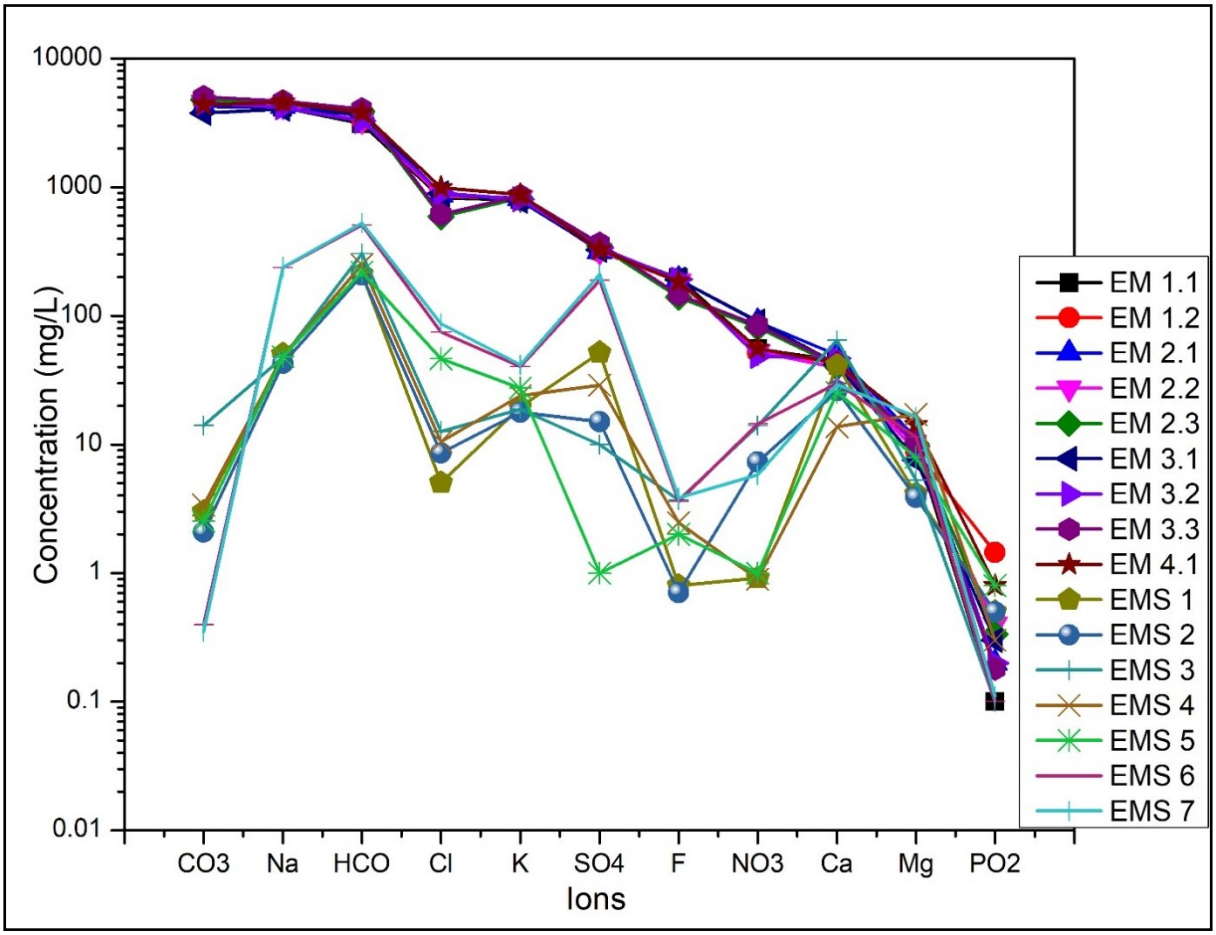

Figure 5: Schoeller plot showing the solute concentration comparison for Emakat Lake and the associated springs

To determine the hydrochemical facies and water type and the dominant hydrochemical processes influencing the chemistry of Emakat Lake and the associated springs, the hydrochemical results were plotted on the piper diagram (Piper, 1944; Ravikumar *et al.,* 2015), the chloro-alkaline indices (CAI-1 and CAI-2) (Liu *et a.,* 2020), Chadha plot (Chadha, 1999) and the Gibbs plots (Gibbs, 1970). The piper plot is divided into six fields (I, II, III, IV, V, and VI) (Fig. 6A) which signify the water type dominance where I and II are classified as a mixing field where no dominant type of cations (Ca-Mg) and anions (Cl-SO_4) for field III and cations (Na-K) and anions (HCO_3-CO_3) for field IV while fields III, IV, V, and VI are Ca-Mg-HCO_3-CO_3, Na-K-Cl-SO_4, Ca-Mg-Cl-SO_4, and Na-K-HCO_3-CO_3 water type respectively (Ravikumar & Somashekar, 2017). The piper plot for the hydrochemical data showed that all lake water samples fall on field VI indicating that Emakat Lake exhibited the Na-K-HCO_3 water type. A majority of spring water, fall on field II which was the mixing zone, indicating that water rock

interaction including dissolution and ionic exchange might be influencing the chemistry. A few samples fell on field III, implying that water from the respective springs are Ca-Mg-HCO_3-CO_3 type characterised by temporary salts (Ravikumar & Somashekar, 2017).

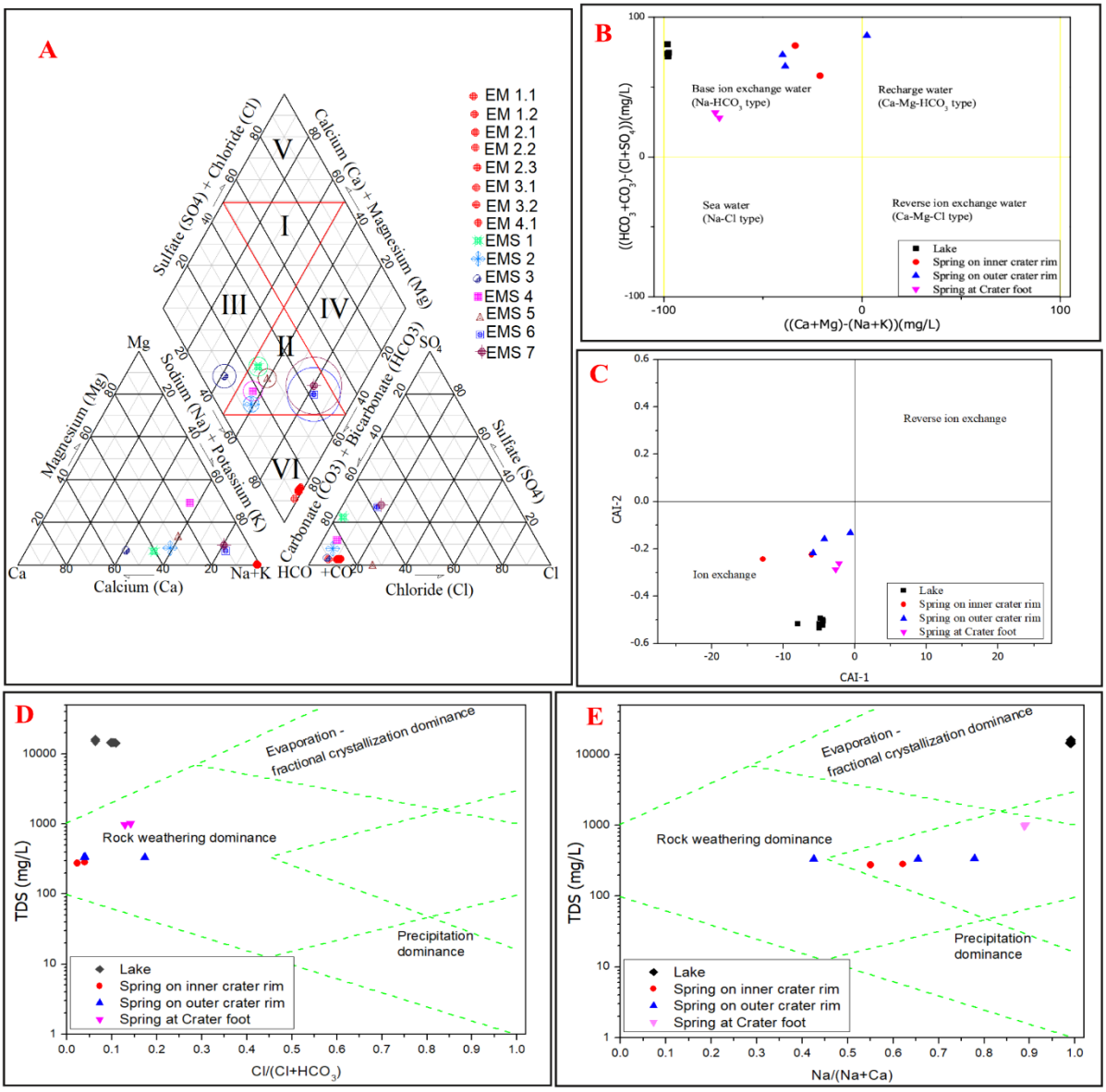

Figure 6: (A) Piper diagram showing the main hydrochemical characteristics of the Emakat Lake and associated springs (B) Chadha plot (Chadha, 1999) (C) Chloro-Alkaline indices (CAI-1 and CAI-2)plot (Liu *et al.*, 2020), and Gibbs plots (D) TDS versus Cl/(Cl+HCO_3) and (E) TDS versus Na/(Na+Ca) (Gibbs, 1970)

The evaluation of the dominant hydrochemical processes influencing the hydrochemistry of Emakat Lake and its associated springs was performed using the Chadha plot (Chadha, 1999). All water samples for Emakat Lake and associated springs fell on the upper–left field except for one spring which fell on the upper-right field (Fig. 6 B), indicating that water evolution in the area is dominated by base ion-exchange processes by which the alkaline metal (Na, K)

exceeded alkaline earth (Ca, Mg) and the weak acids (HCO_3, CO_3) exceeded the strong acids (Cl, SO_4), probably as a result of the dominance in the Na-HCO_3 water type. In contrast, the other spring could represent the recharging water with Ca-Mg-HCO_3 water type. This suggests that the rock-water interaction process through dissolution and the ionic exchange processes of hosting rocks are responsible for the hydrochemical evolution of Emakat Lake and the groundwater of the study area. Further evaluation was done by the chloro-alkaline indices (CAI-1 and CAI-2) plot to understand the ion exchange process's influence on the water chemistry in the area (Liu *et al.,* 2020). The CAI-1 and CAI-2 plot (Fig. 6C) showed that both lake and spring samples fell on the lower-left region, indicating that the evolution of water on both the ground and lake water could occur through an ion exchange process.

The Gibbs plots are essential tools that assist in identifying mechanisms controlling the surface water chemistry (Gibbs, 1970); however, recently, it has been used for groundwater hydrochemistry studies (Liu *et al.,* 2020). Gibbs plot classifies three mechanisms influencing the hydrochemistry of world waters which are atmospheric precipitation, geological influence through weathering processes, and evaporation and fractional-crystallization process, and it is done through the Cl/(Cl+HCO_3) Vs TDS and Na/(Na+Ca) Vs TDS plots (Gibbs, 1970). To understand the mechanism controlling the hydrochemistry of Emakat Lake and the associated springs, the Gibbs plot was employed whereby the Cl/(Cl+HCO_3) Vs TDS plot (Fig. 6 D) showed that spring water samples fell on the rock dominance region and lake waterfall outside the fields. In contrast, the Na/(Na+Ca) Vs TDS plot showed that spring water samples fell inside the rock dominance field and lake water fell on the evaporation dominance field. This implies that the hydrochemistry of springs is controlled by rock-water interaction through the dissolution and ion exchange processes. In contrast, lake chemistry is controlled by diverse processes such as evaporation, fractional crystallization, and rock-water interaction, which indirectly impact it through recharging groundwater and runoff from crater walls (Liu *et al.,* 2020).

4.1.3 Geological Contribution to the Hydrochemical Evolution

The geochemical results from the three rock samples collected from the inner crater rims (RMS 1), outer crater rims (RMS 2), and at the foot (RMS 3) of the Empakai Crater are presented in Table 9. The main phases of the Empakaai Crater were zeolites, oxides, feldspars, amphibole, phosphates, feldspathoids, pyroxenes, sulfosalts, mica, milarites, and nitrates.

Table 9: The dominant geochemical phases of the hosting geological formation as per XRD results

	Sample ID	RMS 1	RMS2	RMS3
Sample Details	Eastings	814250	819956	827190
	Northings	9677555	9674571	9667373
	Altitude	2219	1150	2209
Mineral Phases	Amphibole	11.94	nd	nd
	Feldspar	12.04	nd	19.11
	Feldspathoids	5.62	nd	nd
	Mica	nd*	77.33	10.21
	Milarite	nd	nd	11.22
	Nitrates	nd	17.58	nd
	Oxide	23.37	2.8	10.72
	Phosphate	11.63	1.2	nd
	Pyroxene	5.42	nd	11.12
	Sulfosalt	3.81	nd	nd
	Zeolite	23.57	nd	23.26
	Other silicates	2.61	1.1	nd

*not detected

The domination of zeolites was on the RMS 1 and RMS 3 which are gobbinsite ($Na_{0.6}Ca_{0.2}(Al_{0.7}\ Si_{1.3}).12H_2O$) and philipsites ($KCa_{0.8}Al_{2.7}Si_{5.3}O_{22}.12H_2O$), respectively. Oxides occurred in all three rock samples though dominated the RMS 1 and RMS 2 while in RMS 2 occurred in the minor phase. Oxides on the RMS 1 samples occurred as arsenolit (AsO_3), schmiederite ($Pb_2Cu_2Se_2O_{11}H_4$), senkevichite ($Cs_{0.9}K_{1.1}NaCa_{1.6}Mn_{0.3}Fe$), and walfordite ($Fe_{0.6}Te_{3.3}Ti_{0.1}Mg_{0.1}O_8$) while for the RMS 3 the oxide phase occurred as hollandite ($K_{0.8}Ti_{3.6}Mg_{0.4}O_8$), metamunirite ($NaVO_3$), hollandite ($K_{0.8}Ti_{3.6}Mg_{0.4}O_8$), polycrase ($Y_{0.5}Dy_{0.02}Ti_{0.5}Nb_{0.5}O_3$), redledgeite ($Ba_{0.6}Ti_4O_{0.08}$) and ulvospinel ($Cu_3V_2O_{11}H_6$). Other minerals occurring in the main phase for RMS 1 included feldspars, mainly anorthite ($CaSiAlO_4$), amphibole mainly hornblende (Si6.176Al2.574Mg3.78Fe0.59T), and phosphates as arrojadite ($Fe_{12}Mn_2AlNa_{2.3}K_{0.3}Ba_{0.3}$) and monazite ($EuPO_4$) while feldspathoids such as leucite (KSi_2AlO_6), pyroxenes such as clinoferrosilit ($FeSiO_3$), sulfosalts such as baumhauerite ($Pb_{11.6}As_{16.6}S_{36}$) and cosalite ($Bi_4Pb_{3.9}Cu_{26}S_{10}$) occurred as the minor mineral phases.

The mineral phases of feldspars mainly albite ($NaAlSi_3O_3$), milarite mainly the trattnerite ($K_{0.1}Fe_{2.5}Mg_{2.5}Si_{12}O_{30}$), pyroxene mainly augite ($Ca_{0.6}Fe_{0.1}Mg_{0.4}Mn_{0.01}K_{0.2}O_6$) and mica mainly muscovite ($K_{0.9}Na_{0.07}Al_{2.7}Fe_{0.2}Si_3\ O_6$) dominated the main phase of the RMS 3 in addition to zeolites and oxides. The RMS 2 was mainly dominated by mica which takes about 77.3% with minerals annite ($Al_{1.3}Si_{2.8}Fe_{2.4}Ti_{0.2}$), biotite $Fe_{0.4}Mg_{0.5}Mn(Si_{2.8}Al_{1.2}O_{10})$, chlorite ($Mg_{2.3}Fe_{0.3}Al_{0.9}Si_{1.6}O_{10}(OH)_2.[Mg,Fe)_3(OH)_6$], clinochlore ($Si_3Al_3Ti_{0.01}Fe_{\ 0.01}Mn$), phlogopite

($K_{0.86}Na_{0.05}Ba_{0.05}Mg_{1.4}Fe_{1.1)}$, protolithionite ($K_{0.9}Na_{0.1}Ca_{0.01}Rb_{0.01}Al_{1.5}$), siderophyllite ($Si_{3.2}Al_{1.7}Li_{0.8}Fe_{0.9}$) and vermiculite ($Mg_3Si_4(O_{12}H$) which occupied the main phase. Other minerals for RMS 2 included nitrates namely nitromagnesite ($MgN_2O_{12}H_{12}$) and oxides mainly rodalquilarite ($Fe_2Te_4O_{12}H_3Cl$).

Dissolution of feldspathoids and weathering of feldspars results in unstable zeolites rich in Na and K, which undergo ion exchange with Ca and Mg to produce the stable zeolite rich in Ca and Mg. At the same time, Na and K are released into the solution (Ma *et al.,* 2021). The presence of dominant zeolite minerals of gobbinsite and phillipsite implies the ionic exchange process in the Empakaai Crater. Oxidation of iron in feldspar, feldspathoids and pyroxenes forms various oxides and releases ions, including alkalies (Na, K), into solution (Deniz *et al.,* 2021). The occurrence of oxides of rodalquilarite and walfordite is an indication of the process in the Empakaai Crater.

The occurrence of mica in the area is the result of weathering of pyroxenes; however, its domination in the area is the result of metamorphism, which involves the recrystallization of other minerals, such as clay minerals resulting in the formation of the mica-schist formation, in the area (Żaba & Gaidzik, 2011). Chemical weathering of Amphibole, Feldspars, Feldspathoids and Pyroxenes results in Carbonates, mainly calcite which in turn undergo dissolution and release Ca and Bicarbonate into the solution; in addition, the high calcite amount in the area has also been associated with carbonatite from the eruption of the Oldoinyo Lengai (Greenwood, 2014).

Generally, the domination of the secondary mineral phases in the Empakaai Crater, namely the zeolites, mica, and oxides, implies that the crater is highly weathered, and according to Mollel (2007), the secondary mineral phases are enriched in Ca, Mg and P and depleted in Na and K implying that the weathering process through dissolution and ionic exchange releases Na and K into the solution leaving the rock units depleted in the respective ions (Greenwood, 2014; Mollel, 2007) hence high alkalis (Na and K) in groundwater.

4.1.4 Solute Sources in Emakat Lake

The solute concentration for crater lakes is attributed to several factors such as lithology of the hosting rocks, evaporation, solute loss to mineral crystallization, precipitation, biota, and hydrothermal inputs (Armienta *et al.,* 2008; Deocampo, 2018). The lithological composition of the hosting rocks directly influences the solute composition of a closed lake as they undergo

chemical weathering processes that release solutes to the lake's inflows which are then deposited in the lake basin (Deocampo, 2018).

The lithology and the nature of the mineral type of hosting geology had a direct impact on the springs of the study area since were dominated by major cations of Na, Ca, K and Mg with their associated anions of CO_3^{2-}, HCO_3^-, SO_4^{2-}, Cl^-, NO^{3-}, F^- and PO_4^{3-}. Na and Cl showed a strong correlation of 0.91 indicating their co-occurrence in the groundwater of the study area (Table 10).

Table 10: The ionic ratio of Na/Cl can aid in identifying the source of Na and Cl

Emakat Lake	F	Cl	SO4	NO3	PO2	HCO	CO3	Na	K	Mg	Ca	Springs
F	1	0.65	0.58	0.58	-0.76	0.8	0.24	0.66	0.66	0.58	0.25	**F**
Cl	0.89	1	0.85	0.27	-0.34	0.88	-0.49	0.91	0.97	0.54	-0.21	**Cl**
SO4	-0.79	-0.77	1	0.33	-0.62	0.94	-0.51	0.98	0.91	0.55	-0.14	**SO4**
NO3	-0.41	-0.44	0.29	1	-0.69	0.54	0.38	0.42	0.23	-0.15	0.54	**NO3**
PO2	0.09	0.28	-0.42	-0.4	1	-0.75	-0.24	-0.61	-0.43	-0.42	-0.32	**PO2**
HCO	-0.66	-0.45	0.48	0.77	-0.18	1	-0.27	0.97	0.91	0.57	0.01	**HCO**
CO3	-0.76	-0.68	0.64	-0.13	0.05	0.29	1	-0.48	-0.55	-0.38	0.81	**CO3**
Na	-0.74	-0.47	0.58	0.1	0.12	0.65	0.76	1	0.95	0.55	-0.13	**Na**
K	-0.48	-0.16	0.36	-0.01	0.18	0.59	0.59	0.94	1	0.67	-0.3	**K**
Mg	-0.12	0.16	0.09	-0.09	0.05	0.43	0.24	0.64	0.82	1	-0.56	**Mg**
Ca	0.45	0.32	-0.23	0.1	-0.19	-0.03	-0.27	-0.33	-0.17	0.23	1	**Ca**
	F	**Cl**	**SO4**	**NO3**	**PO2**	**HCO**	**CO3**	**Na**	**K**	**Mg**	**Ca**	

Whereby, a ratio < 1 indicates dissolution of halite and atmosphere contribute to the Cl concentration, and the ratio > 1 indicates additional source of Na exist. The dissolution of silicate minerals contributes to a higher concentration of Na and the ratio of one indicates that halide dissolution is the only source of Cl and Na (Liu *et al.,* 2020). For the springs in the study area, the Na/Cl ratio was > 1 (Fig. 7A), which implies that in addition to halide dissolution, carbonatite and silicate minerals dissolutions account for additional of Na in the system. The strong correlation coefficient of Na and K of 0.95 (Table 10) indicates that dissolution of nephelines and carbonatites contributes to the Na and K in groundwater, however, the weathering of augite and ionic exchange in zeolites could have contributed to the addition of Na as a result of higher Na/K ratio > 1 (Fig. 7 B).

Table 11: The correlation coefficients of chemical constituents for Emakat Lake and the associated springs

Emakat Lake	F	Cl	SO4	NO3	PO2	HCO	CO3	Na	K	Mg	Ca	Springs
F	1	0.65	0.58	0.58	-0.76	0.8	0.24	0.66	0.66	0.58	0.25	**F**
Cl	0.89	1	0.85	0.27	-0.34	0.88	-0.49	0.91	0.97	0.54	-0.21	**Cl**
SO4	-0.79	-0.77	1	0.33	-0.62	0.94	-0.51	0.98	0.91	0.55	-0.14	**SO4**
NO3	-0.41	-0.44	0.29	1	-0.69	0.54	0.38	0.42	0.23	-0.15	0.54	**NO3**
PO2	0.09	0.28	-0.42	-0.4	1	-0.75	-0.24	-0.61	-0.43	-0.42	-0.32	**PO2**
HCO	-0.66	-0.45	0.48	0.77	-0.18	1	-0.27	0.97	0.91	0.57	0.01	**HCO**
CO3	-0.76	-0.68	0.64	-0.13	0.05	0.29	1	-0.48	-0.55	-0.38	0.81	**CO3**
Na	-0.74	-0.47	0.58	0.1	0.12	0.65	0.76	1	0.95	0.55	-0.13	**Na**
K	-0.48	-0.16	0.36	-0.01	0.18	0.59	0.59	0.94	1	0.67	-0.3	**K**
Mg	-0.12	0.16	0.09	-0.09	0.05	0.43	0.24	0.64	0.82	1	-0.56	**Mg**
Ca	0.45	0.32	-0.23	0.1	-0.19	-0.03	-0.27	-0.33	-0.17	0.23	1	**Ca**
	F	**Cl**	**SO4**	**NO3**	**PO2**	**HCO**	**CO3**	**Na**	**K**	**Mg**	**Ca**	

The source of Ca in groundwater can be studied through Ca/Mg ratio whereby the ratio of one is attributed by calcite contribution while a higher Ca/Mg ratio (Ca/Mg > 2) indicate the contribution of dissolution of silicate minerals in addition to calcite (Liu *et al.,* 2020). A majority of samples from springs showed a higher Ca/Mg ratio (Ca/Mg > 2) (Fig. 7 C), implying that in addition to calcite dissolution, the dissolution of silicate minerals mainly augite and melilites accounted for the addition of Ca in groundwater. Since the ratio of $(Ca+Mg)/HCO_3$ vs Cl was < 0.5 did not increase with increased salinity (Fig. 7 D), the release of Ca and Mg to the groundwater was at a lower extent compared to HCO_3 and the major source of Ca and Mg could have been dissolutions of carbonates and weathering of pyroxenes (Kumar *et al.,* 2014).

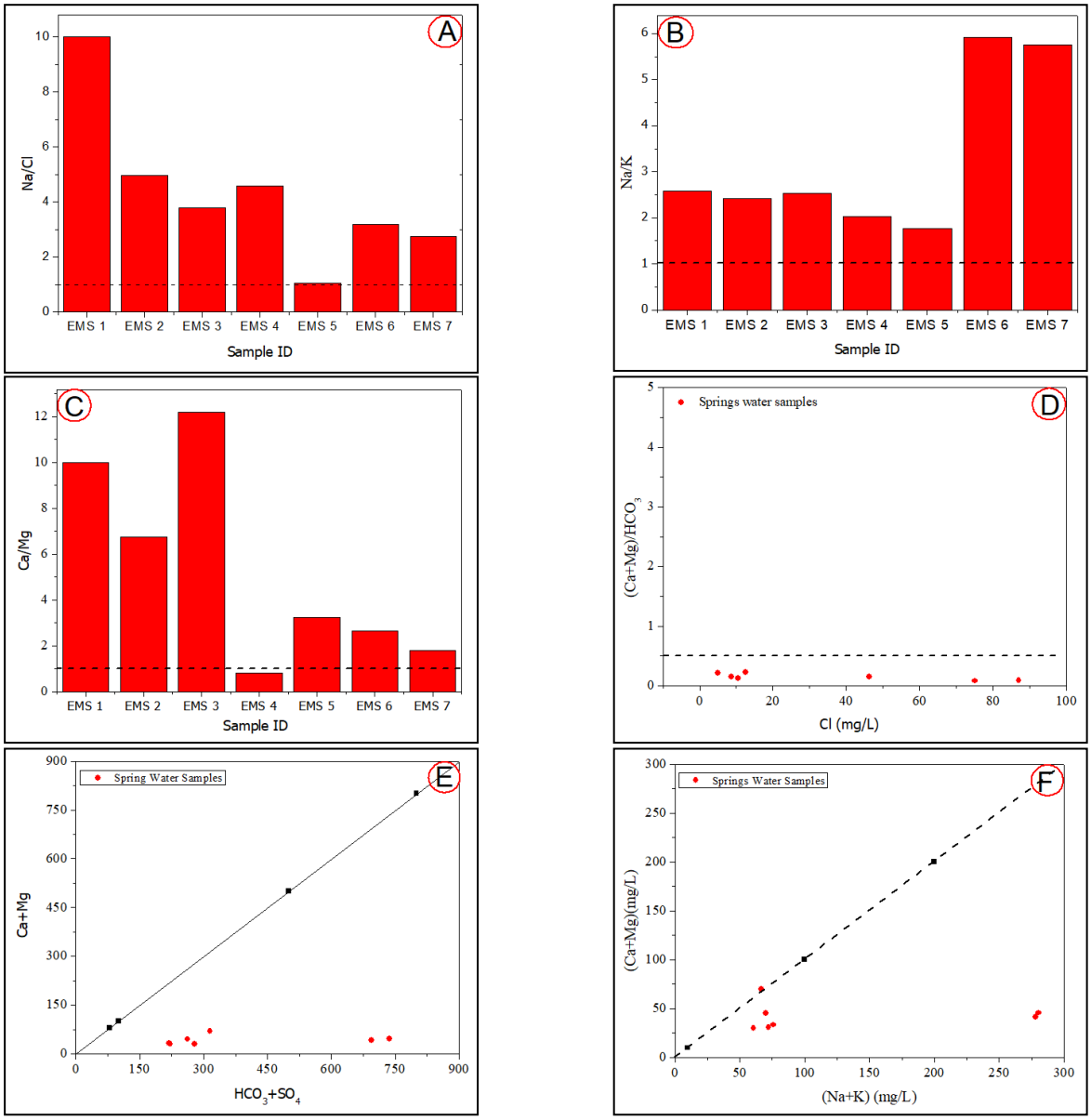

Figure 7: The graphical representation of the chemical characteristics for the springs associated with Emakat Lake

Plots of SO_4+HCO_3 vs Ca+Mg and Na+K vs Ca+Mg can aid in studying the cation exchange processes in groundwater whereby the displacement to right indicate ion exchange and reverse ion exchange occurs when there is displacement to the left of the 1:1 line (Kumar *et al.,* 2014; Liu *et al.,* 2020). The plots for the springs in the study area (Fig. 7 E & F) showed that the springs were displaced to the right of the 1:1 line, indicating that the ion exchange dominated the level of Ca and Mg in the groundwater and the displacement to right was due to excess SO_4+HCO_3 and Na+K over Ca+Mg (Kumar *et al.,* 2014).

Evaporation, solute loss to mineral crystallization, and precipitation are all closely linked to climatic conditions of the crater lakes location whereby evaporation which is more than precipitation results in increased dissolved ions saturating the solution, hence mineral

crystallization (Armienta *et al.,* 2008). The higher evaporation that surpasses rainfall at the Empakaai Crater increased the solute concentration of Emakat Lake. However, some ions may reach saturation point and hence are lost from the lake through mineral crystallization (Armienta *et al.,* 2008). A plot of Cl with other ions can assist in assessing the ions which act conservatively in the system and determine those which act non-conservatively over the evaporative concentration and hence removed from the system (Deocampo, 2004).

The plot of the major ions of Emakat Lake showed that Na, K, and alkalinity acted conservatively while Ca, Mg, Si, and SO_4 acted non-conservatively over the evaporative concentration (Fig. 8) which imply that the conservative ions increased with increasing evaporation while the non-conservative were removed from the lake by mineralization (Deocampo, 2004). The rate of removal of Ca and Mg from the lake through recrystallization is higher than Si and SO_4.

The Saturation Index (SI) of minerals in a water body can aid in depicting the cationic status and source in a water body where $SI > 0$ indicates super saturation and hence mineral precipitation, while $SI<0$ indicates under saturation and hence water remain in a state of weathering more minerals and $SI=0$ indicates that mineral phase remains to be in equilibrium (Zhang *et al.,* 2020).

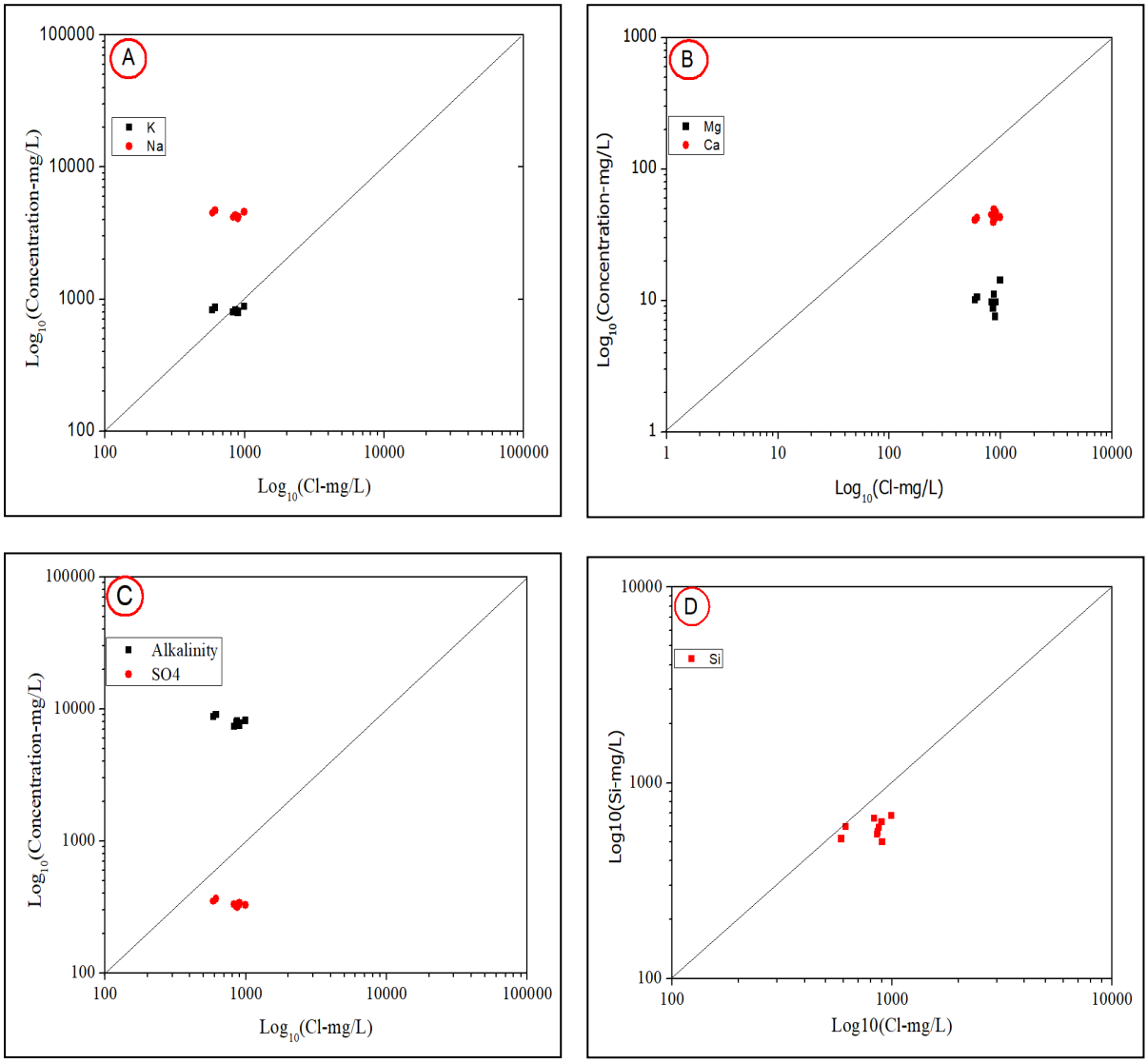

Figure 8: Major solute concentration of Emakat Lake plotted against Cl, a conservative ion over the evaporative

The saturation index of the Emakat Lake, springs inside the Crater, springs outside the crater, and springs at the foot of the crater calculated by PHREEQC software are presented in Table 11. The results showed that mineral precipitation in the lake occur in three phases, the kerolite phase (talc, chrysotile, and sepiolite), calcite phase (dolomite, calcite, and aragonite), and the amorphous phase (quartz and chalcedony) while the springs inside and outside the crater are commonly dominated by calcite and amorphous phases with minor domination of kerolite phases, however, it is different for springs at the foot of the crater which characterized by the occurrence of minor phases of talc and Sylvite.

Table 12: Saturation indices of Emakat Lake and associated springs by which positive values indicate super-saturation, whereas negative values reflect sub-saturation

Mineral	Saturation Indices																		
	Lake													Springs					
	EM 1.1	EM 1.2	EM 2.1	EM 2.2	EM 2.3	EM 3.1	EM 3.2	EM 3.3	EM 3.4	EM 3.5	EM 4.1	EM 4.2	EM 4.3	EMS 1	EMS 2	EMS 3	EMS 4	EMS 5	EMS 6	EMS 7
Talc	16.19	15.24	16.21	15.29	15.19	15.18	15.51	14.9	15.28	19.55	15.39	15.54	15.1	0.07	-0.37	0.61	0.3	-0.47	8.4	-8.26
Chrysotile	10.25	9.46	10.6	9.47	9.39	9.18	9.52	9.05	9.28	9.29	9.8	9.51	9.29	-3.84	-4.23	-1.56	-2.53	-3.44	-9.82	-10.94
Sepiolite	8.66	8.03	8.53	8	7.98	8.01	8.27	7.93	8.25	8.53	8.1	8.32	8.04	-2.11	-2.42	-2.07	-2.14	-2.75	-8.68	-8.31
Dolomite	5.22	4.8	5.05	4.82	4.87	4.76	4.89	4.81	4.81	4.71	5.01	4.83	4.84	-0.51	0.37	1.97	0.67	0.49	-0.47	-1.56
Calcite	2.68	2.49	2.57	2.49	2.5	2.5	2.54	2.49	2.47	2.38	2.51	2.51	2.5	-0.12	0.59	1.41	0.18	0.37	-0.34	-0.76
Aragonite	2.54	2.34	2.43	2.34	-2.87	2.36	2.39	2.34	2.32	2.23	2.36	2.36	2.35	-0.28	0.44	1.26	0.03	0.22	-0.48	-0.91
Fluorite	2.44	2.35	2.31	2.35	2.33	2.23	2.42	2.33	2.32	2.24	2.37	2.39	2.34	-2.81	-1.28	0.2	-0.8	-0.71	-0.15	0.34
Quartz	1.59	1.51	1.4	1.52	1.51	1.62	1.62	1.57	1.65	1.8	1.41	1.65	1.55	0.63	0.61	-0.24	0.1	0.14	-0.71	-0.7
Chalcedony	1.15	1.07	0.97	1.08	1.07	1.18	1.17	1.12	1.2	1.34	0.97	1.2	1.1	0.17	0.15	-0.7	-0.36	-0.32	-1.14	-0.5
Gypsum	-2.35	-2.54	-2.5	-2.53	-2.53	-2.55	-2.48	-2.55	-2.57	-2.67	-2.57	-2.52	-2.54	-3.69	-2.58	-2.62	-2.76	-3.94	-1.66	-2.14
Anhydrite	-2.69	-2.88	-2.82	-2.86	-2.87	-2.89	-2.84	-2.92	-2.95	-3.06	-2.91	-2.87	-2.91	4.1	-3	-3.03	-3.17	-4.32	-1.96	-2.46
Halite	-3.96	-3.95	-3.96	-3.95	-3.94	-3.99	-3.96	-3.95	-3.96	-3.98	-3.88	-3.96	-3.94	-8.95	-8.15	-8.46	-7.84	-7.2	-5.92	-5.89
Sylvite	-4.24	-4.24	-4.23	-4.24	-4.16	-4.25	-4.24	-4.17	-4.18	-4.19	-4.15	-4.24	-4.16	-8.79	-8.02	-8.38	-7.67	-6.97	-6.4	6.78

The domination of kerolite and calcite phases in the lake indicates the existence of continuous removal of Mg^{2+} and Ca^{2+} phases from the system through precipitation whereby Mg^{2+} is removed first from the system as hydrated Mg silicates while Ca^{2+} is removed during carbonate precipitation with minor or no Mg (Campodonico *et al.,* 2019). The amorphous phase in Emakat Lake is the next precipitation phase because the high pH increased the solubility of silica, hence limiting the silica precipitation despite the high silica content resulting from weathering of volcanic formation (Schagerl, 2016). Sub-saturation of SO_4^{2-} phases (gypsum and anhydride) indicates the less removal of SO_4^{2-} from the system which is unusual for the lake system with elevated pH and alkalinity, however, a combination of multiple weathering reaction might have attributed to this (Schagerl, 2016). However, the higher carbonate content in the system buffers the precipitation of SO_4^{2-} with Ca^{2+} (Deocampo, 2018).

The hydrochemical characteristics of rainfall in East Africa reflect the influence of the monsoon winds and the seasonal movements of the Intertropical Convergence Zone (ITCZ) as it is composed of marine aerosols from the Indian Ocean, locally airborne dust, and dissolved gases mainly CO_2 (Schagerl, 2016). The combination of atmospheric moisture and CO_2 gas forms carbonic acid which falls to the ground in its disassociation form (HCO_3^- and H^+) or as acid rain of both states influence the groundwater and lake water evolution since it influences the dissolution and weathering of carbonates and silicate minerals (Wilson, 2004). The interaction of rainwater with the inner walls of the Empakaai Crater influences the weathering of nepheline, pyroxenes, and melilites, the dissolution of carbonates, and the ion exchange in zeolites as a result of enrichment in Ca and depletion in Na and K for the secondary rocks (Greenwood, 2014). This process was reflected in Emakat Lake by the strong correlation coefficient of Na and Mg of 0.64 (Table 10) since they are removed easily in solid-phase during water-rock interaction (Varekamp *et al.,* 2000).

Hydrothermal inputs play a major role in solute contribution to the crater lakes especially on active volcanic craters since they directly impact the concentration of Mg, Na, SO_4, and pH (Armienta *et al.,* 2008). To assess the contribution of the hydrothermal inputs, the $Cl+SO_4$, and pH comparison approach is used where lakes are clustered into three groups based on their neutralizing agents as CO_2-dominated lakes, quiescent lakes, and active acid lakes (Varekamp *et al.,* 2000). A $Cl+SO_4$ vs pH plot for Emakat Lake (Fig. 9A) classified it as a quiescent lake where the dominant neutralizing agents are neither CO_2 dissolution from the atmosphere nor input from active volcanic activities.

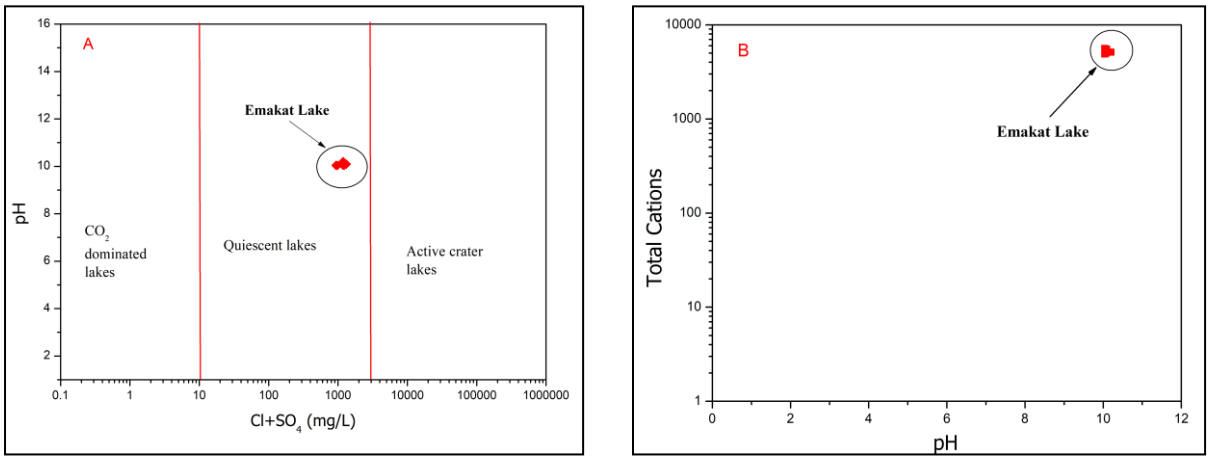

Figure 9: **(A) Lakes classification based on the nature of their neutralization source; (B) Assessment of cation source based on the comparison of pH and total cation of the Emakat Lake**

The cation increase in crater lakes is mostly attributed to the rock-water interaction induced by the volcanic activities which lower pH and increase solubility of rocks hence releasing solutes to the solution. This implies that the higher cationic level in crater lakes occur at lower pH (Armienta *et al.,* 2008). A plot of pH vs total cation of Emakat Lake showed that the total cation increased with increasing pH (Fig. 9 B), implying that the cations of the lake are attributed to other factors than hydrothermal inputs. In this kind of lake, the hydrochemical characteristics of groundwater inflow play a major role in the solute concentration, hence understanding the hydrochemical evolution of the lake requires the understanding of the hydrochemical characteristics and evolution of the lake inflow components (Armienta *et al.,* 2008).

4.2 Water balance of Emakat Lake

4.2.1 Water Balance Parameters Estimations

(i) Lake Volume

The estimation of Emakat Lake volume changes from the combination of the DEM, bathymetric survey, GPS coordinates, and the inter-annual lake volume changes of 0.4 m according to Ryner *et al.* (2008) resulted in an average maximum and minimum lake water levels of 2216.57 MAMSLand 2216.17 MAMSL, respectively. This resulted in a maximum volume of 292 564 175.58 m^3 and a minimum lake volume of 289 515 085.03 m^3 attained in the rainy and dry seasons, respectively, hence, an annual lake water volume change of 3 049 090.55 m^3.

(ii) Rainfall

The validation of the CHIRPS data with the ground-collected data from Monduli, Ngorongoro HQ, and Nainokanoka through the trend analysis monthly rainfall bar chart (Fig. 10) showed a satisfactory trend on Nainokanoka and Monduli compared to the Ngorongoro HQ station. However, there was a variation of the trend which are over-estimation and underestimation of rainfall for the Monduli and Nainokanoka respectively. The performance test of the CHIRPS data against the ground rainfall data collected from the study areas yielded different results (Table 12). The R^2 for the monthly CHIRPS rainfall at the Ngorongoro HQ, Nainokanoka, and Monduli stations resulted in the values of 0.1072, 0.2321, and 0.5140, respectively while the monthly average values resulted in 0.6954, 0.8527, and 0.5149, respectively (Fig. 11). This implies that the CHIRPS performance in rainfall prediction was better on the monthly averages compared to the monthly rainfall estimation.

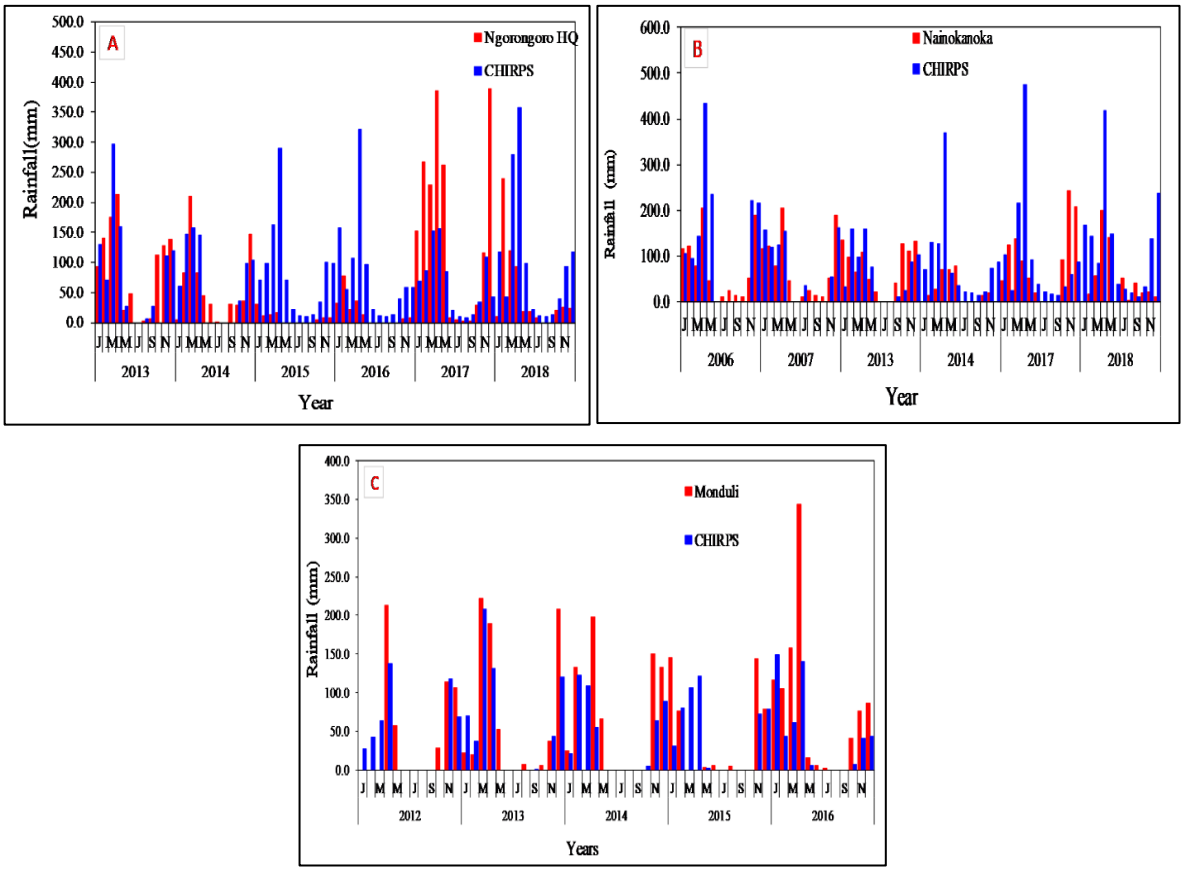

Figure 10: The bar charts for the trend analysis test of rainfall for ground collected and the CHIRPS data; (a) Ngorongoro HQ for 2013 to 2018 (b)Nainokanoka for 2006, 2007, 2013, 2014, 2017, and 2018 (c) Monduli for 2012 to 2016

Table 13: The data performance for validation of the CHIRPS data with three stations: Monduli, Nainokanoka, and Ngorongoro HQ stations

Station	Ngorongoro HQ	Nainokanoka	Monduli
Coefficient of determination (R^2) for Monthly Rainfall	0.1072	0.2321	0.514
Coefficient of determination (R^2) for Average Monthly Rainfall)	0.6954	0.8527	0.7974
Nash Sutcliffe model efficiency coefficient (NSE)	0.72	-1.12	0.32
Root mean square error (RMS)	0.53	0.97	0.69
BIAS	0.74	1.48	1.25

The NSE performance ranges between -∞ to 1. While NSE =1 is considered a perfect prediction, NSE > 0.75 is classified as good, 0.75 > NSE >0.36 is classified as satisfactory while NSE < 0.36 is classified as unsatisfactory (Tomy & Sumam, 2016). Among the three comparisons, the Ngorongoro station yielded a satisfactory NSE of 0.72 while Nainokanoka and Monduli yielded test results of -1.12 and 0.32, respectively (Table 12). The bias test results to 0.74, 1.48, and 1.25 for Ngorongoro HQ, Nainokanoka, and Monduli, respectively which implies that Ngorongoro HQ underestimated rainfall by 26% while Nainokanoka and Monduli over-estimated rainfall by 48% and 25%, respectively. The RMSE test showed that Ngorongoro HQ had the lowest RMSE of 53% followed by Monduli 69% then Nainokanoka 97%. The overall statistical test shows that the CHIRPS data performed better on the two stations; Monduli and Ngorongoro HQ while poor performance was portrayed on most of the statistical tests at Nainokanoka station except for the monthly average of R^2 by which the Nainokanoka station performs better than other stations.

The statistical tests of all stations performed better on R^2 for the monthly average while Nainokanoka outperformed all stations suggesting that the CHIRPS data in the study area could perform better on the prediction of the monthly average rainfall. This result correspond with the recently performed validation of the CHIRPS data excuted with the Arusha station which concluded that, CHIRPS can perform better on monthly timescale in the area (Mwabumba *et al.,* 2022). The average rainfall of the Empakaai Crater was estimated from the extracted rainfall values of the six CHIRPS grids covering the crater for a range of time from 2006 to 2018. The average annual rainfall obtained is 878.68 mm which falls in the same range of 600 to 1000 mm annual rainfall for the Crater Highlands (Ryner *et al.,* 2006).

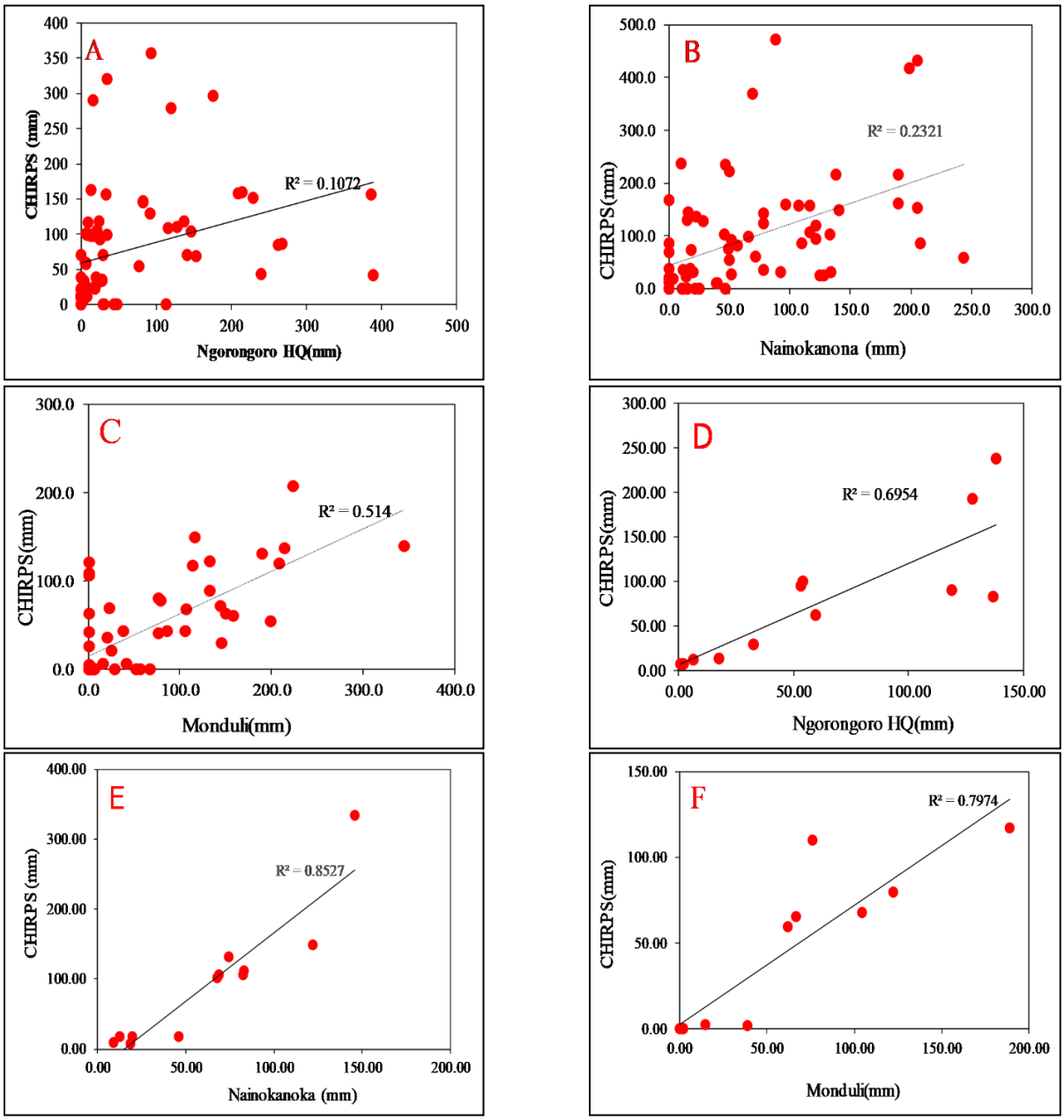

Figure 11: **The graphs of the coefficient of determination (R2) test of the ground collected data against the CHIRPS data; (a) Monthly test at Ngorongoro HQ for 2013-2018 (b) Monthly test at Nainokanoka for 2006, 2007, 2013, 2014, 2016 and 2018 (c) Monthly test at Monduli for 2012-2016; (d) Average monthly test at Ngorongoro HQ for 2013-2018 (e) Average monthly test at Nainokanoka for 2006,2007, 2013, 2014, 2016 and 2018 (f) Average monthly test at Monduli for 2012-2016**

(iii) Runoff by CN Method

Land use and Landcover

The LU/LC map of the Empakaai Crater was obtained from the vegetation type classified according to Ryner *et al.* (2006), which are montane forest about 10%, wooded grassland about 40%, and the highland shrubs (thickets) about 50% (Fig. 12).

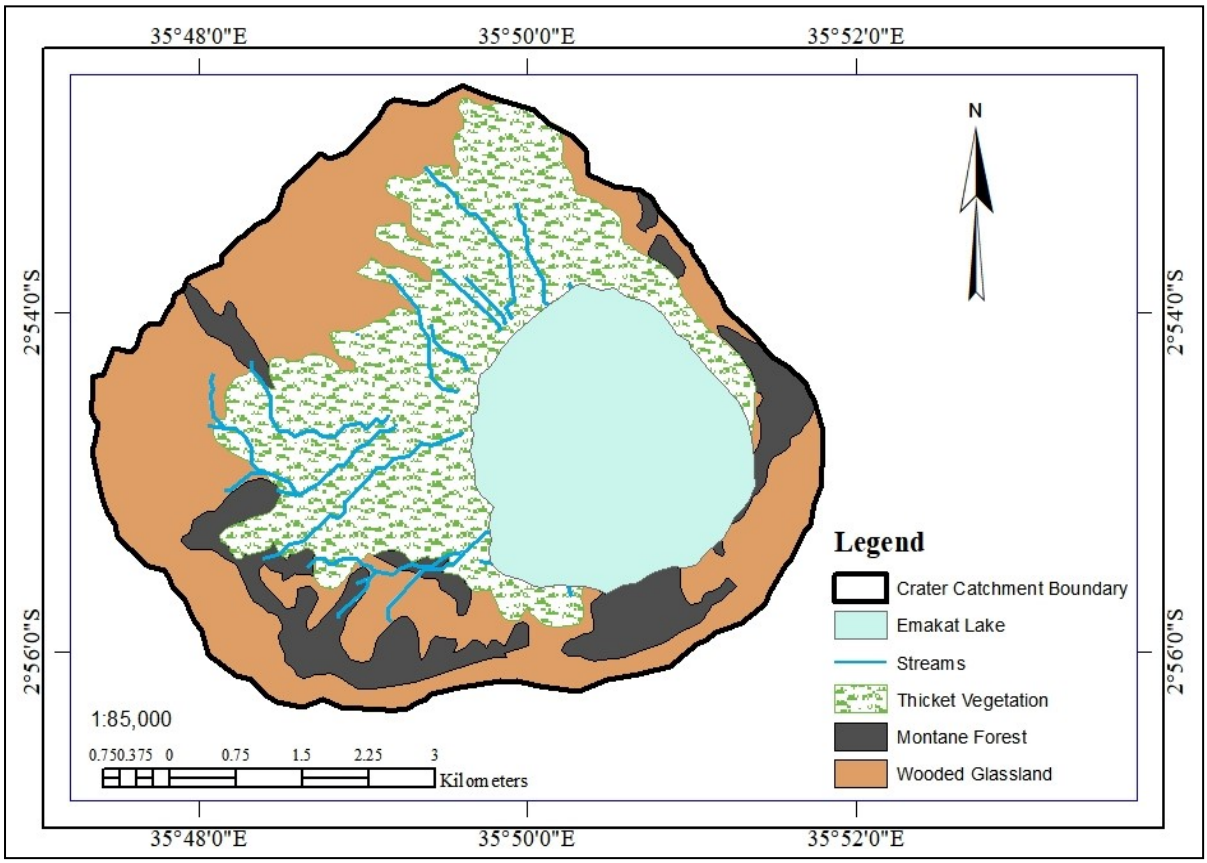

Figure 12: The LU/LC Map based on vegetation distribution

Soil Classification

The Empakaai Crater is covered by volcanic soil classified as the Eutric Nitosol which forms through free drainage in an area with rainfall between 750 to 1000 mm and temperature between 13 and 15ºC while its thickness range above 50 cm (Samki & Baker, 1977). The soil sample collected from the Empakaai Crater indicated that it is sandy loam with 71.59% sand, 17.78% silt, and 10.63% clay (Table 13). The soil classification at Empakaai Crater exhibited a moderately high infiltration rate and hence a low runoff coefficient (Ross *et al.,* 2018).

Table 14: Analysis results for the soil sample collected at Empakaai Crater

Sample Name	Parameter	Description
Empakaai Soil Sample 1	Sand	71.59
	Silt	17.78%
	Clay	10.63%
	Textural Class	Sandy Loam
	Average Moisture Content	31.60%

Hydrological soil group

The combination of the soil characteristics and the slope classification (Fig. 13) done from the DEM, the HSG map (Fig. 14) where HSG were identified which are HSG A, HSG B, HSG C, and HSG D. A combination of the land-use map and the HSG map resulted into three hydrological soil-cover complexes (Fig. 15). A summary of the obtained hydrologic soil-cover complex with their respective curve numbers is presented in Table 14.

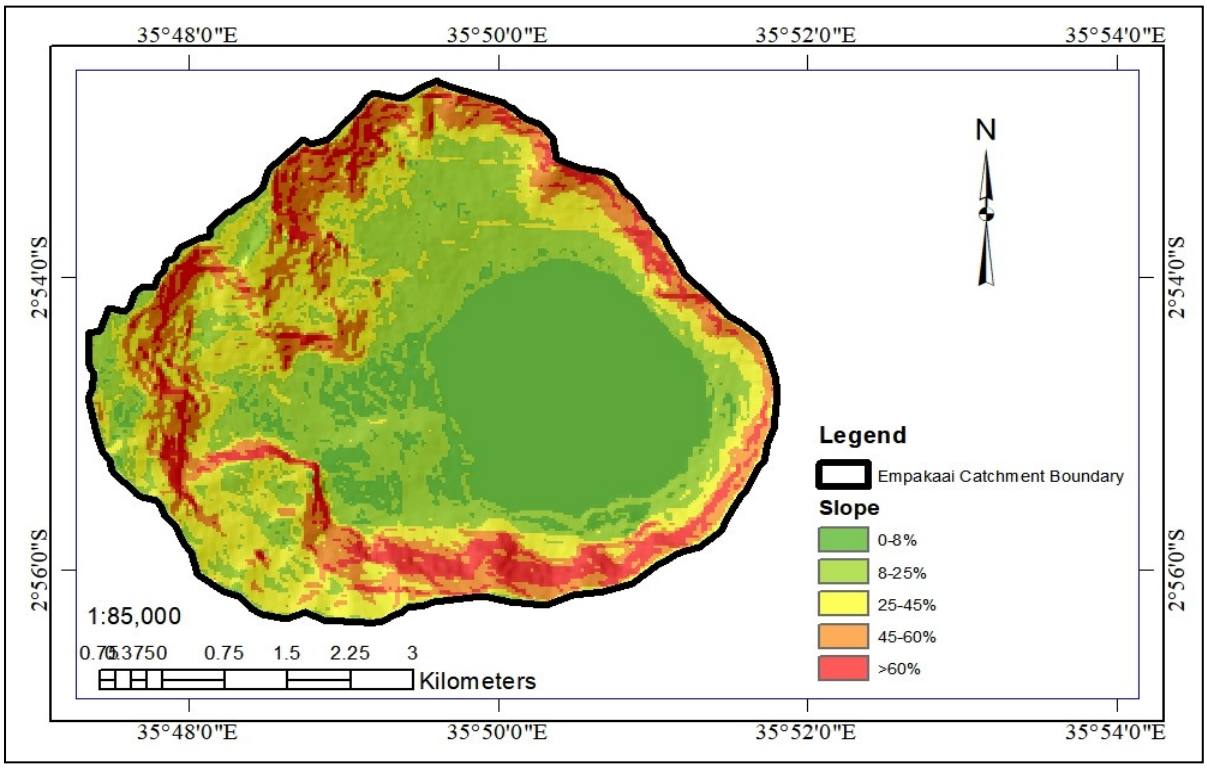

Figure 13: The slope classification map obtained from DEM for the Empakaai Crater

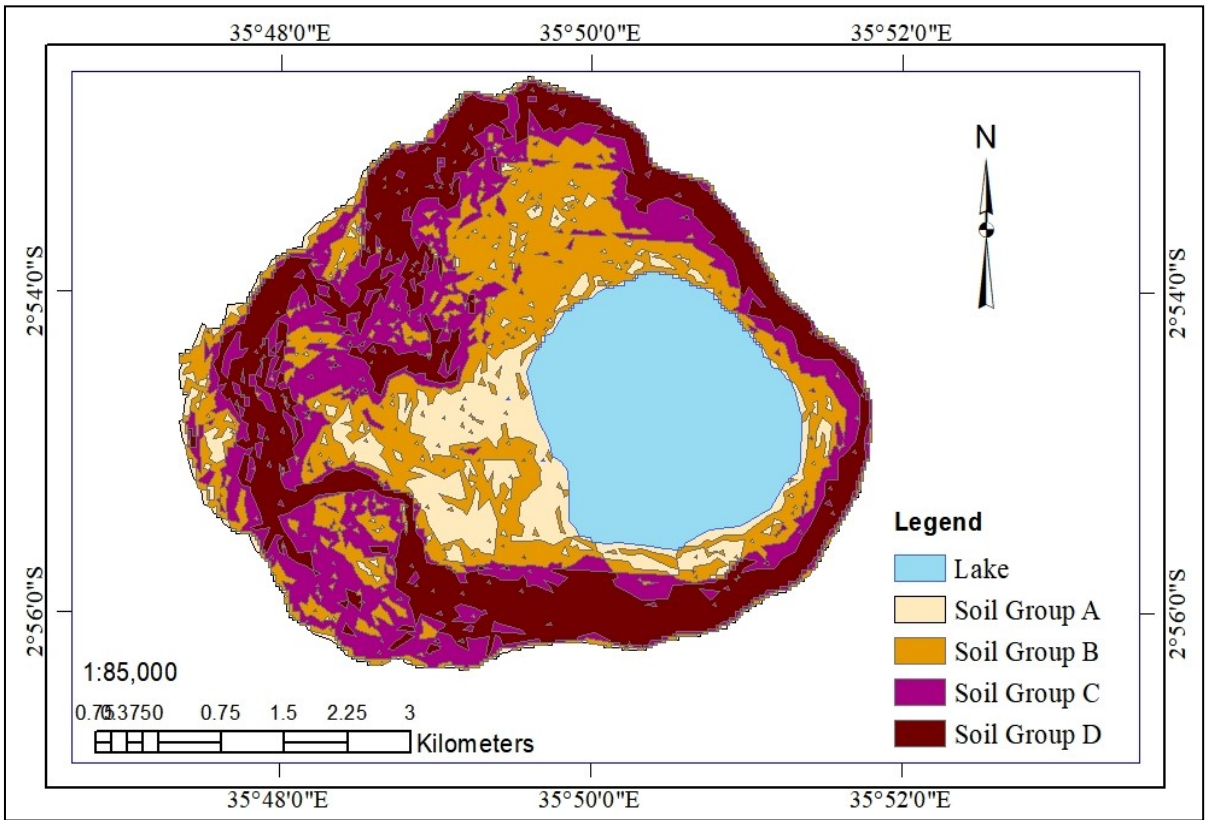

Figure 14: The map showing the hydrologic soil groups (HSG) classification

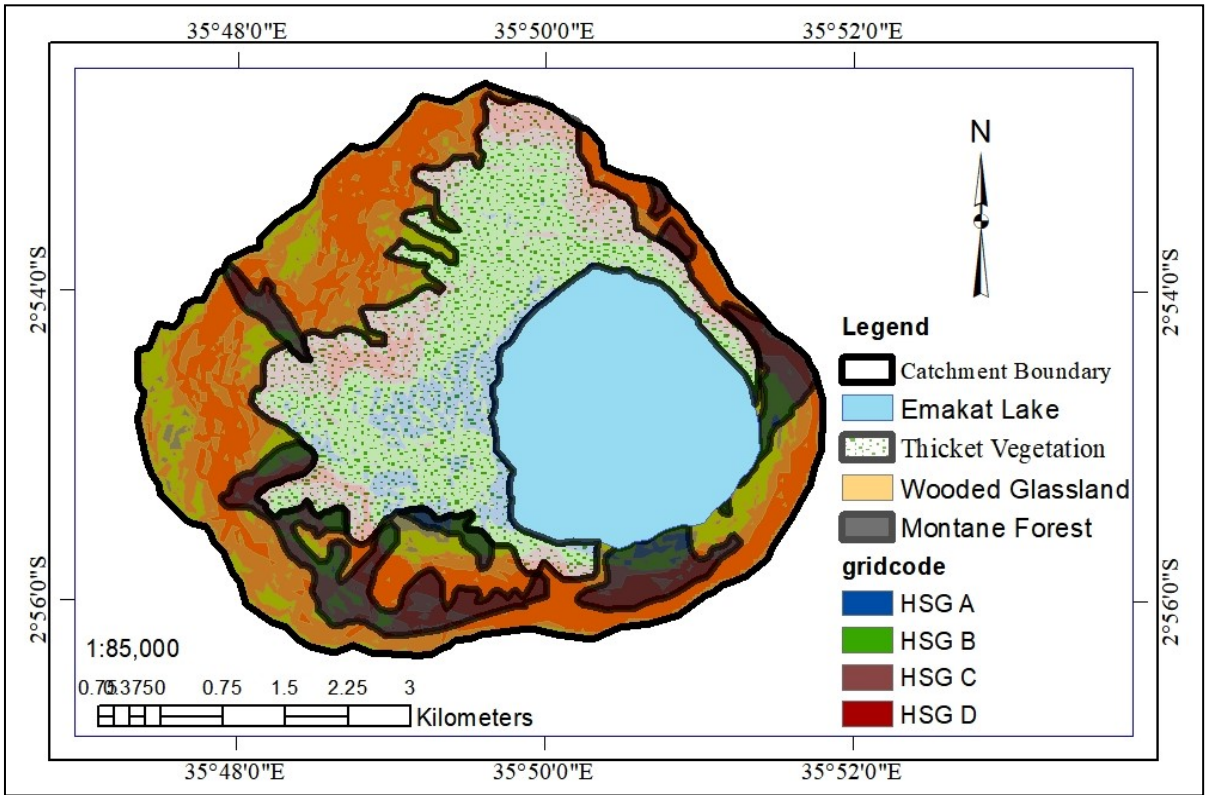

Figure 15: The map of the Empakaai Crater Catchment showing the three hydrological soil cover complex

Table 15: The summary of the hydrological soil-cover complex table corresponding to the hydrological characteristics of Empakaai catchment

Land Cover				Hydrologic Soil Groups (HSG)			
Vegetation type	**Composition**	**Description**	**Hydrologic Condition**	**A**	**B**	**C**	**D**
Montane	*Nuxia congesta*, *Juniperus Procera*, *Croton Machrostachys*, and *Hagenia abyssinica*	Woods protected from grazing and litter and brush adequately cover the soil)	Good	30	55	70	77
Wooded Glassland	*Solanum incunum* and *Croton machrostachys*	Woods glass combination	Fair	43	65	76	82
Thickets	*Clematis simensis*	Meadow-continuous grass protected from grazing	Good	30	58	71	78

Runoff

The area of each hydrological unit in the hydrological soil-cover complex was calculated, the respective CN was identified, and hence a weighted CN of 67.36 potential maximum retention after runoff begins of 109.70 (Table 15). The monthly runoff from the monthly rainfall of the Empakaai Crater estimated from CHIRPS data and the respective runoff is presented in Table 17 but the annual runoff obtained is 332.42 mm.

Table 16: The weighted curve number calculation from the hydrological soil-cover complex

Land Cover		Soil Group	CN	AMC	Area (m^2)	CNxArea
Vegetation	**Hydrological Condition**					
Thicket Vegetation	Good	B	58	AMC II	6 462 360.53	374 816 910.87
	Good	C	71	AMC II	2 640 116.48	187 448 270.23
	Good	A	30	AMC II	1 911 959.97	57 358 799.18
	Good	D	78	AMC II	1 360 710.14	106 135 390.73
Wooded Grassland	Fair	B	65	AMC II	2 972 711.20	193 226 228.17
	Fair	C	76	AMC II	4 634 527.87	352 224 118.11
	Fair	A	43	AMC II	484 319.36	20 825 732.33
	Fair	D	82	AMC II	6 098 554.27	500 081 450.42
Montane Forest	Good	B	55	AMC II	55 581.51	3 056 983.23
	Good	B	55	AMC II	464 976.69	25 573 717.81
	Good	B	55	AMC II	138 011.38	7 590 626.07
	Good	B	55	AMC II	214 285.29	11 785 690.93
	Good	B	55	AMC II	253 948.83	13 967 185.54
	Good	B	55	AMC II	6 985.85	384 221.56
	Good	C	70	AMC II	188 374.95	13 186 246.47
	Good	C	70	AMC II	727 892.10	50 952 447.06
	Good	C	70	AMC II	17 968.34	1 257 783.76
	Good	C	70	AMC II	168 831.15	11 818 180.42
	Good	C	70	AMC II	189 392.44	13 257 470.87
	Good	C	70	AMC II	6 168.14	431 770.10
	Good	C	70	AMC II	13 779.49	964 564.39
	Good	A	30	AMC II	794.03	23 820.83
	Good	A	30	AMC II	14 611.66	438 349.87
	Good	A	30	AMC II	81 088.98	2 432 669.27
	Good	A	30	AMC II	130 277.06	3 908 311.88
	Good	A	30	AMC II	22 097.48	662 924.38
	Good	D	77	AMC II	94 041.64	7 241 206.13
	Good	D	77	AMC II	873 594.48	67 266 775.26
	Good	D	77	AMC II	701.09	53 983.85
	Good	D	77	AMC II	442 955.29	34 107 557.13
	Good	D	77	AMC II	243 660.37	18 761 848.66
	Good	D	77	AMC II	90 954.73	7 003 514.59
	Good	D	77	AMC II	45 832.16	3 529 076.15
				Sum	**31 052 064.96**	**2 091 773 826.24**
				Weighted Curve Number		**67.36**
				Potential Maximum Retention after runoff begins (S)		**109.70**

Table 17: The monthly rainfall of Empakaai Crater obtained as an average of six CHIRPS point grids for the time series of 2006 to 2018 with their respective monthly runoff obtained through the curve number method

Months	Average Rainfall (mm)	Average Runoff (mm)
January	77.26	18.55
February	77.05	18.43
March	133.42	56.19
April	247.14	151.44
May	57.71	8.8
June	20.11	0.03
July	8.19	1.97
August	10.53	1.32
September	5.46	2.91
October	31.07	0.7
November	105.97	36.45
December	104.77	35.64
Annual (mm)	**878.68**	**332.42**

(iv) Evaporation

The evaporation over the Emakat Lake computed by the D-K model utilized ρ_w of 1000 Kg/m^3 and the λ of 2.45 MJ/ kg (Duan *et al.,* 2018). The slope of the saturation curve (Δ) was computed using the monthly average temperature (T) while the psychometric constant (γ) was computed from the atmospheric pressure which is dependent on the altitude (Zotarelli *et al.,* 2018), and the altitude of 2215 MAMSLwas used for Emakat Lake. The annual evaporation from Emakat Lake was established to be 1694.57 mm (Table 17).

Table 18: Parameters for evaporation computation by D-K Model

Month	Air temperature		Surface temp. To(ºC)	Shortwave radiation Rs(W/m^2)	Extra-terrestrial Radiation Ra (W/m^2)	Net Radiation Rn(W/m^2)	Evaporation (mm)
	Tmin(ºC)	Tmax(ºC)					
January	7.09	17.47	20.29	695.11	432.05	483.38	175.65
February	10.44	18.81	20.18	805.08	441.89	564.42	141.36
March	16.72	23.11	19.75	678.78	440.37	475.29	187.84
April	12.01	17.08	15.91	546.28	419.64	375.77	166.00
May	12.56	16.96	16.31	409.61	390.76	273.82	169.63
June	11.42	16.56	17.23	405.61	373.94	266.01	24.84
July	8.97	14.49	17.98	488.70	380.86	323.12	89.27
August	8.97	16.69	19.88	603.82	405.81	409.96	136.78
September	9.49	19.06	21.80	793.57	430.35	551.05	228.93
October	10.06	18.27	22.93	646.77	438.89	452.33	163.26
November	9.42	20.11	20.69	682.88	432.85	475.19	51.91
December	6.99	16.54	18.43	529.40	427.04	366.56	159.12
Annual Evaporation (mm)							**1694.57**

4.2.2 Isotopic characteristics

The stable isotope of Emakat Lake ranged between 3.28 to 3.96‰ with an average of 3.65‰ for $\delta^{18}O$ and range of 31.99 to 33.93‰ with an average of 33.07 for $\delta^{2}H$ while the d-excess range between 1.57 and 5.77‰. The isotopic composition of the springs ranged between -5.18‰ to -4.05‰ with an average of -4.69‰ for $\delta^{18}O$ and range of -26.62 to -19.48‰ with an average of -23.59‰ for $\delta^{2}H$ while the d-excess range from 12.39 to 15.19‰. The isotopic composition of rainfall ranged from -14.2 to 2.52‰ with an average value of -8.06‰ for $\delta^{18}O$ and ranging from -98.25‰ to 4.25‰ with an average of 54.37‰ for $\delta^{2}H$. The isotopic composition of evaporation on the Empakaai Crater estimated by the C-G model resulted in 1.47 and 1.09‰ for $\delta^{18}O$ and $\delta^{2}H$ respectively with a d-excess value of 10.70‰ (Table 18). The collected data from Emakat Lake and springs and the estimated isotopic data of evaporation were both plotted on the meteoric line graph (Fig. 16).

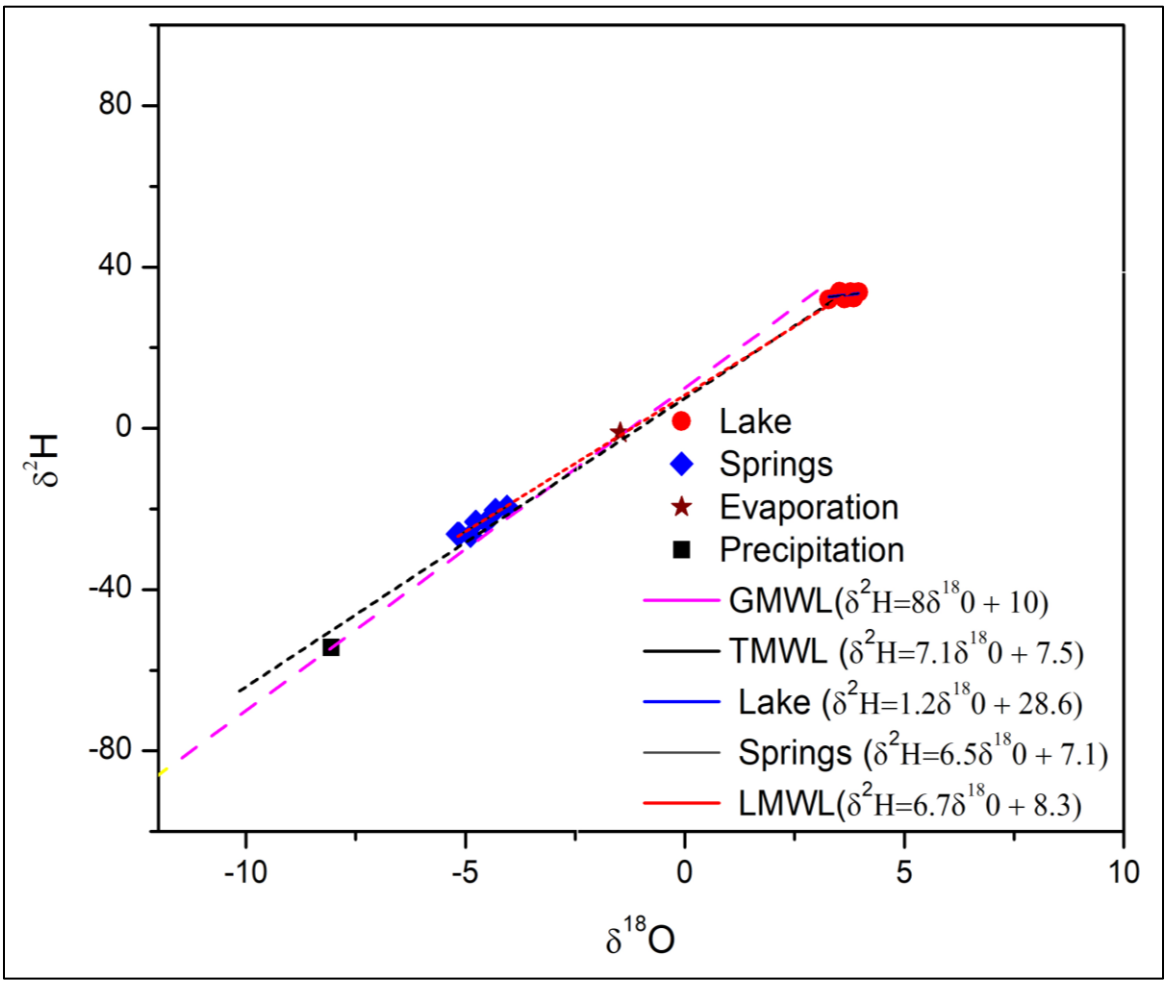

Figure 16: The graph showing the isotopic variation of $\delta^{2}H$ Vs $\delta^{18}O$ along the Global (GMWL) and Tanzania (TML) Meteoric lines

Table 19: The isotopic composition of Emakat Lake and the associated springs

Code	Source	^{18}O ‰	D ‰	d-excess ‰	Code	Source	^{18}O ‰	D ‰	d-excess ‰
EM 1.1	Lake	3.53	33.93	5.69	EMS 3	Spring on outer crater rim	-4.52	-23.14	13.02
EM 1.2	Lake	3.51	33.58	5.5	EMS 4	Spring on outer crater rim	-4.31	-20.29	14.19
EM 2.1	Lake	3.96	33.77	2.09	EMS 5	Spring on outer crater rim	-4.05	-19.48	12.92
EM 2.2	Lake	3.85	32.39	1.59	EMS 6	Spring at Crater foot	-5.14	-26.19	14.93
EM 2.3	Lake	3.61	31.02	2.14	EMS 7	Spring at Crater foot	-4.88	-26.62	12.42
EM 3.1	Lake	3.64	32.13	3.01	EMR 1	Rain Sample	-0.76	4.25	10.33
EM 3.2	Lake	3.78	33.72	3.48	EMR 2	Rain Sample	-9.14	-67.21	5.91
EM 3.3	Lake	3.62	32.35	3.39	EMR 3	Rain Sample	-8.12	-56.25	8.71
EM 4.1	Lake	3.28	31.99	5.75	EMR 4	Rain Sample	-14.2	-98.25	15.35
EMS 1	Spring on inner crater rim	-5.18	-26.22	15.22	EME 1	Evaporation	-1.47	-1.09	10.7
EMS 2	Spring on inner crater rim	-4.76	-23.19	14.89					

The Global Meteoric Water Line (GMWL) was drawn in accordance to the equation $\delta^2H = 8\delta^{18}O + 10$ (Atomic *et al.,* 1992) while the deuterium (δ^2H) and oxygen ($\delta^{18}O$) values for precipitation collected from 1961 to 2016 by International Atomic Energy Agency (IAEA), Dodoma and Dar es salaam was utilized to plot the Tanzania meteoric Water Line (TMWL) while the line yielded an equation of $\delta^2H = 7.1\delta^{18}O + 7.5$. The samples from Emakat Lake and the springs plotted to form the Local Meteoric Water Line (LMWL) with equation $\delta^2H = 6.7\delta^{18}O + 8.3$ whereas the Samples from Emakat Lake formed the Emakat Lake Meteoric Water Line (EMWL) with equation $\delta^2H = 1.2\delta^{18}O + 28$ and springs formed the Springs Meteoric Water Line (SMWL) with equation $\delta^2H = 6.5\delta^{18}O + 7.0$ (Fig. 16).

All samples collected from the Empakaai Crater are concentrated along the TMWL and the slopes of the LMWL (6.7) is close to that of the TMWL (7.1) which is an indication of rainfall as the main source of water in the area (Fig. 16). The slope of the SMWL which is 6.5 is close to the LMWL which is an indication of rainfall to be the main source of water for springs. However, springs are more enriched in stable isotopes compared to rainfall which is an indication of infiltration to have occurred with evaporative loss and isotopic fractionation due to water-rock interactions (Fackrell *et al.,* 2020). The slope of the EMWL (1.2) is much lower than those of the TMWL and LMWL which is an indication of deviation in isotopic composition of lake water compared to the local meteoric water signature as a result of evaporative effects and multiple water sources including groundwater (Yapiyev *et al.,* 2023).

The samples from Emakat Lake plotted below and to the right of both GMWL and TMWL implying that they are highly enriched in $\delta^{18}O$ and δ^2H while the springs plotted to the left and above of both the GMWL and TMWL which implies that they depleted in $\delta^{18}O$ and δ^2H. Enrichment factors for stable isotopes in Empakaai Carter was determined through ascertaining their interrelationship with EC, NO_3^- and Cl^- (Fig. 17). A water body undergoing evaporation exhibits a positive correlation of stable isotopes $\delta^{18}O$ with EC and NO_3^- (Liu *et al.,* 2019). Emakat Lake exhibited a positive correlation of $\delta^{18}O$ with EC while the springs showed a negative correlation, however, the general trend from the springs to Emakat lake showed a strong correlation of 0.9899 for $\delta^{18}O$ with EC (Fig.17. A, B & C). This implies that evaporative effect is higher in the Emakat Lake resulting to the enrichment of stable isotopes $\delta^{18}O$ while groundwater is not affected by evaporation. Nevertheless, there occurred a strong positive correlation of $\delta^{18}O$ with NO_3^- 0.9160 (Fig. 17 E). The springs appeared to be close to the line, indicating that evaporation has no effect on groundwater while lake water samples were displaced to the left and right of the line, indicating that NO_3^- enrichment occur at fair constant $\delta^{18}O$ while NO_3- is reduced at a depth under an anaerobic environment (Talabi & Tijani, 2013).

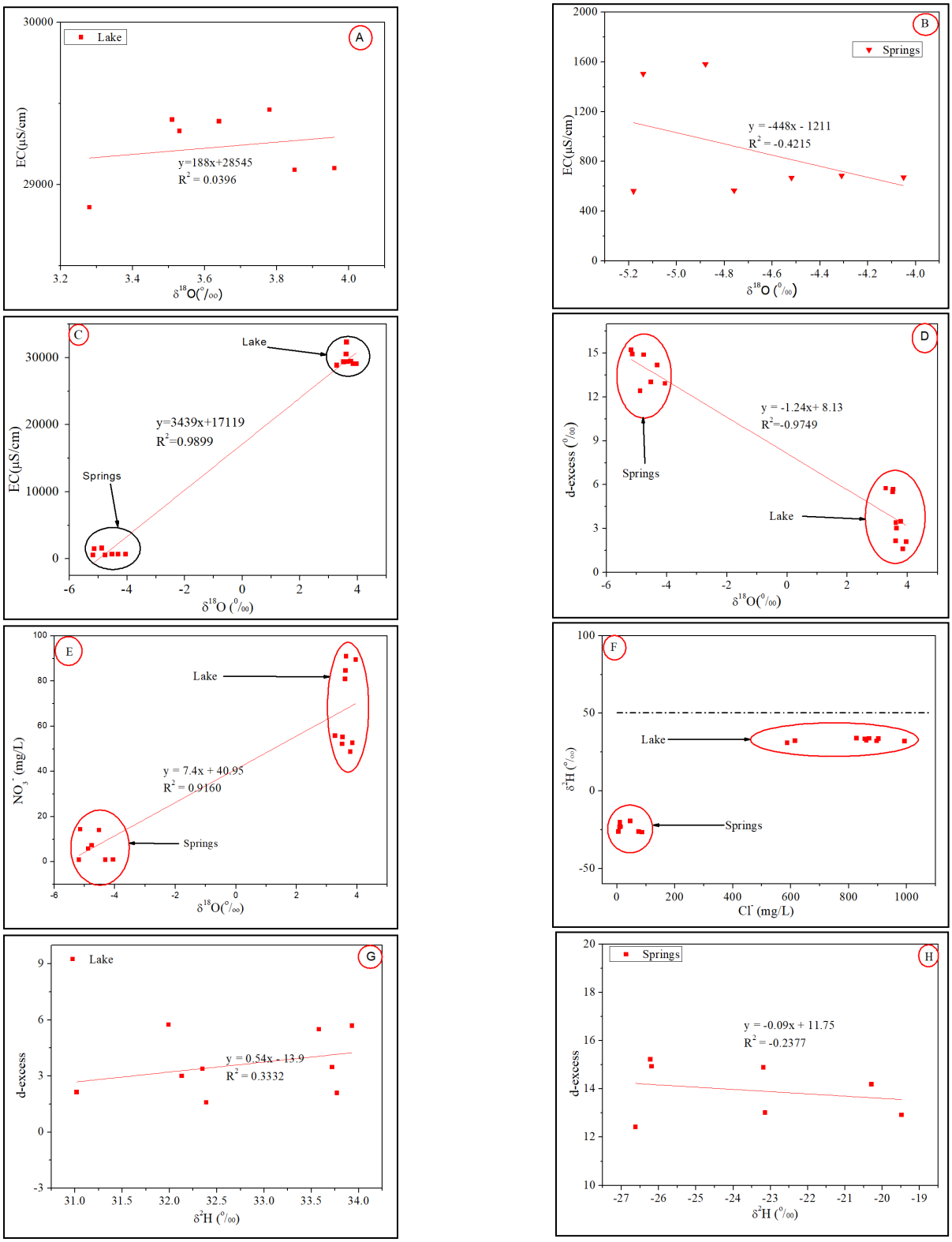

Figure 17: Variation of δ^2H and $\delta^{18}O$ with major ions for Emakat Lake and associated springs (a) $\delta^{18}O$ Vs EC for Emakat Lake (b) $\delta^{18}O$ Vs EC for Emakat Lake (c) $\delta^{18}O$ Vs EC for Emakat Lake and springs (d) $\delta^{18}O$ Vs d-excess (e) $\delta^{18}O$ Vs NO_3^- (f) Cl^- Vs δ^2H (g) δ^2H Vs d-excess for Emakat Lake (h)) δ^2H Vs d-excess for springs

There was limited variation of Cl^- versus δ^2H in both Emakat Lake and the associated springs (Fig. 17 F). The limited variation in springs can be associated with the evapotranspiration

process which tends to concentrate salts in groundwater without fractionation of stable isotopes (Flow *et al.,* 2015) while for Emakat Lake, it can be associated with the partial removal of Cl^- to solid-phase during mineral crystallization as a result of evaporation process (Armienta *et al.,* 2008). The d-excess variation against $\delta^{18}O$ and $\delta^{2}H$ showed that despite a negative correlation of 0.9749 (Fig. 17 D), there still occurred different behaviors among different water sources. The positive correlation of 0.3332 for d-excess versus $\delta^{2}H$ on Emakat Lake and the negative correlation of -0.2377 for the associated springs (Fig. 17 F & G) indicate that a higher evaporative effect occurs on Emakat Lake while no evaporative effects occur on the associated springs (Talabi & Tijani, 2013). The implication of the hydrochemical characteristics and d-excess of Emakat Lake with its associated springs on their respective $\delta^{18}O$ and $\delta^{2}H$ reflected their position on the GMWL (Fig. 16). The higher evaporation in the Emakat Lake results in higher enrichment of $\delta^{18}O$ and $\delta^{2}H$ while the groundwater receives recharge from rainfall however isotopic modification occurs due to rock-water interaction (Fackrell *et al.,* 2020).

4.2.3 Water Balance Parameters from other Lakes in the Vicinity

Since the Emakat Lake is ungauged lake, a combination of satellite data from different sources and the stable isotope data obtained from ground collected water samples from the lake is proposed for the computation of lake water balance. In order to build confidence on the obtained data for the water balance, a comparison of the outputs especially rainfall and evaporation were compared with Lake Babati (Mbanguka *et al.,* 2016), Lake Manyara (Deus *et al.,* 2013), Lake Duluti (Mduma *et al.,* 2016) and the previously study executed at Epakaai Crater (Ryner *et al.,* 2008). The consideration of the selected water bodies was done due to the fact that, all lakes are volcanic lakes which are the result of the Eastern Arm of the East African Great Rift Valley formation processes. Nevertheles, both lakes are located in similar regional climatic condition characterised with bimodal rain seasons occurring in October to December and March to May (Mbanguka *et al.,* 2016).

It was observed that, lakes evaporation surpasses rainfall to a factor of more than 1.65 experienced at Lake Babati (Table 19). The altitudinal plot against rainfall and temperature (Fig. 18) shows that, the rainfall and temperature generally increase with altitude however some local variation can occur as experienced on the Lake Babati.

Table 20: The rainfall and evaporation amount from Manyara, Duluti and Babati Lakes as compared to Lake Emakat

Lake	Altitude (m.a.s.l)	Rainfall (mm/year)	Evaporation (mm/year)	Factor Rain./Evap	Source
Manyara	960	600.00	1120.00	1.87	Deus *et al.* (2013)
Duluti	1290	1012.00	1700.00	1.68	Mduma *et al.* (2016)
Babati	1345	789.00	1300.00	1.65	Mbanguka *et al.* (2016)
Emakat	2300	~800.00	>1000	>1.25	Ryner *et al.* (2008)
Emakat	2300	878.68	1694.57	1.93	Current Study

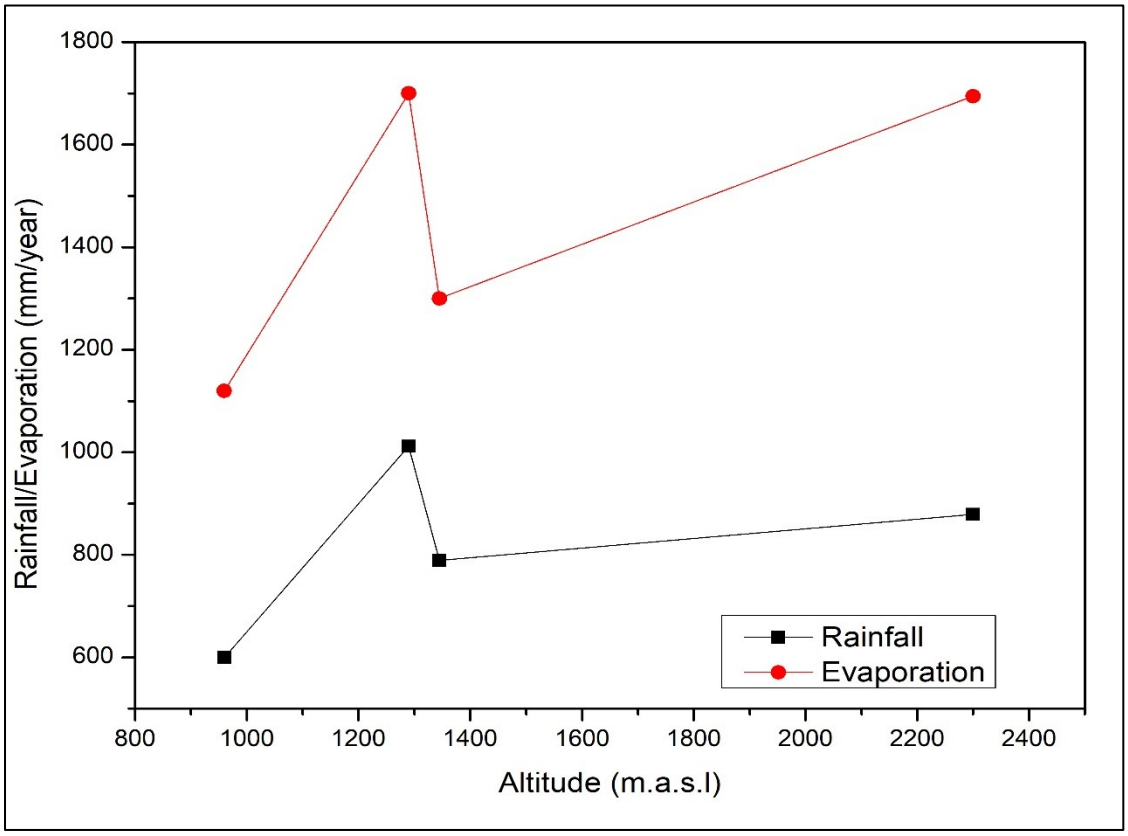

Figure 18: The graph showing Rainfall and Evaporation change with altitude

Ryner *et al.* (2008) on the study about the vegetation dynamics and lake level changes of the Emakat Level reported that, the rainfall in Emakat lake range between 600 and 1000 mm while evaporation in the area surpasses rainfall. This implies that, the obtained values of rainfall (878.68 mm/year) and evaporation (1694.57 mm/year) fall on the same range as observed previously.

4.2.4 Water Balance Estimtions

The water balance of Emakat Lake presented showed that groundwater flow plays a major role in the lake's water balance whereby a total of 16 607 432.39 m^3/year as the groundwater inflow to Emakat Lake which is about 48.83% of total lake inflow while about 17 337 345.27 m^3/year as groundwater outflow which is about 56.00% of total lake outflow were obtained (Table 20). The major lake withdrawals were groundwater outflow and evaporation, however, groundwater outflow surpassed evaporation by 12%. The major inflows were groundwater inflow (48.83%), runoff from crater walls (30.35%), and direct precipitation (20.77%) of the total inflows.

The higher percentage ratio of contribution to lake inflow and outflow implies that the lake depends less on the weather conditions as reported in previous studies (Ryner *et al.,* 2007; Ryner *et al.,* 2008) but drop in the lake level is from its tendency to balance evaporation which surpasses rainfall. While the higher groundwater outflow might have a higher contribution to the Engaresero and Engaruka Rivers which originate on the outer crater rims of the Empakaai Crater and support the life of the downstream residents.

Table 21. The summary of the isotopic mass balance for estimation of the groundwater flow

Parameter	Volume (m^3/year)	Isotopic ($\delta^{18}O$)	Isotopic ($\delta^{2}H$)	Percentage (%)
Lake Volume Change	3 049 090.56	3.65	33.07	
Precipitation over the Lake	7 063 956.54	-8.06	-54.37	20.77%
Runoff from Crater Walls	10 322 309.68	-8.06	-54.37	30.35%
Springs inflow from Crater Walls	15 768.00	-4.75	-23.23	0.05%
Evaporation	13 623 030.78	-1.47	-1.09	44.00%
Groundwater inflow	16 607 432.39	-4.69	-23.59	48.83%
Groundwater Outflow	17 337 345.27	3.65	33.07	56.00%

Therefore, Emakat Lake's water balance reflects its hydrochemistry evolution whereby groundwater inflow and runoff might have evolved due to rock-water interaction through rock weathering and ionic exchange drive ions into it. The evaporation which surpasses rainfall could be responsible for the increase in ionic concentration in the lake as a result some are saturated then crystallized.

CHAPTER FIVE

CONCLUSION AND RECOMMENDATIONS

5.1 Conclusions

The study was undertaken to assess the hydrochemical evolution in Empakaai Crater and water balance of the Emakat Lake where factors influencing the evolution and water balance were assessed. The lake exhibited high TDS and EC, hence was classified as a highly saline lake while its associated springs exhibited lower hydrophysical characteristics. The dominant cations and anions for Emakat Lake and its associated springs were Na^+ and CO_3^{2-}+HCO_3^- which occupied about 80% and 85% for the lake and 60% and 74% of the springs total cation and anion concentrations, respectively.

The order of distribution of cations in Emakat Lake and springs was $Na^+ > K^+ > Ca^{2+} > Mg^{2+}$. Slight difference was obseved in the anions distributions where the lake had distribution of $(CO_3^{2-} + HCO_3^-) > Cl^- > SO_4^{2-} > F^- > NO^{3-} > PO_4^{3-}$ while springs exhibited the anion distribution of $(CO_3^{2-} + HCO_3^-) > SO_4^{2-} > Cl^- > NO^{3-} > F^- > PO_4^{3-}$. The difference in the anion is balanced in the lake due to evaporative effect as SO_4^{2-} is non-conservative in nature hence it is removed in solid phase once discharged from the lake. The hydrochemical facies of Emakat Lake was Na^+-K^+-HCO_3^- while a majority of the springs exhibited mixing hydrochemical facies as a result of water-rock interaction Generally, the hydrochemical characteristics of Emakat Lake reflect weathering of the hosting rocks which are mainly composed of secondary minerals rich in Ca^{2+} and Mg^{2+} such as zeolites and mica by which through ionic exchange and mineral dissolution, release Na^+ and K^+ into the lake inflows such as groundwater inflows and runoff from the inner crater lake.

The hydrochemical chemical evolution in groundwater is attributed by rock-water interaction through the dissolution, ionic exchange and oxidation processed. The processes in groundwater involve the uptake of Ca^{2+} and Mg^{2+} into solid phase and release of Na^+ and K^+ into solution. Hydrochemical evolution of Emakat Lake is mainly influenced by evaporation which surpases rainfall. Due to evaporative effects some ionic concentration in the lake reach saturation and recrystallize removing of the non-conservative elements such as Ca^{2+} and Mg^{2+} from Emakat Lake as talc, chrysotile, sepiolite, dolomite, calcite, and aragonite. Conservative ions such as Na^+ and K^+ remain in solution as a result of their dominance in the Emakat Lake.

The isotopic characteristics revealed that, the source of water in the area is rainfall and it is depleted in stable isotopes ($\delta^{18}O$ and $\delta^{2}H$) compared to the spring and the Emakat Lake. The enrichment of $\delta^{18}O$ and $\delta^{2}H$ in springs is a result of evaporation effect during recharge and isotope fractionation due to rock-water interaction. The EMWL (1.2) is less than that of LMWL (6.7) and TMWL (7.1) which is an indication that, in addition to rainfall the lake receives water from other sources including groundwater. The displacement of the lake to the left below the GMWL and TMWL is an indication of the lake to be subjected to high evaporation.

The water balance of Emakat Lake is mainly controlled by evaporation, precipitation, and groundwater flows. Groundwater flows play a major role in the hydrological system of the lake since they contributed about 49 and 56% of the total lake's inflows and outflows respectively. The water balance of Emakat Lake suggests that groundwater inflow is the major contributor to the solute concentration of the lake followed by runoff from inner crater walls and then precipitation. Despite the lake's outflow being its major withdrawer, the lower percentage that surpasses the inflow does not greatly change the hydrochemistry of the lake but evaporation that surpasses rainfall is responsible for major cations and anions higher cencentration in the lake.

5.2 Recommendations

The study recommends the following;

(i) Strengthening of the field-collected data for the hydrometeorological data is required for a better estimation of the water balance of Emakat Lake as the current study mostly utilized the satellite-collected data.

(ii) Further studies should be undertaken to delineate the contribution of Emakat Lake to the downstream basins of Engaruka and Natron lakes

(iii) Since Emakat Lake is a volcanic lake and the hosting geology is rich in heavy metals, further study should be undertaken to ascertain the heavy metal concentration in Emakat Lake relative to the rivers which are the major suppliers of freshwater to the outer crater rims and the downstream community.

(iv) Since Emakat Lake is located on the highest elevation of the Elanairobi volcanic shield and the present study has revealed that the groundwater dominates the hydrological

system, a detailed study to ascertain the recharge source of the groundwater flowing into Emakat Lake is needed.

(v) Since the study utilized much of the sattellite data to estimate the water balance parameters as it is ungauged, it is recommended to use other methods of water balance to compare findings

REFERENCES

Federation, W. E., & APH Association. (2005). *Standard Methods for the Examination of Water and Wastewater.* American Public Health Association (APHA): Washington, DC, USA, 21. https://scholar.google.com/

Armienta, M. A., Vilaclara, G., De la Cruz-Reyna, S., Ramos, S., Ceniceros, N., Cruz, O., Aguayo, A., & Arcega-Cabrera, F. (2008). Water chemistry of lakes related to active and inactive Mexican volcanoes. *Journal of Volcanology and Geothermal Research*, *178*(2), 249–258. https://doi.org/10.1016/j.jvolgeores.2008.06.019

Askar, M. K. (2013). Rainfall-runoff model using the SCS-CN method and geographic information systems: A case study of Gomal River watershed. *Transactions on Ecology and the Environment*, *178*, 159–170. https://doi.org/10.2495/WS130141

Atomic, I., & Agency, E. (1992). *Isotopic Patterns in Modern Global Precipitation*. https://scholar.google.com

Atomic, I., Agency, E., & Payne, B. R. (1970). Water Balance of Lake Chala and Its Relation. *Atomic Energy*, *11*, 47–58.

Avery, S. T., & Tebbs, E. J. (2018). Lake Turkana, major Omo River developments, associated hydrological cycle change and consequent lake physical and ecological change. *Journal of Great Lakes Research*, *44*(6), 1164–1182. https://doi.org/10.1016/j.jglr.2018.08.014

Ávila-Carrasco, J. R., Hernández-Hernández, M. A., Herrera, G. S., & Hernández-García, G. D. J. (2023). Urbanization effects on the groundwater potential recharge of the aquifers in the southern part of the Basin of Mexico. *Hydrology Research*, *54*(5), 663–685. https://doi.org/10.2166/nh.2023.103

Bocanegra, E., Quiroz Londoño, O. M., Martínez, D. E., & Romanelli, A. (2013). Quantification of the water balance and hydrogeological processes of groundwater-lake interactions in the Pampa Plain, Argentina. *Environmental Earth Sciences*, *68*(8), 2347–2357. https://doi.org/10.1007/s12665-012-1916-4

Boone, R. B., & BurnSilver, S. B. (2002). Integrated assessment results to support policy decisions in Ngorongoro Conservation Area, Tanzania. *Report from the POLEYC Project to the Global Livestock Collaborative Research Support Program, University of*

California, Davis, California, USA.

Boone, R. B., Galvin, K. A., Thornton, P. K., Swift, D. M., & Coughenour, M. B. (2006). Cultivation and conservation in Ngorongoro Conservation Area, Tanzania. *Human Ecology*, *34*(6), 809–828. https://doi.org/10.1007/s10745-006-9031-3

Bowser, C. J., Anderson, M. P., & Valley, J. W. (1990). *Estimating Groundwater Exchange With Lakes 1 . The Stable Isotope Mass Balance Method x = [(Rx / Rstd) by groundwater outflow.* https://scholar.google.com

Branchu, P., & Bergonzini, L. (2004). Chloride concentrations in Lake Tanganyika: An indicator of the hydrological budget? *Hydrology and Earth System Sciences*, *8*(2), 256–265. https://doi.org/10.5194/hess-8-256-2004

Campodonico, V. A., Dapeña, C., Pasquini, A. I., Lecomte, K. L., Piovano, E. L., Investigaciones, C. D., Tierra, D., Nacional, C., Científicas, D. I., Nacional, U., & Mar, L. (2019). Assessing the groundwater inflow using environmental isotopic tracers (Laguna del Plata, Mar Chiquita system , Argentina). *Journal of South American Earth Sciences*, *95*(4), 102305. https://doi.org/10.1016/j.jsames.2019.102305

Chacha, N., Njau, K. N., Lugomela, G. V., & Muzuka, A. N. N. (2018). *Groundwater Age Dating and Recharge Mechanism of Arusha Aquifer, Northern Tanzania: Application of Radioisotope and Stable Isotope Techniques AUWSA 2014*. https://scholar.google.com

Chadha, D. K. (1999). A proposed new diagram for geochemical classification of natural waters and interpretation of chemical data. *Hydrogeology Journal*, *7*(5), 431–439. https://doi.org/10.1007/s100400050216

Chebud, Y. A., & Melesse, A. M. (2009). Modelling lake stage and water balance of Lake Tana, Ethiopia. *Hydrological Processes*, *23*(25), 3534–3544.

Chen, J., Qian, H., Gao, Y., Wang, H., & Zhang, M. (2020). Insights into hydrological and hydrochemical processes in response to water replenishment for lakes in arid regions. *Journal of Hydrology*, 581, 124386.

Chikita, K. A., Goto, A., Okada, J., Yamaguchi, T., Miura, S., & Yamamoto, M. (2022). Hydrological and Chemical Budgets of Okama Crater Lake in Active Zao Volcano, Japan. *Hydrology*, *9*(2), 1-18. https://doi.org/10.3390/hydrology9020028

Childress, B., Hughes, B., Harper, D., & van den Bossche, W. (2007). East African flyway and key site network of the Lesser Flamingo (Phoenicopterus minor) documented through satellite tracking. *Ostrich-Journal of African Ornithology*, *78*(2), 463–468.

Christenson, B. W. (2000). Geochemistry of fluids associated with the 1995-1996 eruption of Mt. Ruapehu, New Zealand: Signatures and processes in the magmatic-hydrothermal system. *Journal of Volcanology and Geothermal Research*, *97*(1–4), 1–30. https://doi.org/10.1016/S0377-0273(99)00167-5

Craig, H., & Gordon, L. (1965). *Craig-Gordon Pisa D and O-18 in the Ocean and the Marine Atmosphere.* https://scholar.google.com

Deacampo, M. D., & Renaut, W. R. (2016). Soda lakes of East Africa. *Soda Lakes of East Africa*, *February*, 2016, 1–408. https://doi.org/10.1007/978-3-319-28622-8

Deniz, K., Kadioğlu, Y. K., Koralay, T., & Güllü, B. (2021). The distribution of elements in the alteration of feldspatic minerals. *Bulletin of the Mineral Research and Exploration*, *166*, 167–188. https://doi.org/10.19111/bulletinofmre.901035

Deocampo, D. M. (2004). Hydrogeochemistry in the Ngorongoro Crater, Tanzania, and implications for land use in a World Heritage Site. *Applied Geochemistry*, *19*(5), 755–767. https://doi.org/10.1016/j.apgeochem.2003.10.006

Deocampo, D. M. (2018). *Geochemistry of Saline Lakes Geochemistry of Saline Lakes: Surface and Ground Water, Weathering and Soils*. Elsevier Ltd. https://doi.org/10.1016/B978-0-08-095975-7.00515-5

Dessie, M., Verhoest, N. E. C., Pauwels, V. R. N., Adgo, E., Deckers, J., Poesen, J., & Nyssen, J. (2015). Water balance of a lake with floodplain buffering: Lake Tana, Blue Nile Basin, Ethiopia. *Journal of Hydrology*, *522*, 174–186.

Deus, D., Gloaguen, R., & Krause, P. (2013). Water balance modeling in a semi-arid environment with limited in situ data using remote sensing in lake manyara, east african rift, tanzania. *Remote Sensing*, *5*(4), 1651–1680. https://doi.org/10.3390/rs5041651

Dinka, M. O. (2020). Estimation of groundwater contribution to Lake Basaka in different hydrologic years using conceptual netgroundwater flux model. *Journal of Hydrology: Regional Studies*, *30*, 1-12. https://doi.org/10.1016/j.ejrh.2020.100696

Dinku, T., Ceccato, P., Grover-Kopec, E., Lemma, M., Connor, S. J., & Ropelewski, C. F. (2007). Validation of satellite rainfall products over East Africa's complex topography. *International Journal of Remote Sensing*, *28*(7), 1503–1526.

Dinku, T., Funk, C., Peterson, P., Maidment, R., Tadesse, T., Gadain, H., & Ceccato, P. (2018). Validation of the CHIRPS satellite rainfall estimates over eastern Africa. *Quarterly Journal of the Royal Meteorological Society*, 144, 292-312.

Duan, Z., & Bastiaanssen, W. G. M. 2015 A new empirical procedure for estimating intra-annual heat storage changes in lakes and reservoirs: Review and analysis of 22 lakes. *Remote Sensing of Environment*, *156*, 143–156. https://doi.org/10.1016/j.rse.2014.09.009

Duan, Z., & Bastiaanssen, W. G. M. (2017). Evaluation of three energy balance-based evaporation models for estimating monthly evaporation for five lakes using derived heat storage changes from a hysteresis model. *Environmental Research Letters,* 12(2), 024005.

Duan, Z., Gao, H., & Ke, C. (2018). Estimation of lake outflow from the poorly gauged Lake Tana (Ethiopia) using satellite remote sensing data. *Remote Sensing*, *10*(7), 1–21. https://doi.org/10.3390/rs10071060

Duan, Z., Gao, H., & Ke, C. (2018). Estimation of lake outflow from the poorly gauged Lake Tana (Ethiopia) using satellite remote sensing data. *Remote Sensing*, *10*(7), 1–21. https://doi.org/10.3390/rs10071060

Elsawwaf, M., Willems, P., Pagano, A., & Berlamont, J. (2010). Evaporation estimates from Nasser Lake, Egypt, based on three floating station data and Bowen ratio energy budget. *Theoretical and Applied Climatology*, *100*(3), 439–465. https://doi.org/10.1007/s00704-009-0168-z

Fackrell, J. K., Glenn, C. R., Thomas, D., Whittier, R., & Popp, B. N. (2020). Stable isotopes of precipitation and groundwater provide new insight into groundwater recharge and flow in a structurally complex hydrogeologic system: West Hawai'i, USA. *Hydrogeology Journal*, *28*(4), 1191–1207. https://doi.org/10.1007/s10040-020-02143-9

Fazlollahi, M. M., Jalali, S. G. H., Kooch, Y., & Said-Pullicino, D. (2016). Slope gradient and shape effects on soil profiles in the northern mountainous forests of Iran. *Eurasian Soil Science*, *49*(12), 1366–1374. https://doi.org/10.1134/S1064229316120061

Finch, J., & Calver, A. (2008). *Methods for the Quantification of Evaporation from Lakes.* https://scholar.google.com

Flow, G., Park, N., Hedley, P., Dogramaci, S., & Dodson, W. (2015). *The Use of Major Ion Analysis and Stable Isotopes O^{18} and H^{2} to Distinguish The Use of Major Ion Analysis and Stable Isotopes O^{18} and H^{2} to Distinguish Groundwater Flow in Karijini National Park , Western Australia February*. https://scholar.google.com

Frame, G., Frame, L. H., & Spillett, J. J. (1975). An ecological survey and development plan for the Empakaai Crater ecosystem (Ngorongoro Conservation Area). *Serengeti Research Contribution*, *212*, 472.

Gaidzik, K. (2011). *The Ngorongoro Crater as the Biggest Geotouristic Attraction of the Gregory Rift (Northern Tanzania, Africa): Geological Heritage Krater Ngorongoro Największą Atrakcją Geoturystyczną Ryftu Gregory' Ego January*. https://scholar.google.com

Gat, J. R., Mook, W. G., & Meijer, H. A. J. (2001). Environmental isotopes in the hydrological cycle. *Principles and Applications UNESCO/IAEA Series*, *2*, 63–67.

Getenet, M., García-Ruiz, J. M., Otálora, F., Emmerling, F., Al-Sabbagh, D., & Verdugo-Escamilla, C. (2022). A Comprehensive Methodology for Monitoring Evaporitic Mineral Precipitation and Hydrochemical Evolution of Saline Lakes: The Case of Lake Magadi Soda Brine (East African Rift Valley, Kenya). *Crystal Growth and Design*, *22*(4), 2307–2317. https://doi.org/10.1021/acs.cgd.1c01391

Gibbs, R. J. (1970). Mechanisms controlling world water chemistry. *Science*, *170*(3962), 1088–1090. https://doi.org/10.1126/science.170.3962.1088

Gibson, J. J., Birks, S. J., & Yi, Y. (2016). Stable isotope mass balance of lakes: A contemporary perspective *Quaternary Science Reviews*, *131*, 316–328. https://doi.org/10.1016/j.quascirev.2015.04.013

Gibson, J. J., Birks, S. J., Yi, Y., Shaw, P., & Moncur, M. C. (2018). Isotopic and geochemical surveys of lakes in coastal B.C.: Insights into regional water balance and water quality controls. *Journal of Hydrology: Regional Studies*, *17*, 47–63.

Gibson, J. J., Edwards, T. W. D., & Prowse, T. D. (1996). Development and validation of an

isotopic method for estimating lake evaporation. *Hydrological Processes*, 10(10), 1369-1382.

Gibson, J. J., Mydłowski, A., Skrzypek, G., Dogramaci, S., Grierson, P. F., & Hedley, P. (2015). Estimation of evaporative loss based on the stable isotope composition of water using Hydrocalculator. *Journal of Hydrology*, *523*, 781–789.

Gonfiantini, R., Roche, M., Olivry, J., Fontes, J., & Maria, G. (2001). *The altitude Effect on the Isotopic Composition of Tropical Rains*. https://scholar.google.com

Greenwood, S. M. (2014). *Mineralogy and Geochemistry of Pleistocene Volcanics at Embagai Caldera and Natron Basin, Tanzania: Potential Constraints on the Stratigraphy of Olduvai Gorge (Doctoral dissertation, The University of Wisconsin-Milwaukee).* https://scholar.google.com

Guest, N. J., James, T. C., Pickering, R., & Dawson, J. B. (1961). Angeta Salei Tanzania. *Geological Survey*, 39 (40), 53- 54.

Guswa, A. J., Hamel, P., & Meyer, K. (2018). Curve number approach to estimate monthly and annual direct runoff. *Journal of Hydrologic Engineering*, *23*(2), 1–10.

Horita, J., & Wesolowski, D. J. (1994). *Horita and Wesolowski, 1994 58*(16), 1–13.

Horita, J., Rozanski, K., & Cohen, S. (2008). Isotope effects in the evaporation of water: A status report of the Craig-Gordon model. *Isotopes in Environmental and Health Studies*, *44*(1), 23–49. https://doi.org/10.1080/10256010801887174

Hutchinson, G. E. (1957). *A Treatise on Limnology: Georgraphy, Physics and Chemistry.* John Wiley & Sons.

IAEA/GNIP. (2014). *IAEA/GNIP precipitation sampling guide Introduction: The Global Network of Isotopes in Precipitation (GNIP)*. http://www.iaea.org/water

Jain, S. K., & Singh, V. P. (2003). Chapter 10: Reservoir sizing. *Water Sci*, 51, 555-612.

Kalacheva, E. G., Melnikov, D. V., Voloshina, E. V., & Karpov, G. A. (2022). Water Geochemistry of the Crater Lake on Maly Semyachik Volcano. *Journal of Volcanology and Seismology,* 16(3), 192-205.

Kansoh, R., Abd-El-Mooty, M., & Abd-El-Baky, R. (2020). Computing the water budget components for lakes by using meteorological data. *Civil Engineering Journal*, *6*(7), 1255–1265. https://doi.org/10.28991/cej-2020-03091545

Karmakar, S., & Musthafa, O. M. (2020). *Lakes and reservoirs Pollution: Managing Water Resources and Hydrological Systems. CRC Press*

Karolyte, R., Johnson, G., Serno, S., & Gilfillan, S. M. V. (2017). The Influence of Water-rock Reactions and O Isotope Exchange with CO_2 on Water Stable Isotope Composition of CO_2 Springs in SE Australia. *Energy Procedia*, *114*(2016), 3832–3839. https://doi.org/10.1016/j.egypro.2017.03.1515

Katsanos, D., Retalis, A., & Michaelides, S. (2016) Validation of a high-resolution precipitation database over Cyprus for a 30-year period. *Atmospheric Research*, *169*, 459–464. https://doi.org/10.1016/j.atmosres.2015.05.015

Krabbenhoft, D. P., Bowser, C. J., Anderson, M. P., & Valley, J. W. (1990). *Estimating Groundwater Exchange With Lakes: The Stable Isotope Mass Balance Method x = [(Rx / Rstd) by groundwater outflow.* https://scholar.google.com

Kumambala, P. G., & Ervine, A. (2010). Water Balance Model of Lake Malawi and its Sensitivity to Climate Change. *The Open Hydrology Journal*, *4*, 152–162.

Kumar, M., Ramanathan, A., & Rao, M. S. (2014). *Identification and Evaluation of Hydrogeochemical Processes in the Groundwater Environment of Delhi, India August 2006*. https://doi.org/10.1007/s00254-006-0275-4

Kusakabe, M. (1994). Geochemistry of Crater Lakes Preface. *Geochemical Journal*, *28*(3), 137–138.

Levin, N. E., Zipser, E. J., & Cerling, T. E. (2009). *Isotopic Composition of Waters from Ethiopia and Kenya: Insights into Moisture Sources for Eastern Africa* https://www.google.com

Liu, F., Wang, S., Wang, L., Shi, L., Song, X., Yeh, T. C. J., & Zhen, P. (2019). Coupling hydrochemistry and stable isotopes to identify the major factors affecting groundwater geochemical evolution in the Heilongdong Spring Basin, North China. *Journal of Geochemical Exploration*, 205, 106352.

Matt, C., Hess, T., & Benlian, A. (2015). Digital transformation strategies. *Business & Information Systems Engineering*, 57, 339-343.

Lyimo, E., Kohi, E., Maliti, H., Kimaro, J., Mwita, M., & Kija, H. (2020). *Population trends in the Ngorongoro Conservation Area since 1995 to 2018. Tanzania: Tanzania Wildlife Research Institute*. https://scholar.google.com

Ma, D., Zhou, J., Li, Q., Dou, J., Huang, J., Zhu, G., Wang, L., & Hu, K. (2021). Temporal variations of hydrochemical characteristics and their controlling factors in the xiying river basin in the eastern qilian mountains, china. *Polish Journal of Environmental Studies*, *30*(4), 3741–3751. https://doi.org/10.15244/pjoes/131948

Maidment, R. I., Grimes, D., Black, E., Tarnavsky, E., Young, M., Greatrex, H., Allan, R. P., Stein, T., Nkonde, E., Senkunda, S., & Alcántara, E. M. U. (2017) A new, long-term daily satellite-based rainfall dataset for operational monitoring in Africa. *Scientific Data*, *4*, 1–17. https://doi.org/10.1038/sdata.2017.63

Majoube, M. (1971). Fractionnement en oxygène 18 et en deutérium entre l'eau et sa vapeur. *Journal de Chimie Physique*, *68*, 1423–1436. https://doi.org/10.1051/jcp/1971681423

Mbanguka, R. P., Lyon, S. W., Holmgren, K., Girons Lopez, M., & Jarsjö, J. (2016). Water balance and level change of Lake Babati, Tanzania: Sensitivity to hydroclimatic forcings. *Water*, 8(12), 572.

Mduma, N. P., Komakech, H. C., Zhang, J., & Muzuka, A. N. (2016). Application of isotopes and water balance on Lake Duluti -groundwater interaction, Arusha, Tanzania of isotopes and water balance on lake duluti-groundwater interaction, Arusha, Tanzania. *Hydrology and Earth System Sciences Discussions*, 2016, 1-24.

Mohajerani, H., Zema, D. A., Lucas-Borja, M. E., & Casper, M. (2021). *Understanding the Water Balance and Its Estimation Methods*. https://scholar.google.com

Mollel, G. F. (2007). *Petrochemistry and Geochronology of Ngorongoro Volcanic Highland Complex and its Relationship to Laetoli and Olduvai Gorge, Tanzania*. Rutgers The State University of New Jersey, School of Graduate Studies.

Mollel, G. F., Swisher III, C. C., Feigenson, M. D., & Carr, M. J. (2008). Geochemical evolution of Ngorongoro Caldera, Northern Tanzania: Implications for crust–magma interaction. *Earth and Planetary Science Letters*, 271(1-4), 337-347.

Muzuka, A. N. N. (2004). Elemental and isotopic compositions of organic carbon and nitrogen of recently deposited organic matter in Empakai crater and its implication for climatic changes in northern Tanzania. *Tanzania Journal of Science*, *30*(2), 87–96. https://doi.org/10.4314/tjs.v30i2.18403

Muzuka, A. N., Ryner, M., & Holmgren, K. (2004). 12 000-Year, preliminary results of the stable nitrogen and carbon isotope record from the Empakai Crater lake sediments, Northern Tanzania. *Journal of African Earth Sciences*, 40(5), 293-303.

Mwabumba, M., Yadav, B. K., Rwiza, M. J., Larbi, I., Dotse, S. Q., Limantol, A. M., Sarpong, S., & Kwawuvi, D. (2022). Rainfall and temperature changes under different climate scenarios at the watersheds surrounding the Ngorongoro Conservation Area in Tanzania. *Environmental Challenges, 7, 100446.*

Nathenson, M. (1992) *Water balance for Crater Lake, Oregon*. https://scholar.google.com

Navarre-Sitchler, A., & Jung, H. (2017). Complex coupling of fluid transport and geochemical reaction rates: Insights from reactive transport models. *Procedia Earth and Planetary Science*, 17, 5-8.

NCAA, & MNRT. (1996). *Ngorongoro Conservation Area General Plan*. https://scholar.google.com

Nkotagu, H. (1996a). Application of environmental isotopes to groundwater recharge studies in a semi-arid fractured crystalline basement area of Dodoma, Tanzania. *Journal of African Earth Sciences*, *22*(4), 443–457.

Nkotagu, H. (1996). Origins of high nitrate in groundwater in Tanzania. *Journal of African Earth Sciences*, 22(4), 471-478.

Özaydin, V., Şendil, U., & Altinbilek, D. (2001). Stable isotope mass balance method to find the water budget of a lake Turkish. *Journal of Engineering and Environmental Sciences*, *25*(4), 329–344. https://doi.org/10.1128/JVI.00693-11

Pamela, P., Yukni, A., Imam, S. A., & Kartiko, R. D. (2018). The selective causative factors on landslide susceptibility assessment: Case study Takengon, Aceh, Indonesia. https://scholar.google.com

Parasuraman, S. B., Consultancy, K., Mishra, S., & Singh, V. P. (2007). *SCS-CN Method*

Revisited January. https://scholar.google.com

Philip, J. Y., & Mosha, D. M. S. (2012). Salt Lakes of the African rift system: A valuable research opportunity for insight into nature's concenrtated multi-electrolyte science. *Tanzania Journal of Science*, 38(3), 1-13.

Piper, A. M. (1944). A graphic procedure in the geochemical interpretation of water-analyses. *Eos, Transactions American Geophysical Union*, *25*(6), 914–928.

Ravikumar, P., & Somashekar, R. K. (2017). Principal component analysis and hydrochemical facies characterization to evaluate groundwater quality in Varahi river basin, Karnataka state, India. *Applied Water Science*, *7*(2), 745–755. https://doi.org/10.1007/s13201-015-0287-x

Ravikumar, P., Somashekar, R. K., & Prakash, K. L. (2015). A comparative study on usage of Durov and Piper diagrams to interpret hydrochemical processes in groundwater from SRLIS river basin, Karnataka, India. *Elixir International Journal,* 80(2015), 31073-31077.

Rezaei, H., Jafarzadeh, A. A., Alijanpour, A., Shahbazi, F., & Kamran, K. V. (2015). Effect of slope position on soil properties and types along an elevation gradient of arasbaran forest, Iran. *International Journal on Advanced Science, Engineering and Information Technology*, *5*(6), 449–456. https://doi.org/10.18517/ijaseit.5.6.589

Rice, E. W., Baird, R. B., Eaton, A. D., & Clesceri, L. S. (2012). *Standard Methods for the Examination of Water and Wastewater*. American Public Health Association Washington, DC.

Ritzema, H. P. (1994). Edepotlink_I183157_001. *Drainage Principles and Applications*, *16*, 121–144. http://www.ircwash.org/resources/drainage-principles-and-applications

Rosenberry, D. O., Winter, T. C., Buso, D. C., & Likens, G. E. (2007). Comparison of 15 evaporation methods applied to a small mountain lake in the northeastern USA. *Journal of Hydrology*, *340*(3–4), 149–166. https://doi.org/10.1016/j.jhydrol.2007.03.018

Ross, C. W., Prihodko, L., Anchang, J., Kumar, S., Ji, W., & Hanan, N. P. (2018). HYSOGs250m, global gridded hydrologic soil groups for curve-number-based runoff modeling. *Scientific Data*, *5*(5), 180091. https://doi.org/10.1038/sdata.2018.91

Rouwet, D., Christenson, B., Tassi, F., & Vandemeulebrouck, J. (Eds.). (2015). *Volcanic Lakes (Vol. 2)*. Berlin: Springer. https://scholar.google.com

Rozanski, K., Cohen, S., & Horita, J. (2008). Isotopes in Environmental and Health Studies Isotope effects in the evaporation of water: A status report of the Craig–Gordon model Isotope effects in the evaporation of water: A status report of the Craig–Gordon model. *Isotopes in Environmental and Health Studies*, *44*(1), 23–49.

Rusydi, A. F. (2018, February). Correlation between conductivity and total dissolved solid in various type of water: A review. In IOP conference Series: *Earth and Environmental Science,* 118, 012019.

Ryner, M. (2007). *Past Environmental and Climate Changes in Northern Tanzania: Vegetation and Lake Level Variability in Empakaai Crater [Doctoral dissertation]*. Institutionen för naturgeografi och kvartärgeologi.

Ryner, M. A., Bonnefille, R., Holmgren, K., & Muzuka, A. (2006). Vegetation changes in Empakaai Crater, northern Tanzania, at 14 800-9300 cal yr BP. *Review of Palaeobotany and Palynology*, *140*(3–4), 163–174. https://doi.org/10.1016/j.revpalbo.2006.03.006

Ryner, M. A., Gasse, F., Rumes, B., & Verschuren, D. (2007). Climatic and hydrological instability in semi-arid equatorial East Africa during the late Glacial to Holocene transition: A multi-proxy reconstruction of aquatic ecosystem response in northern Tanzania *Palaeogeography, Palaeoclimatology, Palaeoecology*, *248*(3–4), 440–458. https://doi.org/10.1016/j.palaeo.2006.12.014

Ryner, M., Holmgren, K., & Taylor, D. (2008). A record of vegetation dynamics and lake level changes from Lake Emakat, northern Tanzania, during the last c. 1200 years. *Journal of Paleolimnology*, *40*(2), 583–601. https://doi.org/10.1007/s10933-007-9184-0

Samki, J., & Baker, R. (1977). *Provisional Soils Map of Tanzania.* Geological Survey Department, Dodoma.

Satheeshkumar, S., Venkateswaran, S., & Kannan, R. (2017). Rainfall–runoff estimation using SCS–CN and GIS approach in the Pappiredipatti watershed of the Vaniyar sub basin, South India. *Modeling Earth Systems and Environment*, *3*(1), 1–8.

Schagerl, M. (2016). *Soda lakes of East Africa Soda Lakes of East Africa*.

https://scholar.google.com

Schoeller, H. (1965). *Hydrodynamique Lans Le Karst. Actes du Colloque de Dubrovnik, IAHS* UNESCO. https://scholar.google.com

Scoon, R. N. (2018). Geology of National Parks of Central/Southern Kenya and Northern Tanzania. *Geology of National Parks of Central/Southern Kenya and Northern Tanzania*, 2018, 39–57. https://doi.org/10.1007/978-3-319-73785-0_5

Shiklomanov, I. A. (1993). *World Freshwater Resources. Water in Crisis: A Guide to the World's Fresh Water Resources* Oxford University Press, New York.

Sokolov, A., & Chapman, T. G. (1974). *Methods for Water Balance Computations: An International Guide for Research and Practice*. https://scholar.google.com

Swenson, S., & Wahr, J. (2009). Monitoring the water balance of Lake Victoria, East Africa, from space. *Journal of Hydrology*, *370*(1–4), 163–176.

Talabi, A. O., & Tijani, M. N. 2013 Hydrochemical and stable isotopic characterization of shallow groundwater system in the crystalline basement terrain of Ekiti area, southwestern Nigeria. *Applied Water Science*, *3*(1), 229–245. https://doi.org/10.1007/s13201-013-0076-3

Tate, E., Sutcliffe, J., Conway, D., & Farquharson, F. (2004). Water balance of Lake Victoria: update to 2000 and climate change modelling to 2100/Bilan hydrologique du Lac Victoria: mise à jour jusqu'en 2000 et modélisation des impacts du changement climatique jusqu'en 2100. *Hydrological Sciences Journal,* 49(4), 1-12.

Thapa, B. R., Ishidaira, H., Pandey, V. P., & Shakya, N. M. (2017). A multi-model approach for analyzing water balance dynamics in Kathmandu Valley, Nepal. *Journal of Hydrology: Regional Studies*, *9*, 149–162. https://doi.org/10.1016/j.ejrh.2016.12.080

Thomas, R., Meybeck, M., & Beim, A. (1996). *Water Quality Assessments - A Guide to Use of Biota, Sediments and Water in Environmental Monitoring*. https://scholar.google.com

Tolf, M. O. P., Lasaga, A. O. C., Pan, C., & White, W. B. (1985). *The kinetics of Dissolution of Nepheline.* https://scholar.google.com

Tomy, T., & Sumam, K. S. (2016). Determining the Adequacy of CFSR Data for Rainfall-

Runoff Modeling Using SWAT. *Procedia Technology*, *24*, 309–316.

Troitskaya, Y. I., Rybushkina, G. V., Soustova, I. A., Balandina, G. N., Lebedev, S. A., Kostyanoi, A. G., Panyutin, A. A., & Filina, L. V. (2012). Satellite altimetry of inland water bodies. *Water Resources*, *39*(2), 184–199.

UNESCO. (1971). *Scientific Framework of World Water Balance Unesco.* https://scholar.google.com

URT. (2022). *The United Republic of Tanzania Administrative Units Population Distribution Report*. https://scholar.google.com

USDA, S. (1975). Urban hydrology for small watersheds. *Soil Conservation*, *Technical Release, 55 (TR-55)*, 164.

USGS. (2018). *Lakes and Reservoirs: Guidelines for Study Design and Sampling: Handbooks for Water-Resources Investigations*. http://library.usgs.gov

Varekamp, J. C., Pasternack, G. B., & Rowe, G. L. (2000) Volcanic lake systematics II. Chemical constraints. *Journal of Volcanology and Geothermal Research*, *97*(1–4), 161–179. https://doi.org/10.1016/S0377-0273(99)00182-1

Vereecken, H., Weihermüller, L., Assouline, S., Šimůnek, J., Verhoef, A., Herbst, M., Archer, N., Mohanty, B., Montzka, C., Vanderborght, J., Balsamo, G., Bechtold, M., Boone, A., Chadburn, S., Cuntz, M., Decharme, B., Ducharne, A., Ek, M., Garrigues, S., … Xue, Y. (2019). Infiltration from the pedon to global grid scales: An overview and outlook for land surface modeling. *Vadose Zone Journal*, *18*(1), 1-53.

Westerberg, L. O., Holmgren, K., Börjeson, L., Håkansson, N. T., Laulumaa, V., Ryner, M. A., & Öberg, H. (2010). The development of the ancient irrigation system at Engaruka, northern Tanzania: Physical and societal factors. *Geographical Journal*, *176*(4), 304–318. https://doi.org/10.1111/j.1475-4959.2010.00370.x

Widgren, M., & Sutton, J. E. G. (2004). *Islands of Intensive Agriculture in Eastern Africa: Past & Present*. https://scholar.google.com

Wilson, M. J. (2004). Weathering of the primary rock-forming minerals: Processes, products and rates. *Clay Minerals*, *39*(3), 233–266. https://doi.org/10.1180/0009855043930133

Winter, T. C., Rosenberry, D. O., & Sturrock, A. M. (1995). Evaluation of 11 equations for determining evaporation. *Water Resources Research*, *31*(4), 983–993.

YAO, H. (2009). Long-Term Study of Lake Evaporation and Evaluation of Seven Estimation Methods: Results from Dickie Lake, South-Central Ontario, Canada. *Journal of Water Resource and Protection*, *01*(02), 59–77. https://doi.org/10.4236/jwarp.2009.12010

Yapiyev, V., Rossi, P. M., Ala-Aho, P., & Marttila, H. (2023). Stable water isotopes as an indicator of surface water intrusion in shallow aquifer wells: A cold climate perspective. *Water Resources Research*, 59(2), e2022WR033056.

Żaba, J., & Gaidzik, K. (2011). The Ngorongoro Crater as the biggest geotouristic attraction of the Gregory Rift (Northern Tanzania, Africa): Geological heritage. Geotourism/Geoturystyka, (24-25), 27-27.

Zhang, B., Zhao, D., Zhou, P., Qu, S., Liao, F., & Wang, G. (2020). Hydrochemical characteristics of groundwater and dominant water–rock interactions in the Delingha Area, Qaidam Basin, Northwest China. *Water*, 12(3), 836.

Zhang, G., Bolch, T., Chen, W., & Crétaux, J. F. (2021). Comprehensive estimation of lake volume changes on the Tibetan Plateau during 1976–2019 and basin-wide glacier contribution. *Science of the Total Environment,* 772, 145463

Zhang, Z., Huang, Y., Xu, C. Y., Chen, X., Moss, E. M., Jin, Q., & Bailey, A. M. (2016). Analysis of Poyang Lake water balance and its indication of river–lake interaction. *SpringerPlus,* 5(1), 1-15.

Zotarelli, L., Dukes, M. D., Romero, C. C., Migliaccio, K. W., & Morgan, K. T. (2010). *Step by step Calculation of the Penman-Monteith Evapotranspiration (FAO-56 Method)*. Institute of Food and Agricultural Sciences. University of Florida, 8. https://scholar.google.com

RESEARCH OUTPUTS

(i) Accepted Article for Publication

Godwin, L., Kapama, H. K., & Ceven, S. (2023). The hydrological system and water balance of ungauged Crater Lakes of the Northern Crater Highlands. *Tanzania Journal of Engineering and Technology*, 42(3), xx-xx.

(ii) Poster Presentation